Progress in Energy and Combustion Science 112 (2026) 101262

Contents lists available at ScienceDirect

Progress in Energy and Combustion Science

journal homepage: www.elsevier.com/locate/pecs

Thermocatalytic ammonia synthesis beyond conventional Haber-Bosch: Principles, advances, challenges and opportunities

Tianbao Gu [a,*], Matej Huš [b,c,**], Samuel Simon Araya [d], Blaž Likozar [b], Fausto Gallucci [e], Vincenzo Liso [a]

[a] AAU Energy, Aalborg University, Aalborg, Denmark
[b] National Institute of Chemistry, Ljubljana, Slovenia
[c] Association for Technical Culture of Slovenia (ZOTKS), Ljubljana, Slovenia
[d] Luxembourg Institute of Science and Technology (LIST), Luxembourg
[e] Department of Chemical Engineering & Chemistry, Eindhoven University of Technology, Eindhoven, Netherlands

ARTICLE INFO

Keywords:
Ammonia synthesis
Mild thermocatalysis
Process intensification
System integration
Green NH_3

ABSTRACT

Transforming ammonia (NH_3) synthesis from the energy-intensive, fossil-fuel-dependent conventional Haber-Bosch (HB) process to a flexible, green hydrogen-based process is pivotal for decarbonization and enabling NH_3 utilization in the energy sector. The conventional HB process, operating under high temperature and pressure, is incompatible with green hydrogen systems and economically unviable for downscaled NH_3 production integrated with intermittent renewable energies . Therefore, developing alternatives capable of synthesizing NH_3 under moderate conditions is crucial for achieving green NH_3 production. This necessity has driven the development of a range of emerging technologies, including thermocatalytic, electrocatalytic, photocatalytic, and plasma-assisted processes, amongst which thermocatalysis stands out in terms of production rate, technology readiness, and economic feasibility, demonstrating the greatest potential for NH_3 synthesis transformation. This review provides a comprehensive overview of advanced thermocatalytic NH_3 synthesis beyond conventional HB process and the system integration with renewable sources. It highlights key limitations and advances in implementing new materials and auxiliary techniques, outlining the challenges and mitigation strategies for achieving high NH_3 productivity under mild conditions. Alongside multiscale modeling studies, the review covers catalyst development, reactor intensification, process integration, and system evaluation, examining progress and conducting meta-analysis in reaction mechanisms, emerging separation technologies, and system integration. Scientific obstacles, economic analysis, and environmental impacts are thoroughly discussed, offering state-of-the-art insights into mild NH_3 synthesis from fundamental research to practical applications. Additionally, recent industrial projects of green NH_3 production are summarized, showcasing scalability and commercial viability. Finally, the remaining challenges and opportunities in advanced thermocatalytic NH_3 synthesis are outlined, identifying future research frontiers.

Contents

* Corresponding author.
** Corresponding author. National Institute of Chemistry, Ljubljana, Slovenia.
E-mail addresses: tig@energy.aau.dk (T. Gu), matej.hus@ki.si (M. Huš).

https://doi.org/10.1016/j.pecs.2025.101262
Received 13 December 2024; Received in revised form 6 October 2025; Accepted 6 October 2025

1. Introduction

Ammonia (NH_3) is an indispensable chemical with widespread applications in multiple sectors, serving as a cornerstone for sustaining modern society. Its primary use is in the production of fertilizers, which contribute to global food production, providing necessary nutrients for crops. Beyond its role in agriculture, NH_3 and its derivatives find applications in the pharmaceutical, synthetic fibers, resins, and explosives industries [1]. More recently, NH_3 has gained recognition as a promising candidate for sustainable fuels and a carbon-free hydrogen (H_2) carrier through the concept of Power-to-X (PtX), in which renewable energy is converted into H_2 by water electrolysis or into other synthetic fuels such as methanol, methane and NH_3 [2]. It is one of the most effective solutions for storing intermittent energy in long-term and at large-scale [3]. The properties of the H_2-based secondary chemicals are systematically reviewed in Ref. [4], highlighting the suitability of NH_3 as a carbon-neutral, easy-to-store, and high-density-energy carrier. The recent progress and prospects of NH_3 fuel are reviewed in Ref. [5]. The International Energy Agency (IEA) has presented the scenario of using NH_3 as an energy carrier in the report 'Ammonia Technology Roadmap' in 2021, as shown in Fig. 1 [6].

However, the current dominant method of NH_3 production, the conventional Haber-Bosch (HB) process, has a substantial carbon footprint and energy consumption. This century-old process requires high temperatures (400–500 °C) and pressures (150–300 bar), relying heavily on fossil fuels for both energy and H_2 production [7]. Due to its operational features, typical HB plants are always built in a centralized and large-scale form to efficiently and cost-effectively produce NH_3, which requires stable H_2 supply of high purity. Fossil fuel-based H_2 as the main source is supplied massively to maintain HB reactors operation, leading to a substantial carbon emission and energy consumption [8]. According to IEA [6], more than 70 % of NH_3 production is based on natural gas steam reforming, with the remainder based on coal gasification, giving a large carbon footprint, which contributes to 1.3 % of global carbon dioxide (CO_2) emissions. On the other hand, the energy consumption of NH_3 production is substantial, accounting for around 2 % of the annual global energy use (IEA). Replacing the fossil fuel-based energy and H_2 supply with renewable sources promises an order-of-magnitude carbon emissions reduction [2]. Therefore, decarbonizing NH_3 production is critical for mitigating its environmental

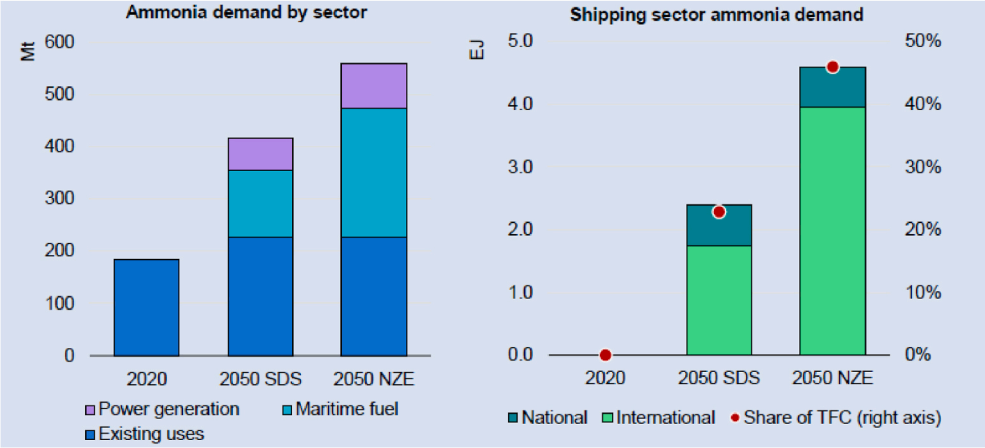

Fig. 1. Ammonia use as an energy carrier in the Sustainable Development Scenario (SDS) and the Net Zero Emissions (NZE) by 2050, as a fraction of TFC (final energy consumption) in the maritime shipping sector. Reproduced from Ref. [6] with permission from the International Energy Agency.

impact and achieving global sustainability goals and net zero emission. While significant strides have been made in developing alternative NH_3 synthesis technologies, such as electrochemical synthesis [7,9], photocatalytic synthesis [10], and plasma-assisted synthesis [11,12]. These methods are still in their early stages of development and face various challenges, including low NH_3 yield, low energy efficiency, and the need for further research to optimize reaction pathways and develop more efficient catalysts.

For example, the emerging electrochemical NH_3 synthesis or nitrogen (N_2) reduction reaction (NRR) represents a promising approach that could facilitate decentralized, small-scale NH_3 production with lower environmental impact. Unlike the HB process, electrochemical synthesis can operate at ambient pressures and lower temperatures, depending on the electrochemical cell used, and can use water directly as the H_2 source, reducing dependence on fossil fuels [13,14]. However, low NH_3 yields and Faradaic efficiency primarily due to the competing H_2 evolution reaction, high costs, and limited durability of certain electrolytes currently limit its practical application [7]. The advancements of electrochemical NH_3 synthesis have been thoroughly reviewed in Ref. [15], with focus on atomic-level fundamentals. The review highlights advanced theoretical screening and experimental practices for rational electrocatalyst design, addressing current challenges and proposing strategies for enhancing electrocatalytic NH_3 production. It reports that recent progress has seen improvements in NH_3 generation rates from $\sim 10^{-12}$ mol s^{-1} cm^{-2} to 10^{-11}-10^{-10} mol s^{-1} cm^{-2}, and Faradaic efficiencies from <1 % to ~10 %, respectively. However, these advancements remain more than an order of magnitude below the threshold required for practical applications. The review of techno-economic assessment (TEA) for different electrochemical NH_3 synthesis units are recently reported in Ref. [16], highlighting the significant gap from current research status to commercial application.

Plasma-assisted NH_3 synthesis also shows promise, particularly for its ability to activate N_2 and H_2 at ambient conditions, potentially reducing the high energy demands associated with traditional synthesis [12]. This method is compatible with renewable energy, making it a promising route for NH_3 production. The use of dielectric barrier discharge plasma offers additional benefits, such as simpler reactor construction and low operating costs under atmospheric conditions [11,17]. However, plasma-assisted synthesis suffers from low NH_3 yield and energy inefficiency. Scaling up the process for industrial production poses significant challenges. Furthermore, high-energy electrons in the plasma can lead to NH_3 decomposition, which impacts overall efficiency, and catalyst development is needed to enhance the selectivity and efficiency of NH_3 formation [18].

Photocatalytic NH_3 synthesis, directly uses solar energy to drive the reaction, operates under mild conditions without high-temperature and pressure demands [10]. Photocatalytic N_2 fixation to NH_3 has been reviewed in Ref. [19], covering the fundamental aspects of photocatalytic reactions, effective photocatalysts, and reactor design strategies. Notable progress and discoveries have been recorded, indicating that solar-driven NH_3 production on a modest scale may become feasible in the future. However, photocatalytic methods currently suffer from very low NH_3 yields, making large-scale application impractical. To improve the efficiency of this method, advances in photocatalyst development that can effectively capture solar energy and facilitate N_2 reduction, are needed. Additionally, scaling up photocatalytic synthesis to industrial levels meets technical and economic challenges that require further research. Chemical looping NH_3 synthesis offers another novel approach by decoupling N_2 fixation and hydrogenation steps, which could provide a more controlled reaction environment and reduce energy requirements through operation at lower temperatures and pressures [20]. While promising, chemical looping technology is still in its infancy and generally exhibits lower yields of NH_3 compared to more established methods. A key challenge is identifying stable and effective N_2 carrier materials that can reliably transport and release N_2 [21]. Moreover, a deeper understanding of the underlying reaction mechanisms and kinetics is necessary to optimize the process and improve NH_3 yields in chemical looping-based processes.

Each emerging NH_3 production technology involves a distinct synthesis pathway, addressing specific challenges associated with moving away from traditional fossil fuel-based methods. Beyond individual approaches, ammonia production can also benefit from multi-technology coupled synthesis, an emerging and promising innovation that integrates complementary technologies to improve efficiency and sustainability. One example is the tandem use of non-thermal plasma and electrocatalysis under ambient conditions, where plasma-driven oxidation is combined with electrochemical reduction to enhance overall system performance and mitigate the limitations of each individual technology [22,23]. This hybrid method achieves better selectivity through decoupled optimization, allowing the independent enhancement of nitrogen activation and NH_3 formation processes under their optimal conditions, delivering NH_3 yield rate of 3 mmol h^{-1} cm^{-2} and a corresponding Faradaic efficiency of 92 % at −0.25 V versus reversible hydrogen electrode in batch experiments [23]. Even though still in its infancy, this technology demonstrates superior performance metrics through two-step processes that differentiate the complex N_2 activation step from the more efficient NH_3 production stage, allowing for nearly complete selectivity in ammonia generation while maintaining scalability through flow-mode operation.

In contrast, integrating green H_2 into the existing HB process offers a

Table 1
Summary of technology development for NH_3 production.

Technology	Process	Required conditions	H_2 source	TRL	Plant scale	Comments	Ref.
Thermocatalysis	Conventional HB: SMR-HB	400–500 °C, 150–300 bar	Fossil- H_2	9	Commercial >2000 t/d	- Centralized production with high capital cost - High production rate with low cost - Producing more than 95 % NH_3 currently - High energy consumption and carbon emission	[20, 27]
	SMR-HB + CCS		Fossil- H_2	7–9	Pilot - Commercial	- Promising to be used in existing large-scale plants for carbon reduction - High production rate - High cost for CCS, possibly economical competitive with carbon tax in future	[28, 29]
	Green HB: Grid-eH_2O-HB		eH_2	6–9	Pilot – Commercial	- Normally in large scale - Potential for reaching net zero emission - Connect with grid power for stable operation - TRL depends on the electrolysis technology integrated, e.g., ALK and PEM	[27, 30]
Advanced thermocatalysis	eH_2O-Adv. HB	300–400 °C, 30–150 bar	eH_2	5–8	Pilot <30 kg/d	- Can be downscaled and due to mild operation conditions - Connect with dynamic renewable power - Requires flexible operation - Integrate with SOE electrolyser remains lower TRL	[8,26]
	eH_2O-Adv. HB + Abs.	300–400 °C, 30–150 bar	eH_2	4–5	Small	- Use ex-situ sorption to replace condensation, which is more efficient - Different operation conditions of catalyst and sorbent leads to more energy cost in operation and system complexity - Durability and capability challenge of materials after many circles - Lots of thermal mass (sorbents) are needed for large-scale units	[25, 31]
	eH_2O-Adv. HB with in-situ Abs.	300–350 °C, 30–150 bar	eH_2	1–3	Small	- Potential to exceed equilibrium - High conversion with many layers without gas recycling - Load catalyst bed and sorbent bed in the same reactor - Operation conditions trade-off is needed for catalyst and sorbent - Challenges in material poisoning and cycling - Lower space velocity is usually required for longer residence time	[26, 32]
	eH_2O-Adv. HB with Membrane	200–350 °C, 10–100 bar	eH_2	1–3	Small	- Enhance the forward reaction to format NH_3 - Low productivity due to mild conditions - Challenge of membrane tolerance under high temperature - Expensive cost of membrane	[25]
Electrocatalysis	Non-aqueous eNH_3	200–500 °C, <20 bar	eH_2	1–3	Small <1 kg/d	- Non-aqueous (organic) electrolyte used - Higher Faradaic efficiency compared to aqueous eNH_3, especially for Li-mediated NRR - Low NH_3 production rate - Proton/H+ doner is needed - Challenge in N_2 triple bond dissociation, durability and continuous operation - Difficulties in measurement and characterization - Promising for long-term future	[15, 16]
	Aqueous eNH_3	<100 °C, <20 bar	H_2O	1–3	Small	- Synthesize NH_3 directly from water - Higher voltage is needed to overcome the overpotential - Struggling with the competitive H_2 evolution reaction - Challenge in N_2 triple bond dissociation - Low Faradaic efficiency and NH_3 production rate - Huge electrode surface and catalyst loading - Promising for long-term future	[33]
Photocatalysis	Batch reactor	Ambient temperature and pressure	H_2O	1–3	Small	- Use solar energy to synthesize NH_3 from water - Competing H_2 evolution reaction - Photocatalysts with highly active sites are desired - Challenges of electrons supply through light - Ammonia production rate is very low - The solar-driven N_2 fixation is promising for distributed NH_3 production	[19]
Non-thermal plasma	Batch reactor	Around 50 °C, atmosphere pressure	H_2O vapor; H_2	1–3	Small	- Active N_2 bond by free electrons in plasma - Potential for on-site NH_3 synthesis under atmospheric condition - The efficiency and conversion are very low - High cost due to the plasma source	[17, 18, 34]
Hybrid plasma-electrocatalysis	Flow reactor	Ambient pressure temperature	eH_2	1–3	Small	- High selectivity, decoupled optimization - System complexity, early stage	[22, 23]

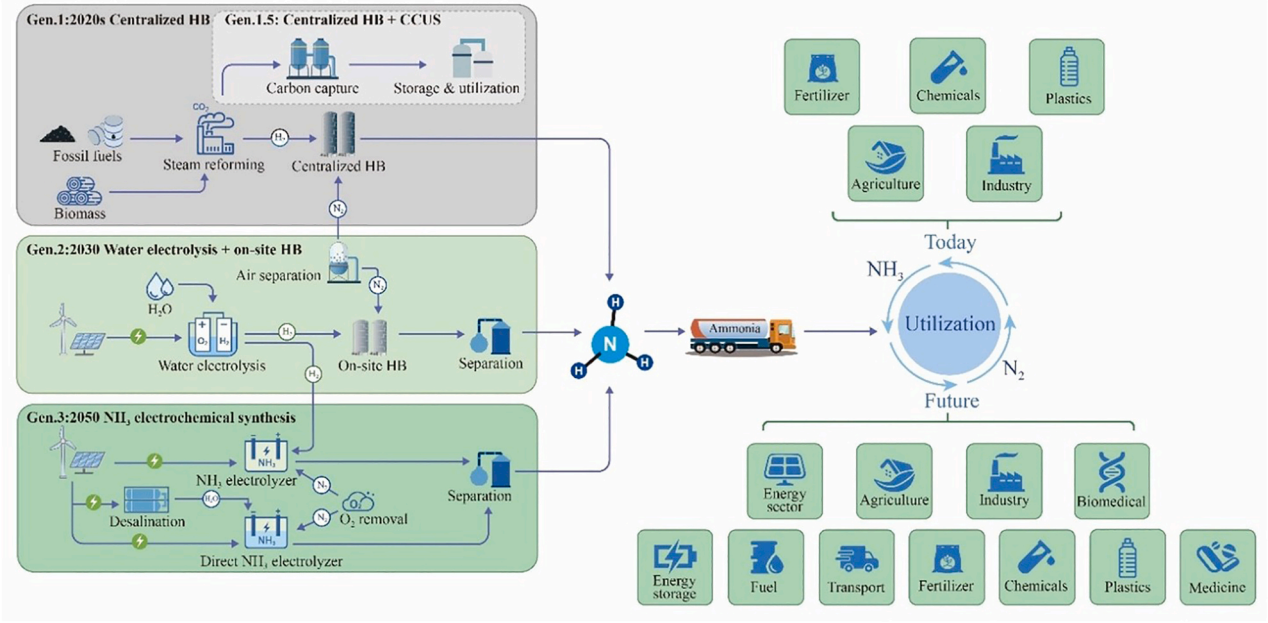

Fig. 2. Vision of renewable NH_3 production and utilization. Gen. 1: Steam reforming-based HB process (+CCS for Gen 1.5), Gen. 2: Water electrolysis-based HB process, Gen. 3: Electrochemical NH_3 synthesis.

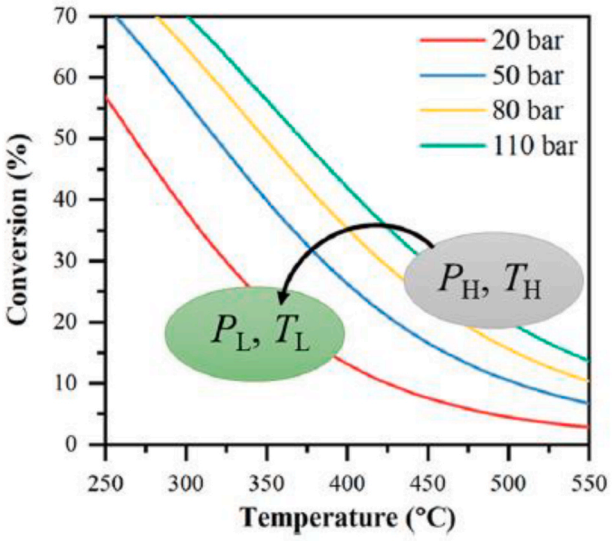

Fig. 3. Theoretical equilibrium conversion of NH_3 synthesis. Reprint from Ref. [25] with permission from American Chemical Society.

more immediate path, that can significantly reduce the carbon footprint of NH_3 production. By substituting fossil fuel-derived H_2 with green H_2 from renewable sources, the green Haber-Bosch process is promising to cut the carbon emissions of traditional NH_3 production [24]. This approach retains the infrastructural advantages of the conventional process while lowering CO_2 emissions. However, the HB process is not inherently compatible with green H_2 systems, necessitating downscaling and adjustments to operating conditions. Efforts on novel catalyst development, efficient separation methods and process intensification have been attempted, driving improvements in the HB process over the past century [25] that led to the development of advanced thermocatalytic NH_3 synthesis beyond the conventional HB process, which can operate under milder conditions [26]. These advancements achieved enable the integration of thermocatalytic NH_3 synthesis with water splitting, paving the way for alternative NH_3 production. Based on the latest studies and reports, the operation conditions, technology readiness level (TRL), pros and cons of various NH_3 synthesis technologies and processes are summarized in Table 1.

Despite the rapid development and significant achievements in advanced NH_3 production, the conventional steam methane reforming (SMR)-based HB process is expected to persist for several decades until it can be phased out by other zero-emission alternatives [16]. Among the existing NH_3 synthesis technologies, advanced small-scale thermocatalytic process integrated with water electrolysis remains the most promising in terms of maturity, cost, and energy efficiency [16,35]. Drawing upon state-of-the-art reviews in literature, the envisioned future of NH_3 production and utilization has been outlined. In the long-term future (beyond 2050), electrocatalytic synthesis is anticipated to dominate NH_3 production [30], whereas advanced thermocatalytic processes are expected to prevail in the near term (the next several decades) [35]. The progression of NH_3 production technologies, from conventional Haber-Bosch process (Gen. 1) to near-future systems integrating water electrolysis with advanced HB (Gen. 2), and ultimately to direct electrocatalytic NH_3 synthesis in the long term (Gen. 3), is depicted in Fig. 2.

Reviews in Refs. [20,25] summarize advances in milder NH_3 synthesis technologies, comparing thermocatalytic, electrocatalytic, and photocatalytic methods for dinitrogen reduction under moderate conditions, as well as emerging separation technologies. The NH_3 production system via the Gen. 2 route has been reviewed and assessed in Refs. [35,36]. The societal and environmental implications of modern thermocatalytic NH_3 synthesis are discussed in the context of the future role of the Haber-Bosch process in Ref. [26] and the broader NH_3 economy in Ref. [30]. Despite these efforts, a comprehensive review that systematically explores thermochemical NH_3 synthesis beyond conventional HB process, encompassing and linking catalyst development, reactor design, process intensification, and system integration, has yet to be reported. Such a review is crucial for bridging fundamental advances with practical applications, identifying the current challenges and opportunities for diverse stakeholders, and ultimately facilitating the transition to green NH_3 production.

This article presents a comprehensive overview of the progress, challenges and opportunities in NH_3 synthesis via thermocatalysis beyond conventional Haber-Bosch process, examining the advances in

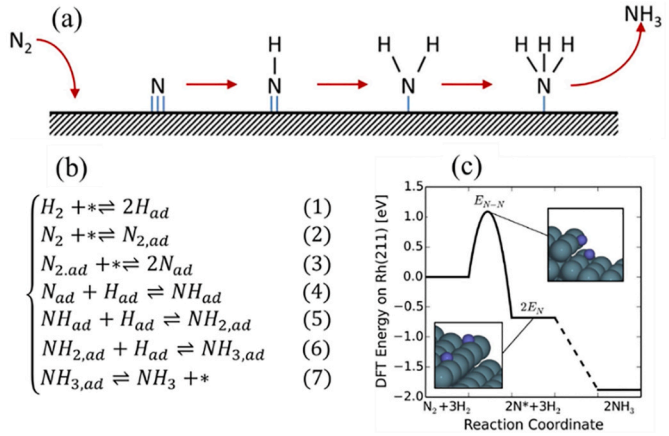

Fig. 4. Typical HB loop reaction scheme (a) reproduced from Ref. [45] with permission from Elsevier; elemental steps (b) reproduced from Ref. [46] with permission from Springer Science; energy barrier calculation example (c) reproduced from Ref. [20] with permission from Elsevier.

mechanistic, reactor scale, and system level perspectives. The integration of advanced processes with renewable energy sources are also discussed to facilitate the widespread adoption of NH_3 production. By providing a critical analysis of existing technologies and emerging trends, this review emphasizes the role of NH_3 in energy sector and ongoing efforts to redefine NH_3 production via thermocatalysis. This paper is structured into seven chapters. Chapters 1 and 2 introduce the background of mild thermocatalytic NH_3 synthesis, along with its limitations and mitigation strategies. Chapters 3, 4, and 5 constitute the core of the review, focusing on advances in novel catalyst development and mechanism exploration, process intensification and conceptual reactor design, and the integration of green NH_3 production systems, respectively. Modeling studies, ranging from the microscale to the system level, are incorporated where relevant. Chapter 6 outlines the current challenges and future perspectives from both research and policymaking viewpoints, mapping out strategies for advancing NH_3 production. The review concludes with a summary of key insights in Chapter 7.

2. Limitations and mitigations of ammonia mild synthesis

The thermocatalytic NH_3 synthesis beyond conventional HB process is interpreted as using compensation technologies to enhance the synthesis process which allow it to operate at mild conditions (<400 °C, 100 bar) and thereby maintain competitive NH_3 productivity [37]. Owing to the moderate operation conditions, the advanced synthesis process can be downscaled, exhibiting compatibility with water splitting powered by renewable energies, to achieve the Power-to-Ammonia (PtA) vision [38].

From a thermochemical point of view, synthesis of NH_3 with reactants of H_2 and N_2 is an exothermic and reversible reaction,

$$3H_2 + N_2 \rightleftharpoons 2NH_3, \Delta H_{298} = -92.22\ \text{kJ/mol} \quad \text{(R1)}$$

where low temperature and high pressure favor the forward reaction as seen in the equilibrium plot Fig. 3 [25].

This plot shows that it is theoretically possible to achieve a high conversion of H_2 and N_2 under low temperature and high pressure. It is fundamental to develop low-temperature NH_3 thermocatalytic synthesis beyond the conventional HB process. However, neither modifying the extreme operational conditions of HB nor its integration with water electrolysis is easy [25,27]. The first primary issue is the activation of N_2 at reduced temperature. The strong triple bond in N_2, with its high energy barrier, demands significant external energy for cleavage, making it the rate-determining step in the synthesis process. This limitation results in low production rates at lower temperatures. The second critical issue is the catalyst oxygenate tolerance, as H_2 from water splitting often contains small amounts of impurities of oxygen (O_2) and moisture that can poison the iron-based catalysts traditionally used in the HB process [39]. Addressing these two issues requires the development of catalysts that are active enough at low temperature and tolerant to these oxygenates, allowing for the effective use of renewable H_2 in existing NH_3 plants [40]. The third challenge is that the HB process is finely tuned for fossil-based H_2. Adapting operating conditions to maximize efficiency and NH_3 yield with dynamic H_2 production, though essential, is challenging [26]. Additionally, while the high-pressure environment of the Haber-Bosch is advantageous for both NH_3 synthesis and efficient product separation, water electrolysis typically occurs at lower pressures [35]. This pressure difference may necessitate additional compression, potentially diminishing some of the energy gains from using H_2. Finally, effective separation of NH_3 from unreacted N_2 and H_2 at these lower pressures remains challenging [41]. Conventional condensation methods are less effective under such conditions, potentially requiring costly refrigeration. Developing alternative separation techniques is critical for enabling efficient, low-pressure NH_3 synthesis with sustainable H_2 [42,43]. For decades, the efforts to improve HB process and its combination with water splitting have been mainly made to overcome these limitations. The overview for the limitations in three scales and their corresponding mitigation strategies are illustrated in the sections of this chapter, as follows.

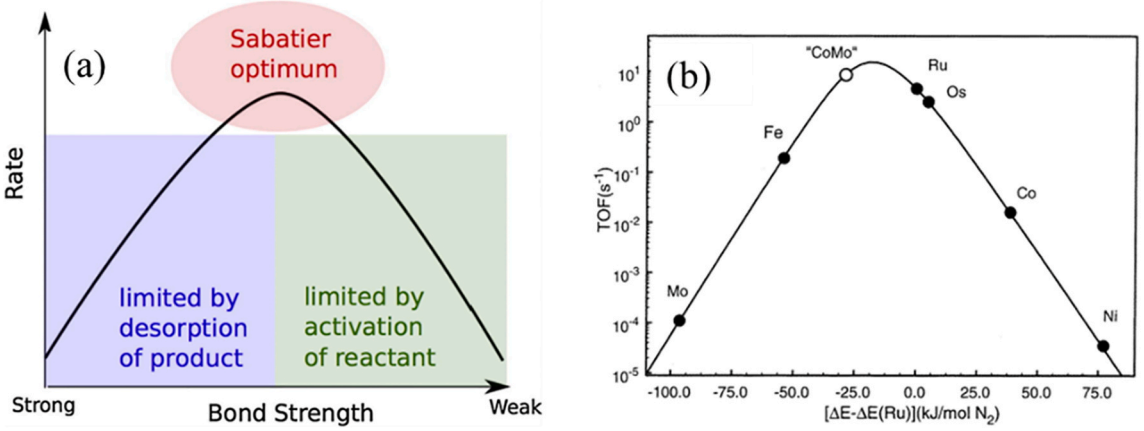

Fig. 5. Illustration of the Sabatier principle (a) reproduced from Ref. [47] with permission from Elsevier; Volcano plot of NH_3 synthesis turnover frequencies over TMs reprinted (b) reproduced from Ref. [48] with permission from American Chemical Society.

2.1. Nitrogen activation

At molecular level, the NH_3 thermocatalytic synthesis is complicated, consisting of many sequential and parallel reaction steps. Numerous studies have investigated the synthesis mechanism based on surface science, theoretical calculation, material science and so on, exploring several catalytic mechanisms under certain circumstances. For the industrial HB process over iron-based catalysts, the well-accepted reaction scheme is the dissociative pathway, i.e., the process undergoes N_2 activation through dissociative adsorption ($N_2 \rightarrow 2N^*$), followed by the hydrogenation of N adatoms and finally NH_3 desorption, as illustrated in Fig. 4(a) [44].

The encompassing elementary steps are presented in Fig. 4(b) [46], amongst which N_2 activation is the rate-determining step for the synthesis [40] due to its high energy barrier compared to others, as shown in Fig. 4(c). The high barrier is directly caused by the stability of the triple bond between the two N atoms. Although theoretically low temperatures favor the NH_3 synthesis equilibrium, the catalytic reaction cannot be triggered at low temperatures owing to the aforementioned high energy barrier. Therefore, high temperature is normally used in the HB process to activate N_2 and thereby force the catalytic reaction.

To address this, more active catalysts that can activate N_2 molecules at reduced temperatures are desired. The research on catalyst development for NH_3 synthesis in some sense is to investigate the activation of N_2 and its nature [49]. In the principle of Sabatier, the optimum catalyst should bind atoms and molecules with a trade-off strength, i.e., strong enough to activate the reactants, and weak enough to desorb the products, leading to the volcano plot of activities along the catalyst bond strength as shown in Fig. 5(a) [47]. Fortunately, the typically used catalyst (Fe-based) is not the optimum one, there are some other transition metals (TMs) such as ruthenium (Ru) and Molybdenum (Mo) which show better performance in the volcano plot as shown in Fig. 5(b) [20]. This figure shows the theoretical feasibility of developing more active catalysts based on other TMs, opening the gate of NH_3 synthesis under mild conditions.

Moreover, the activity of N_2 adsorption on catalyst surface is not only on the basis of the transition metal, some materials such as alkali and potassium (K) can also make positive effects on the structural and/or electronic aspects of the catalyst [50]. Hence, promoters are often considered in novel catalyst development, to further enhance the catalyst activity. The state-of-the-art for NH_3 synthesis novel catalysts and mechanism investigations under moderate conditions, are elaborated upon in Chapter 3.

2.2. Ammonia separation

Another critical challenge for mild NH_3 synthesis is separation of the NH_3 produced [26]. In general, physical condensation is used after the conventional HB loop, separating NH_3 from the gas mixture of N_2, H_2 and NH_3 by their different saturation temperatures. The condensation process is energy-intensive, and the separation efficiency is highly favored by high pressure according to the vapor-liquid equilibrium curve [51]. The condensation-based separation can be achieved with cooling water under high pressure, while a much lower temperature is needed for separation under lower pressure requiring an expensive refrigeration system [35]. Currently, most of the centralized HB plants can achieve reported conversions of 10 %–15 % under 425–450 °C over 100 bar [40,52]. Therefore, physical condensation technology is applicable. However, for a mild process that is operated at low pressure and with a low yield of NH_3 (few percent or less), cryogenic condensation is neither efficient for separating NH_3 nor viable to completely remove the low-concentrated NH_3 from unconverted H_2 and N_2.

The mitigation strategy is to develop more efficient NH_3 separation technologies that align with the conditions of mildly operated HB units. Solid sorption (including adsorption and absorption) and membrane separation are the two main emerging separation approaches to be used in mild HB process [35,51]. Ammonia can also be captured with by liquid solvents such as ionic liquid, whereas liquid matters are normally not compatible with catalyst-filled reactors, hence rarely implemented in advanced NH_3 synthesis process. Adsorption of NH_3 is based on the theory of surface sorption, i.e., fixing the molecule on solid surface by the weak binding strength or chemical bonds, which is typically effective only at low temperature [42]. The materials utilized normally possess a high surface area such as MOFs and ionic networks. Conversely, NH_3 absorption occurs when NH_3 enters the crystalline matrix of the absorbent, forming stable metal ammine complexes inside [53]. The absorption-based NH_3 uptake is still effective at high temperatures (e.g., 300 °C) compared to adsorption, and therefore shows more promise for in-situ separation during NH_3 synthesis. In fact, many absorbents developed also have an adsorption capacity of NH_3, namely composite sorbents, resulting in combined sorption.

On the other hand, membrane separation utilizes the different permeabilities of gases through specific thin membranes to separate gas mixtures, which exhibits advantages in energy consumption [54]. A slightly smaller kinetic diameter of NH_3 (2.60 Å) compared to H_2 (2.89 Å) makes the size exclusion-based separation insufficient for the membrane NH_3 separation. The mechanisms of NH_3 transport through membranes are thus complicated and different according to different types of membranes such as polymeric membranes and inorganic membranes. For the purpose of separating NH_3 in the HB process, the membranes require not only selective permeability of NH_3, but also thermal and mechanical stability under the working conditions of the integrated HB process [25]. From this perspective, inorganic membranes, which have more tolerance to high temperature, show more compatibility with the advanced thermocatalytic NH_3 synthesis. The different technologies for NH_3 separation are compared in Table 2.

Moreover, NH_3 separation also can be used as a process intensification technique for NH_3 synthesis reactor, to exceed the single-pass equilibrium. The combination of solid absorption or membrane separation with synthesis can intensify the synthesis process in two ways: 1) shift the chemical equilibrium to the forward reaction; 2) accelerate the reaction rate by removing the inhibition effects of the instantly

Table 2
Comparison of different NH_3 separation methods.

Technology	Mechanism	Materials	Pros.	Cons.
Physical condensation	Separate gas mixture by their different boiling points through a cryogenic process	N.A.	Mature technology in large-scale NH_3 synthesis; simple process and easy to use	Cooling tower water is needed; large energy expenditure, requires high pressures [51]; hard to downscale
Solid adsorption	Bind gas molecules on the solid surface with different surface affinities	Active carbon, zeolites, metal halides, MOFs	Useful under low pressure	Requires large amounts of adsorbents; requires low temperatures [42]
Solid absorption	Associate gas molecules by forming ammine complex	Salt, MOFs, alkali metal	Low pressure useable; high capacity [53]	Additional desorption process is needed to collect NH_3
Membrane separation	Separate gases by filtering the gas mixture through a selective permeability thin membrane	Polymer, metal alloy	Energy efficient; potential to be used in-situ	Expensive; favored at low temperature; difficult to upscale [25]

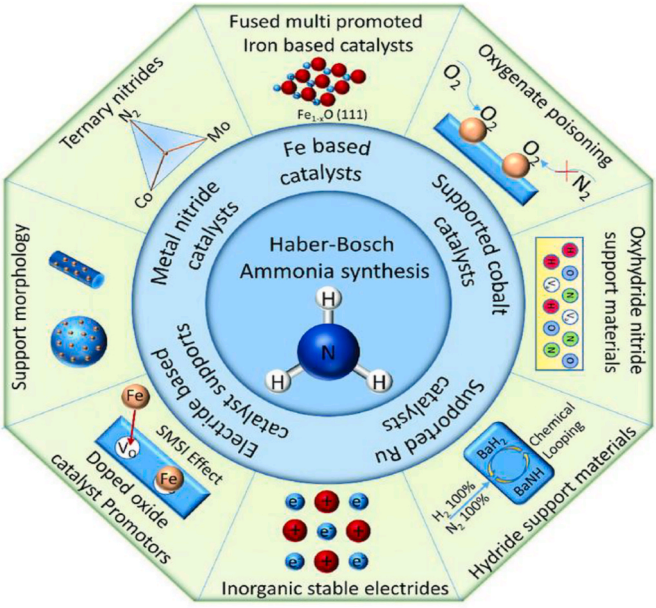

Fig. 6. Graphical overview of strategies to advancing NH_3 catalyst. Reproduced from Ref. [40] with permission from Wiley.

generated NH_3 [55]. The state-of-the-art for novel NH_3 separation technologies and its-based intensified reactors are extensively reviewed in Chapter 4.

2.3. System integration

To accomplish the Gen. 2 scenario of NH_3 production, the on-site HB reactor is required to integrate with water electrolysis stacks powered by renewable energy to supply H_2 to the HB loop [4]. However, the HB reactor would have operational challenges due to the unstable or uneven continuous H_2 supply caused by intermittent renewable energy sources such as wind and solar [56]. Since the HB process normally requires continuous and stable operation, especially for large-scale and heavily operated plants, fluctuating H_2 supply could lead to safety and inefficiency problems. Some components of the HB process, such as the NH_3 reactor and air separation unit, need longer startup times than the electric intermittency. Whereby the unmatched delay would cause energy waste and/or other operation problems [57].

There are two mitigation methods for intermittency. Method 1: eliminate the intermittency before the HB process; Method 2: develop dynamic operation HB process which aligns with upstream intermittent electrolysis stack. For Method 1, a battery can be employed prior to water electrolysis to store renewable electricity and mitigate its intermittency. Alternatively, an H_2 buffer can be used to temporarily store the generated H_2, ensuring a steady supply to the downstream HB process [26]. For Method 2, necessary flexibility of the HB reactor is required, for instance, the catalyst effective temperature and pressure swings, and components startup times [58]. In principle, mildly operated smaller-scale HB units have better operation flexibility than the conventional large-scale plants, while rigorous dynamic operation guidelines and control strategies are still required, where modeling and simulation tools play a pivotal role [59]. Besides, there are several other key challenges for the NH_3 system integration, for instance, incompatible operation conditions and impurities from H_2 sources. The state-of-the-art for the water-electrolysis integrated HB process is thoroughly reviewed in Chapter 5, including the intermittent renewables challenge, H_2 impurities, system modeling and assessments.

3. Novel catalysts and mechanisms of ammonia synthesis

Despite its deceivingly simple atomic composition, NH_3 can be synthesized via several different mechanisms. Broadly speaking, there is the dissociative mechanism, where the triple N ≡ N bond in molecular N_2 is cleaved upon adsorption and each atom is individually hydrogenated via NH and NH_2 intermediates, and the associative mechanisms, where hydrogenation precedes the N ≡ N bond cleavage [60]. Barring different adsorption modes of N_2 and the H* source, there is little variability in the dissociative mechanism. The associative mechanism, however, can follow the distal pathway, where one N_2 atom is sequentially hydrogenated via NNH, NNH_2, NNH_3, or the alternating pathway via NNH, NHNH, $NHNH_2$, NH_2NH_2, NH_2NH_3 [60]. The mechanism is determined by the adsorption interaction of N_2 and intermediates and possible steric hindrance on the catalyst surface, while the rate determining step is always the cleavage of the N ≡ N bond. The Langmuir-Hinshelwood mechanism is used in modeling thermocatalytic NH_3 synthesis because both reactants must adsorb before reacting. Under industrial conditions, the dissociative mechanism predominates [61]. This chapter reviews the advances on novel catalyst development, focusing on:

1) Material preparation including noble/non-noble metals, promoters, supports and other innovative materials, as well as their potential for large-scale applications.
2) Reaction mechanism discovery to understand the complex catalytic reactions over novel catalysts.
3) Microscale modeling studies for describing and predicting the catalytic reaction process.

3.1. Material preparation and development

Before the introduction of the Haber-Bosch process, NH_3 synthesis routes were cumbersome, expensive and inefficient. Dry distillation of organic matter or the reduction of nitrous acid gave way to the cyanamide process, where calcium carbide was reacted with molecular N_2. Immediately before the World War I, the Haber-Bosch process was discovered, boasting superior efficiency, conversion and practicality [49]. Ever since, research has focused on improving the catalytic materials, which have enabled lower operating temperatures and improved efficiency. The graphical overview of developing advanced catalyst for improving HB process is depicted in Fig. 6 [40]. Five categories, Fe-based, supported Ru, supported cobalt, metal nitride and electride-based catalysts, are divided, leveraging on the approaches such as using promotors and oxygenate poisoning. In this section, the efforts for developing advanced catalysts are reviewed from three aspects: transition metals, promoters and other innovative materials.

3.1.1. Transition metal-based catalysts

When Haber proposed to use high pressures in NH_3 synthesis and efficient ways of procuring cheap H_2 and N_2 were established, a low-cost, efficient and stable catalyst was needed. Several metals were tested, ranging from carbides and nitrides to osmium. In 1909, Haber was convinced that the best catalyst had to be multi-component. Despite extensive search at BASF, iron, first proposed in 1905, remained the best performing catalyst for the original Haber-Bosch process [62]. Even today, fused iron catalysts remain unrivalled in the industrial applications. Several new types have been developed (A102, A106, A109, A110 family), which are all magnetite-based. In the 1990s, an iron-based catalyst with the wustite structure ($Fe_{1-x}O$) was also shown to perform well [63].

A great leap forward was made in the 1990s, when ruthenium catalysts were invented and quickly became second-generation catalysts [64]. That ruthenium, iron and osmium are the best pure metal catalysts has been known for over a century, but volcano-shaped activity curves have since provided rationale for these observations. However, they are

plagued by a high affinity for H_2, making them prone to poisoning. Among those, osmium has not seen commercialization due to its rarity and the corresponding high cost, as well as extreme toxicity. As a foray into less expensive materials, cobalt-based catalysts were developed already in the 1970s in the UK but the true renaissance had to wait until the computational methods in the 2000s showed that Co-Mo-N catalysts could outperform iron [48], which was quickly confirmed experimentally [65]. This discovery paved the way to finding several different binary formulations, such as rhenium nitride [66] or cobalt-rhenium [67]. The general idea, however, is not new by any means. It has been speculated since the 1960s that an efficient formulation requires an electron donor species, such as alkali metals, and a transition metal (iron, ruthenium, osmium, potassium) as an electron acceptor [68].

3.1.2. Promoters and supports

It was observed very early that pure iron performs disappointingly in NH_3 synthesis. It is now known that the activity of different facets decreases in the following order (111)>(211)>(100)>(210)>(110) [69] and that seven-fold coordinated sites (C7) on the (111) bcc facet contribute disproportionately to the activity. However, inadvertent contamination of the catalyst with Al_2O_3, CaO_2 and potassium, which were present in iron ore from Sweden, improved the catalyst remarkably [49]. Ever since, promoters were investigated heavily for improvements of the catalyst performance along with the effect of different supports, such as carbon-supported ruthenium catalysts. A wide variety of promoters and supports have been discovered in recent decades [40], which combined with Fe, Co, and Ni offer a promising alternative to conventional fused-Fe catalysts.

Iron catalysts were first promoted with Al_2O_3, which prevented sintering [70]. Soon, potassium was shown to improve the performance at high pressures [50]. Alloying with other metals showed further improvements, such as Fe-Co [71] and Fe-Ni catalysts [72]. Small amounts of zirconium benefitted the reaction, as well [73]. More recently, Nb_2O_5-promoted wustite iron was shown to perform well when melted with other promoters [74]. Lithium hydride can help break the scaling relations of iron in NH_3 synthesis but is highly sensitive to moisture [75]. Further research is oriented towards low iron content catalysts [76], which can have as little as one percent of iron. These incorporate N_2 into oxynitride-hydride formulations and can entirely exclude iron [77].

Ruthenium catalyst studies traditionally focused on the use of different supporting materials with the aim of exposing as many finely dispersed ruthenium atoms as possible due to the cost of ruthenium. First graphite-supported ruthenium was discovered already in 1979. Recently, research has also focused on finding supports that interact with ruthenium and modify its electronic properties. Lanthanum cobaltite stood out as a promising material due to the synergistic effects of Co with Ru [78]. On one hand, nitrides, amides and hydrides can supply active intermediates from the lattice, bringing about the Mars-van Krevelen mechanism, which is embodied by TiH_2 [79], and may have small amounts of BaO added [80]. This paved the way for core-shell Ru/Ba–$Ca(NH_2)_2$ catalysts [81], and CaFH solid solution supports [44]. and various MgO or CaO supports [82]. On the other hand, small amounts of barium or other earth alkali metals have been shown to favorably modify the electronic properties of ruthenium, explaining the addition of small amounts of BaO [80] and using MgO or CaO supports [82]. Another approach is to trap ruthenium atoms as low concentration substitutes in perovskites, such as in lanthanum cobaltite [78]. Using pure intermetallics, such as YRu_2, is commercially untenable [83].

3.1.3. Other innovative materials

Recently, third-generation catalysts have been developed, such as electrides, hydrides, nitrides, rare-earth oxides (cerium, promethium-based), oxy-hydrides, perovskites, amides and intermetallics [84]. Special emphasis is being placed on developing non-noble metal-based and catalysts without critical raw materials (CRM). In general, the third-generation catalysts are distinguished by the avoidance of the scaling relations of the second-generation materials, which is achieved by the manipulation of metal-support interactions and unique storage properties of electrons [84]. Still, the principal metal in these catalysts remains iron, ruthenium, cobalt or molybdenum, while the readily available electrons decrease the activation barrier to cleave the N≡N bond down to as low as 60 kJ/mol.

Electrides are a type of materials having electrons trapped in cavities. Mostly unstable even at room temperature, for instance $C_{12}A_7{:}e^-$ synthesized in 2003. In its structure, two superoxide ions are substituted with four electrons, which can be readily replaced by hydride ions [85], and this prevents catalyst poisoning with H_2 and therefore exhibits a good catalytic activity in NH_3 synthesis when used in conjunction with Ru [86]. Since, several other electrides have been tested, such as $Ca_2N{:}e^-$, $[Y_5Si_3]^{0.79+}{:}e^{0.79-}$ [87] and Ru/LaScSi [88]. Other rare earth-transition metal-Si combinations were also probed [89].

Hydrides are conceptually similar materials in a sense that anions activate the N_2 molecule through injecting the electrons. The hydride ion is rather large, has a low electron affinity and can move between the surface and the bulk [90]. Lithium hydride was first reported in 2016 to mediate the reaction when used with transition metals or their nitrides [75]. While the latter easily break the strong N ≡ N bond, NH_3 synthesis is thwarted by the catalyst poisoning with N atoms. LiH mitigates this effect by transforming itself into LiNH, improving yields in the process [75]. Several other hydrides have been tested (sodium, potassium, calcium, barium) and their performance is dependent on the stability of the imide formed [91]. However, the role of hydrides goes beyond using up N adatoms, as shown by the discovery of $[Li_4FeH_6]^-$ clusters [92], where hydride ions both assume a structural role in the lattice and facilitate dinitrogen activation and hydrogenation. It is also possible to use hydrides without transition metals, such as TiH_2 [79] or barium oxyhydride [76], which can be used with ruthenium or iron. Solid solutions, such as CaFH, can also be classified as hydrides and have been shown to operate at very low temperatures (down to 50 °C) [44].

Recent research has focused on ternary nitrides, due to their higher stability and activity, than the already well researched binary nitrides (such as molybdenum, uranium, vanadium or rhenium) [93]. As predicted by the volcano plot of N_2 adsorption energies [48], Cs-promoted Co_3Mo_3N achieved a superior NH_3 synthesis rate compared to traditional Fe catalysts with two promoters. This high activity is attributed to optimal atomic mixing of metals and Cs inhibiting NH_3 poisoning [94]. Lattice N atoms are highly mobile and participate in the reaction through the Mars van Krevelen mechanism, although they are gradually lost at higher temperature. Other nitrides, such as Fe_3Mo_3N performs better at higher temperatures [95]. Similar performance is observed in antiperovskite nitrides (Co_3ZnN, Ni_3ZnN, Co_3InN, and Ni_3InN). Ni-loaded LaN and Ru/ZrH_2 catalysts demonstrate efficient N_2 activation through dual-site mechanisms, rivaling conventional catalysts [96].

Intermetallic compounds (IMCs) have garnered interest in heterogeneous catalysis due to their unique ordered structural and electronic properties. In addition to the IMCs with an electride character, which were already discussed, others achieve catalytic activity via structural and ligand effects. Historically, rare-earth IMCs were combined with transition metals, although post-reaction analysis revealed they often decompose into rare earth metal nitrides and transition metals. Recently, Ru_2Y [83] and $RhCo_3$/CoO(011) have been shown to catalyse the reaction [97]. Alloys with disordered structures have not received much attention but computational studies suggest alloying Ru or Fe with Pt or Rh might improve their performance at the B5 sites [84].

Lanthanum oxides, particularly when used as supports in NH_3 synthesis, enhance catalytic activity by strengthening metal-support interactions, especially in cerium-based oxides like CeO_2 and Pr_2O_3 [98]. Doping with metals such as Zr [99] and Ti [100] further enriches O_2 vacancies, significantly boosting NH_3 synthesis rates. Ru/$La_{0.5}Ce_{0.5}O_{1.64}$, particularly when promoted with Ba, has shown the highest activity among oxide-supported catalysts [101]. Perovskites with an

ABO_3 structure are promising supports due to their stability and tunable electronic properties, while their catalytic activity depends on the alkaline-earth elements (A in ABO_3) and metals (B in ABO_3) [102]. For example, Ru/$CaTiO_3$, Ru/$SrTiO_3$ and Ru/$BaTiO_3$ show high synthesis rates [103].

Traditional catalysts have been extensively characterized in the past, allowing us to assign individual components as active sites, promoters, and supports. In industrial Fe-based catalysts, iron is widely considered an active component and Al_2O_3 a support, while the definition of the active site is less precise. The distinction between support and promoters is also blurred, extending to active sites, since the reaction usually proceeds fastest at interface sites. Particularly in innovative materials, such prescriptive labels become wholly untenable and are preferably avoided. Instead, we acknowledge their multifunctionality and the coupling between the components.

3.1.4. Feasibility for large-scale industrial application

Despite having potentially superior activity, several catalyst formulations remain unsuitable for large-scale industrial applications because of prohibitively high cost or other market forces, limitations in activity and operation conditions, difficulty in up-scaling or durability-related factors. While it is possible to assess all these aspects of established catalysts, innovative materials have so far remained constrained to lab-scale experiments, allowing us little insight into long-term durability. Often, no commercial vendors exist, making the assessment of their supply chain and marketability moot. For those, we can only discuss the pricing of catalyst raw materials.

Pricing, market conditions and supply chains. With iron priced at less than $1 per kilogram, Fe-based catalysts cost a few dollars per kilogram and typically last 5–10 years in commercial reactors. Market prices of metallic ruthenium hover around 20,000–25,000 US dollars per kilogram, making Ru-based catalysts extremely expensive [104]. Consequently, highly dispersed catalysts with as low Ru loading as possible are used. Intermetallic alloys, such as Ru_2Y [83] and $RhCo_3$/-CoO(011), are commercially not suitable due to their high metal content. Ternary hydrides, such as Co_3Mo_3N, Fe_3Mo_3N, are two-to-three orders of magnitude more expensive than iron-based catalysts, yet still cheaper than ruthenium-based catalysts. Innovative materials, such as electrides and exotic hydrides ($[Li_4FeH_6]^-$), are currently prepared only on a lab-scale. Promoters usually do not add substantial financial burdens, generally ranging from negligible (Al_2O_3, K_2O, KOH, MgO, CaO) to very inexpensive at 25–50 US dollars per kg (Zr, Ni, Co, Mo) up to moderately inexpensive with a couple hundred dollars per kg (BaO, Nb_2O_5) [105]. Among those, rhenium is a notable exception with a cost

Table 3
Characteristics of recently developed novel NH_3 catalysts.

Catalyst full composition	Temperature (°C)	Pressure (MPa)	Space velocity	NH_3 production rate	Ref.
5 % Ru on LaCoSi electrides	400	0.1	18,000 mL g^{-1} h^{-1}	2.88 mmol g^{-1} h^{-1}	[115]
5 % Ru on LaFeSi electrides				5.45 mmol g^{-1} h^{-1}	
5 % Ru on LaMnSi electrides				5.78 mmol g^{-1} h^{-1}	
Ru-$BaAl_2O_{4-y}e^-_y$/graphite	300–400	0.1	36,000 mL g^{-1} h^{-1}	0.4–3.7 mmol g^{-1} h^{-1}	[116]
$KH_{0.19}C_{24}$	240–400	1	36,000 mL g^{-1} h^{-1}	3.9 mmol g^{-1} h^{-1}	[110]
LaRuSi(001)	400	0.1	60 mL min^{-1}	1.7 mmol g^{-1} h^{-1}	[117]
CaRuSi(001)				0.053 mmol g^{-1} h^{-1}	
Micrometer-size Ru				0.02 mmol g^{-1} h^{-1}	
1.9 % Ru on ZrH_2/Ba	400	1	60,000 mL g^{-1} h^{-1}	27.5 mmol g^{-1} h^{-1}	[118]
1.9 % Ru on ZrH_2	400	1	60,000 mL g^{-1} h^{-1}	8.98 mmol g^{-1} h^{-1}	
1.9 % Ru on ZrN				2.61 mmol g^{-1} h^{-1}	
1.9 % Ru on ZrO_2				5.44 mmol g^{-1} h^{-1}	
1.5 % Ru on CeO_2	400	1	72,000 mL g^{-1} h^{-1}	1395 mmol g^{-1} h^{-1}	[119]
16 wt % Ce-Ru/HZ/CeO_2	400	1	–	24.6 mmol g^{-1} h^{-1}	[120]
4.5 % Ru on LaN/C_{60}	400	1	60,000 mL g^{-1} h^{-1}	34.7 mmol g^{-1} h^{-1}	[121]
Ru/3TiCN/ZrH_2	400	1–3	60,000 mL g^{-1} h^{-1}	25.6–35.6 mmol g^{-1} h^{-1}	[122]
Mo_2C with 0.1 wt%Co	400	1	36,000 mL g^{-1} h^{-1}	6.29 mmol g^{-1} h^{-1}	[123]
Fe/$BaTiO_{3-x}N_y$	400	0.9	–	8.8 mmol g^{-1} h^{-1}	[124]
Co–$BaCeO_3$	400	5	18,000 mL g^{-1} h^{-1}	14.94 mmol g^{-1} h^{-1}	[125]
AMn[RuH_m] (AM = Li, Na, K, Ca, or Ba) with MgO	300	0.1	60,000 mL g^{-1} h^{-1}	1–15 mmol g^{-1} h^{-1}	[126]
Fe/K(3)/MgO	350	1–3	36,000/72,000 mL g^{-1} h^{-1}	17.5–29.6 mmol g^{-1} h^{-1}	[111]
Ru-O-Ce	330–400	1	600 mL g^{-1} min^{-1}	4.1–6.7 mmol g^{-1} h^{-1}	[127]
FeN4©G-K with graphene lattice	150–190	0.1	30,000 mL g^{-1} h^{-1}	1.1–10.3 μmol g^{-1} h^{-1}	[108]
Co//$BaAl_2O_{4-x}$Hy Electrides	340	0.9	36,000 mL g^{-1} h^{-1}	500 mmol·g_{Co}^{-1} h^{-1}	[128]
Co/SrNH	400	0.9	–	1686.7 mmol·g_{Co}^{-1} h^{-1}	[129]
Ru/$La_2Ce_2O_7$/BaCsKLi	400	1	90 mL min^{-1}	6.6–35.9 mmol g^{-1} h^{-1}	[130]
Ru/LaScSi	400	1	60 mL min^{-1}	1.37 mmol g^{-1} h^{-1}	[131]
Ru/CeTiGe	400	1	60 mL min^{-1}	0.75 mmol g^{-1} h^{-1}	
Ba–Ru/GC	400	1	60,000 mL g^{-1} h^{-1}	18.7 mmol g^{-1} h^{-1}	[132]
1 wt%Cs–5wt%Ru/CeO_2	400	1–5	27,000 mL g^{-1} h^{-1}	43–73 mmol g^{-1} h^{-1}	[133]
Co(10 wt %)/$SrCN_2$/Al_2O_3	300	0.9	36,000 mL g^{-1} h^{-1}	4.43 mmol g^{-1} h^{-1}	[112]
Ru/10SiO_2/CeO_2	340–400	0.1	18,000–36,000 mL g^{-1} h^{-1}	3.3–5.5 mmol g^{-1} h^{-1}	[134]
Co/Ln_2O_3	420–470	6.3/9.0	–	0.05–0.8 g/g/h	[135]
Graphene oxide (rGO)/K	190–230	0.1	–	0.1–2.1 μmol g^{-1} h^{-1}	[136]
Ru-BaO/MgO/$MgAlO_x$	405	5	18,000 mL g^{-1} h^{-1}	2.93–37.08 mmol g^{-1} h^{-1}	[137]
Fe/Co-CeO_2	400	1	36,000 mL g^{-1} h^{-1}	1.3–2.93 mmol g^{-1} h^{-1}	[138]
Ru ACCs (2 wt% Ru)/Ba/Ce	400	1	60,000 mL g^{-1} h^{-1}	56.2 mmol g^{-1} h^{-1}	[139]
Ru nanoparticles/Pr_6O_{11}	400	0.1	72,000 mL g^{-1} h^{-1}	6.45 mmol g^{-1} h^{-1}	[140]
Nano-Ru/MgO	400	0.2	60,000 mL g^{-1} h^{-1}	21.7 mmol g^{-1} h^{-1}	[141]
Fe/Ba/MgO	350	1	72,000 mL g^{-1} h^{-1}	13.8 mmol g^{-1} h^{-1}	[142]
Fe–N–C on porphyrinic MOF	300	0.1	30,000 mL g^{-1} h^{-1}	0.56 mmol g^{-1} h^{-1}	[143]
$(H_3O)_2[(Mo_6Cl_8)Cl_6]\cdot 6H_2O$/HY-zeolite	400	1	18,000 mL g^{-1} h^{-1}	20.5 mmol g_{Mo}^{-1} h^{-1}	[144]
Re/Mo_2CTx	400	1	36,000 mL g^{-1} h^{-1}	22.4 mmol g^{-1} h^{-1}	[109]
Ni/Mo_2CTx	400	1	36,000 mL g^{-1} h^{-1}	21.5 mmol g^{-1} h^{-1}	
Ru/$Cs_{0.68}Ti_{1.83}O_4$	500	5	–	0.28 mmol g^{-1} h^{-1}	[145]
Ru/CeTX/MgO (T = Ti, Sc; X = Ge, Si)	300–400	0.1-0.3	–	0.6–4.39 mmol g^{-1} h^{-1}	[146]
$Ba_3SiO_{5-x}N_yH_z$	300	0.9	–	40.1 mmol g^{-1} h^{-1}	[147]

of ~2500 dollars per kilogram, limiting its use. A well-known drawback of iron is the required harsh reaction parameters (150–300 bar, 400–500 °C). Ru-based catalysts operate at milder conditions (10–100 bar, 300–450 °C) and exhibit higher yields, but this is eclipsed by the higher cost of catalytic materials.

Marketability is a broader aspect of commercialization, taking all market conditions into account, such as global demand for ammonia and its outlook. As of 2025, approximately 200 Mt of NH_3 is produced annually, projected to increase three-to four-fold by 2050 under net-zero emissions scenario [106]. For a catalyst with a space-time yield of ~1 g_{NH3} $cm_{cat.}^{-3}$ h^{-1} with a density of 1 g cm^{-3}, roughly 50–60 kt of catalyst will be required by 2050. Supply chains for novel materials of such capacity currently do not exist, while the annual ruthenium production is about 30–50 t annually, far behind the projected requirements. Non-noble metal catalysts, such as iron, cobalt and nickel, will therefore remain the bedrock of ammonia synthesis for a foreseeable future.

Operating conditions. Naively, operation at low temperature and low pressure would be desired to decrease energy expenditure for the operation of the reactor vessel itself. However, these might effectuate low ammonia concentration at the outlet, which makes its separation and purification in the second heat exchanger and subsequent recompression more energy intensive. Conventional Haber-Bosch process operates viably with a single-pass feed conversion of 25 %, which yields a 14 % NH_3 concentration at the outlet. A typical GHSV of 10,000 h^{-1} therefore implies a space-time yield of 0.93 g_{NH3} cm_{cat}^{-3} h^{-1} or more [107].

Due to thermodynamic constraints, higher temperatures decrease the conversion at a constant pressure. A useful operating-temperature envelope at lower pressures is therefore exceedingly low (below 473 K at 0.1 MPa and below 593 K at 1 MPa), requiring very efficient catalysts to speed the reaction up. Most of the innovative catalyst materials (with the exception of FeN4©G-K/graphene [108]) were tested at 673 K and 0.1−1 MPa, which is outside the operating envelope and unsuitable for industrial applications unless their activity is brought down to lower temperatures or they are used at 5 MPa or more, the latter negating most of the economical savings in their operation.

Stability, durability and operability. Commercially viable ammonia plants have lifetimes of several decades and require highly stable catalysts, which retain their activity for a decade or more. This is a distinction of commercial catalysts, while novel materials are rarely tested for months prior to publication, let alone years. A notable exception is Re/Mo_2CT_x, which was tested for 1100 h (45 days) and exhibited minimal deactivation [109]. Other catalysts were tested for shorter periods of time, commonly for less than 100 h [110]. Most often, stability is only hinted at qualitatively, not going beyond “steady initial rate […] for at least 100 h” [111].

Furthermore, the catalysts should be durable, *i.e.* tolerate various contaminants including oxygen and moisture, and exposure to the atmosphere. Their operability refers to their ability to withstand rather frequent powering down and restarting of the reactor for operational reasons without noticeable effects on activity. These aspects are hardly ever assessed during catalyst-discovery and lab tests with very few exceptions, such as air-durable Co/$SrCN_2$ [112]. Industrial-grade validation (>1000 h, contaminant tolerance, cycling robustness) remains an exception rather than the rule.

Formability. In large-scale operations, powder catalysts are not desired since they cause pipe clogging and can even damage delicate equipment, such as sensors [113]. Instead, stable shapes such as pellets, tablets or rings, are preferred. Formability of the catalysts for technical use is an important aspect, which is wholly overlooked when reporting novel catalyst formulations. This is arguably the largest gap between lab-scale catalyst discovery and industrial applicability as none of the recent novel catalysts (as shown in Table 3) report formability considerations.

Nevertheless, several novel catalysts have shown promising performance near ambient conditions, but their production remains limited to lab-scale and upscaling has not been proved feasible yet [114]. Several reviews in the literature report on the development of novel catalysts for thermochemical NH_3 synthesis [7,40], summarizing studies up to the time of publication. A non-exhaustive list of novel catalysts developed to date is provided in Table 3.

3.2. Reaction mechanisms

3.2.1. Dissociative pathway

Regardless of reaction mechanisms, there must be the N≡N cleavage at one step. As this is the rate determining step in most instances, great effort has been put into understanding this step. Theoretical studies using the Sabatier principle and Brønsted-Evans-Polanyi (BEP) relations have shown that Fe, Ru and the CoMo intermetallic lie near the maximum attainable turnover frequencies (TOF) without breaking the scaling relations [148]. These first- and second-generation catalysts follow the dissociative mechanism, as shown in Fig. 4.

Physisorption of N_2 or H_2 and its respective dissociation are often grouped together into a dissociative adsorption, assuming that physisorption is weak. Invariably, N_2 dissociation is the rate-determining step. It is initiated by the injection of electrons in the antibonding orbital of N_2, weakening the bond. These electrons stem from the transition metal itself or from the electronegative support material (such as electrides or hydrides) [128]. On second-generation catalysts, surface H_2 accumulation inhibits the reaction rate, similar to catalyst poisons. The effective removal of surface H_2 rapidly becomes the true reaction bottleneck. On other novel catalysts, the accumulation of surface N poses a significant challenge, which can be effectively mitigated using electrides or hydrides, which sequester surface N and break the scaling relations. A diagram example over Ru (0001) catalyst is displayed in Fig. 7.

3.2.2. Associative pathway

The associative pathway is less common and only contributes noticeably to the reaction on some metal nitrides and other seldom used materials. Examples include Ni/CeN [150] or rare earth perovskites oxy-nitride hydrides [151], where the following steps take place.

$$N_2 + * \rightarrow N_2* \quad \text{(I)}$$

$$H_2 + * \rightarrow H_2* \quad \text{(II)}$$

$$H_2* + * \rightarrow 2H* \quad \text{(III)}$$

$$N_2* + H* \rightarrow N_2H* + * \quad \text{(IV)}$$

$$N_2H* + H* \rightarrow N_2H_2* + * \quad \text{(V)}$$

$$N_2H_2* + H* \rightarrow N_2H_3* + * \quad \text{(VI)}$$

$$N_2H_3* + H* \rightarrow N_2H_4* + * \quad \text{(VII)}$$

$$N_2H_4* + * \rightarrow 2NH_2* \quad \text{(VIII)}$$

$$NH_2* + H* \rightarrow NH_3* + H* \quad \text{(IX)}$$

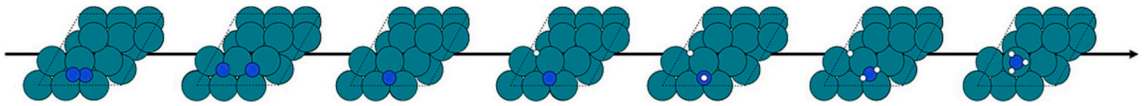

Fig. 7. Surface reaction steps during NH_3 synthesis over a Ru (0001) catalyst. Reproduced from Ref. [149] with permission from Elsevier.

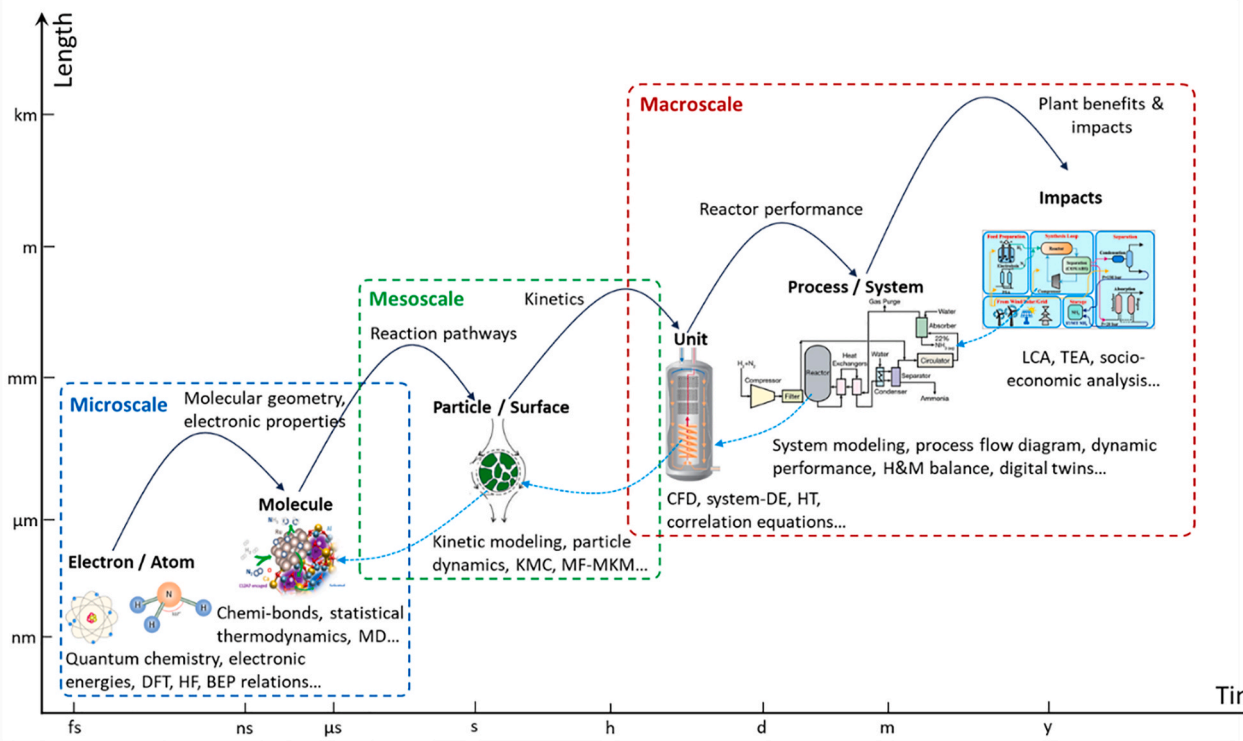

Fig. 8. Illustration and coupling of multiscale modeling study for NH_3 synthesis.

$$NH_3^* \rightarrow NH_3 + * \quad (X)$$

Electron transfer plays a crucial role in efficient NH_3 synthesis. As discussed earlier, this explains the performance gains of third-generation catalysts. In particular, metal-support interactions, surface electrides, hydride mobility and other electronic phenomena make them well suited for producing NH_3. In many cases, the barriers for N≡N dissociation are lowered sufficiently for the formation of NH_x species to become the rate determining step.

3.3. *Microscopic models for mechanism exploration*

Ammonia synthesis possesses a sufficiently small reaction network that it can be described with a broad array of methods, ranging from the atomistic to reactor-level descriptors. On the one hand, the largest conceivable intermediate in the reaction consists of seven atoms (NH_2NH_3) but realistically no larger than four-atom species are encountered, making the reaction suitable for first-principles modeling [152]. On the other hand, the complex thermodynamics with exothermic phenomenon, requiring low temperatures, which are in stark contrast with kinetic requirements, call for higher level modelling at the macroscale to understand the optimum reactor geometry and conditions [149]. In essence, the catalyst surface coverage is impacted by the chemical potential and sticking coefficients. The former is a function of intensive variables (pressure, temperature) and phenomena (composition, material and heat transport), while the latter is particularly influenced by surface rearrangements, segregation, deposition, subsurface compounds and potential phase changes.

Multiscale modelling, spanning from the atomic scale to the system level, is thus preferred to couple the different simulation models of NH_3 synthesis, as illustrated in Fig. 8. This approach encompasses a broad temporal and spatial range, from femtoseconds to years and nanometers to kilometers. For mechanism exploration in this chapter, microscale and mesoscale models are focused. The macroscale modeling studies will be summarized in Chapter 4 (reactor scale) and Chapter 5 (system and impact level).

3.3.1. *Density functional theory calculations*

The density functional theory (DFT) is the most used *ab initio* method of describing the reaction at the electronic level. While it can be used to calculate the thermodynamic equilibria involved in the synthesis, costlier higher-level methods, such as CCSD(T) or GW, are better suited for this purpose. While several functionals used in DFT describe the net reaction with admirable accuracy, individual steps can be different as large as 100 kJ/mol even in the most popular functionals (PBE, RPBE, or B3LYP) [153]. Hence, precise CCSD(T) computations with large basis sets are used as benchmark when the size of the system allows it. Since introducing surfaces necessitates larger systems, heterogeneous catalysis has to resort to DFT and higher-level methods remain feasible only for equilibria calculations or, at best, single-point electronic calculations on pre-optimized structures.

Among all computational techniques, DFT is the most ubiquitous in NH_3 synthesis research [149]. In some capacity, DFT is included in a majority of novel papers, making a short review impractical. Instead, we focus on what can be achieved with it. In DFT simulations, different atomistic aspects of the process can be computed. Generally, they can be grouped into structure computations and mechanistic investigation. In the former, the catalyst itself is studied. DFT is used to predict the most stable catalyst facet, its surface termination, phase diagrams, *d*-band gap values, band structure, electrostatic potential, charge transfer, bond orders etc [154]. On the other hand, mechanistic investigations usually follow once the most reliable structure(s) is (are) pinpointed and focus on the adsorption of different species and the energetics of their interconversion [155]. In postprocessing, these data are converted into individual kinetic rate constants via the transition state theory (TST) or similar approaches, which serve as the input for various kinetic models (microkinetics, kinetic Monte Carlo, etc.) [156]. Often, quantitative values are less important than the qualitative picture and overall trends. In these instances, the more likely reaction mechanism or the relative performance of different catalysts is sought after.

3.3.2. Molecular dynamics simulations

Molecular dynamics (MD) simulations are well suited for studying kinetic phenomena at the mesoscale, such as mass transfer through interfaces [157], adsorption [158]. Depending on the aspect investigated, very different types of MD can be used. In general, conventional MD simulations use classical force fields, where the interaction between particles is some combination of electrostatics and van der Waals interaction, which is computationally fast. Since such simulations cannot capture bond formation and cleavage, they are limited to dynamic properties in (quasi-) equilibrium conditions, such as clusters of liquid NH_3 [159] or NH_3 adsorption and diffusion [160].

When reactions are of interest, either reactive force fields (ReaxFF) must be used [161] or we resort to *ab initio* MD (AIMD), such as Born–Oppenheimer molecular dynamics (BOMD) or Car–Parrinello molecular dynamics (CPMD) [162]. Various ReaxFFs can describe larger molecular structures, such as 10-nm ruthenium nanoparticles for NH_3 synthesis [163].

on the contrary, AIMD is useful when simulating smaller systems where precise quantum-chemical behaviour must be known, such as the stability of ruthenium nanoparticles in molten salts [164], ruthenium clusters during the reaction [165] or overall motif stability on a particular catalyst [166]. This supporting role of AIMD is especially common, as it is used to ascertain the stability of some structure used in other types of modelling. More extreme environments, such as plasma-based NH_3 synthesis can also be described [158].

Another case study of dynamics provides a more detailed insight than a simple search for stationary points at the potential energy surface (PES) [167]. Specifically, it enables the study of temperature dependence of the individual reaction steps and the evolution of the catalyst surface with respect to different active sites. In dynamics calculations, collective variables can be used to obtain ensemble quantities with great precision, such as the free energy. More importantly, it can describe the sticking coefficients and the local chemical potential in a way that is unattainable otherwise [167]. Being the rate determining step, the cleavage of N≡N bond is usually the focus of these studies on iron-based [168], ruthenium and third-generation catalysts. Catalyst poisoning is an inherent surface phenomenon, which was studied with surface molecular dynamics. On Fe(111), N_2 atoms stabilize surface structures, which are responsible for the formation of vacancies and thus auto-regulate the poisoning effect [169].

3.3.3. Microkinetic models

Microkinetic modelling is the classical method to describe catalytic systems, which has been around since the dawn of chemical engineering. Starting from simple power laws, microkinetic modelling has also benefited from the advances in available computation power to the point of being able to solve complex systems of several differential equations. An important advantage of microkinetic modelling is its versatility. Depending on the available computational power and known data points, the models can vary greatly in their complexity.

In a microkinetic model, the reaction pathway is postulated to consist of several reaction steps, which have individual reaction rates. They are proportional to the reaction rate constant and the activity (concentration, surface coverage etc.) of the participating species and must comply with the principle of microscopic reversibility [170]. A mass balance for each participating species, surface or gaseous, is written and a set of differential equations is solved based on the geometry of the system in question.

The provenience of the data used, however, lends itself to grouping the models according to their purpose. When experimental data is to be reproduced for the sake of tweaking the reaction conditions and optimizing performance, little thought is given to the microscopic background of the microkinetic parameters ($A_{i,\mathrm{for}}$, $A_{i,\mathrm{rev}}$, $E_{i,\mathrm{for}}$, $E_{i,\mathrm{rev}}$), and they are instead fitted to experimental data [37]. Similarly, structure-based and conditions-related parameters are obtained (pressures, flow rates, active site density, sticking coefficients, catalyst weight, space time) empirically. Such models are particularly useful when elaborate phenomena are to be described, such as the kinetics under non-steady conditions and cycling behaviour [171]. On the other hand, when fundamental understanding is sought after, modern microkinetic models make use of *ab initio* input (surface site density, reaction mechanisms, rate constants) [172]. Before that, surface science results were used to feed the microkinetic models with.

Early microkinetic models have already used the conventional associative and dissociative mechanisms. Kinetic models with a minimum number of assumptions, which neglected adsorbate-adsorbate interactions and presume an energetically homogeneous surface, were already able to describe NH_3 synthesis rates in reactors at industrial conditions. Already in 1980s, rudimentary quantum chemical calculations [173,174] yielded useful information that was incorporated into microkinetic models. Based on kinetic models alone, it was possible to identify the dissociation of N_2 as the slow step in the mechanism [175] and study its adsorption [176]. Most importantly, microkinetic models allowed for the extrapolation from surface science studies at lower pressures and surface coverages to industrial conditions [177]. Before the broad availability of quantum chemical methods, kinetic models were already able to qualitatively describe the role of promoters, such as potassium [155]. Countless other studies on iron-based catalysts followed [178].

Modern microkinetic models follow the same set of elementary steps regardless of the catalyst, being valid for Ru-based [179], Co-Mo [180] or other catalysts [181]. Recently, the models have gained additional degrees of freedom, such as accounting for various types of active sites (multisite MKM) [182], lateral interactions [183] and kinetics on nanoparticles.

3.3.4. Kinetic Monte Carlo models

Kinetic Monte Carlo (kMC) models offer more detailed information into the temporal evolution of the catalyst surface than mean-field microkinetic models (MF-MKM). Since kMC describes the reaction (adsorption, desorption, diffusion, interconversion) on an arbitrarily granular level, the lower limit being the atomistic active site but more coarse-grained approaches are also possible, surface reconstruction, adsorbate-adsorbate lateral interactions and spectator species effects can be observed. In essence, kMC incorporates spatial inhomogeneities and correlations. The major drawback of the kMC approach is the computational cost. While the first-principles methods for computing the potential energy surface (PES) for individual steps do not differ between kMC and MF-MKM, the kMC simulation itself is computationally much costlier. This is, however, offset by its insensitivity to the issue of stiffness or convergence problems [156].

Even when using purely theoretically derived data, such as DFT energetics on Fe(111) and Fe(211)R, kMC can approximate the experimentally observed TOF to within the factor of 1.8, which correspond to a 0.04 eV change of the apparent activation energy [184,185]. Such models are often extended to describe similar surfaces, which are decorated or doped [186–188] and can ultimately serve to perform computational catalyst screening [189] or nanoparticle control [190].

Despite its versatility, kMC is rather seldomly used for describing thermocatalytic NH_3 synthesis. A notable example is the seminal first-principles calculation of NH_3 synthesis on Ru [191]. However, kMC is nowadays prevalent in the description of the electrocatalytic N_2 reduction reaction (NRR). In thermocatalysis, NH_3 decomposition is more often studied with kMC.

3.3.5. Machine learning

Machine learning (ML) is a nascent method for learning from vast quantities of data and generalization of the non-obvious underlying trends. Hence, ML is not a method tailored to a specific level of process description but rather a tool for rationalizing very different sets of data. The biggest obstacle to using ML successfully is a relative lack of abundant high-quality data. ML excels when the number of data points

increases, at least in low four-digit numbers of data points and preferably even more. Unfortunately, very few single sources satisfy these requirements, while broad acquisition produces datasets of questionable quality due to the incomparability of the data acquisition techniques. ML has been used at various levels for describing ammonia synthesis process and its variants or successors but no attempts at harnessing ML to describe multiple levels concomitantly have been successful. Instead, catalyst discovery or reactor optimization are mostly tackled with ML.

An example of a problem with a natively large configurational space is high-entropy alloys, which can only realistically be assessed with ML [192] applied on existing first-principles data. Alternatively, ML is used to study a specific parameter, such as electric field-dipole effects, with correlations to reaction energies identified through ML analysis [193]. Furthermore, it can be used to predict new reaction pathways [194]. ML can exploit experimental data and provide optimum catalyst formulations, for instance different ruthenium-based catalysts [195], supports thereof [196] or lower ruthenium loading [197]. At higher levels, models of entire reactors can be modified and optimized to solve the maximum yield problem of NH_3 synthesis [198], improve the energy efficiency [199] or regulate individual parameters, such as reactor hotspot temperature [200]. This approach is not limited to thermocatalytic processes but can be applied to plasma catalysis and so forth [201].

In summary, despite their differences in scale and methodology, the microscopic modeling approaches for the ammonia synthesis follow a common framework: starting from the accurate description of elementary steps (via DFT and *ab initio* methods), progressing through the dynamic evaluation of kinetic phenomena (using MD and AIMD), and culminating in the construction of kinetic models (microkinetic or kMC) to bridge molecular insights with macroscale observables. These models are increasingly supported by data-driven tools such as machine learning, which aid in parameter optimization and trend discovery across high-dimensional spaces. A recurring theme is the reliance on high-quality, first-principles-derived data as the foundation for all subsequent modeling layers. Furthermore, the integration of multiscale models, linking electronic structure, surface dynamics, and reactor-level kinetics, is emerging as a key strategy to achieve predictive capability and mechanistic clarity. The readers are referred to Ref. [149] for a list of recent studies implementing various micro-to mesoscale modeling approaches for NH_3 synthesis. Collectively, these approaches not only deepen the understanding of NH_3 synthesis but also establish generalizable workflows applicable to other catalytic systems.

4. Emerging ammonia separation and enhanced reactor

Apart from catalyst development, NH_3 separation other than by traditional condensation is a critical step for achieving NH_3 production beyond conventional Haber-Bosch process. Solid sorption and membrane separation are the two main techniques to separate NH_3 from mildly thermocatalytic synthesis units, demonstrating potential for reactor enhancement or intensification [25]. This chapter offers a comprehensive review of the progress in solid sorption and membrane separation techniques for isolating NH_3 from unreacted H_2 and N_2. The chapter covers material development, intensified reactor prototypes, and unit-scale modeling studies, systematically summarizing the advances of implementing solid sorption and membrane separation technologies in moderate thermocatalytic NH_3 synthesis.

4.1. Separation material development

Development of advanced materials with good separation ability and reactor compatibility is the cornerstone of the implementation of NH_3 solid sorption and membrane separation technologies [51]. The state-of-the-art material developments in terms of solid sorbents and membranes are elaborated in subsequent sections.

4.1.1. Solid sorbents

Solid sorbents for NH_3 uptake can be divided into 2 categories: adsorbents, where sorption occurs primarily at the surface, and absorbents, where sorption takes place in the bulk of the solid [202]. Within surface sorption, physisorption is driven by weak van der Waals forces, typically filling NH_3 molecules into the pores of the adsorbent, while chemisorption involves stronger interactions through the formation of chemical bonds with reactive surface sites [202]. Accordingly, the commonly used adsorbents always have porous or microporous structures, such as carbon-based materials, zeolites, metal organic frameworks (MOFs) and

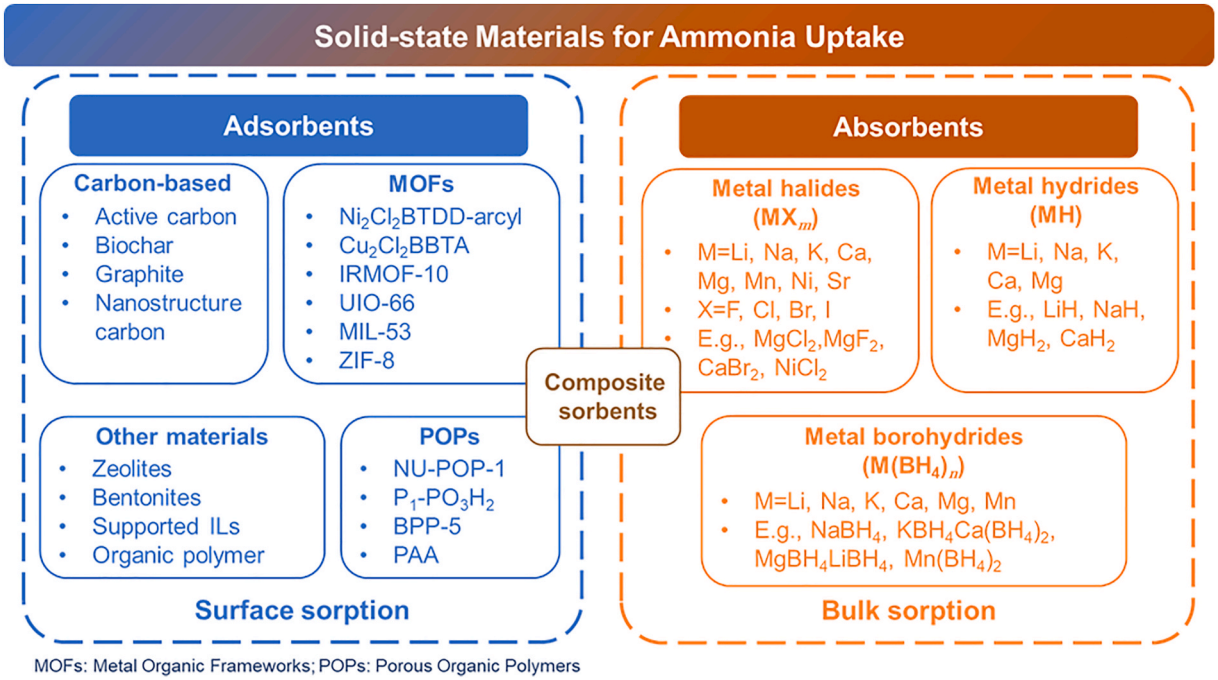

Fig. 9. Categories of commonly used solid-state materials for NH_3 sorption.

porous organic polymers (POPs) [51], which are favored by reactive sites. In contrast, absorption involves bulk uptake, where NH_3 molecules penetrate the solid and form more stable coordination complexes with metal centers [203]. The underlying principle is the formation of ammine complexes that store NH_3 in a stoichiometric manner [53]. Representative bulk absorbents include metal halides, metal hydrides, and metal borohydrides, which take up NH_3 through coordination or reactive absorption [204]. In general, the position of sorption (surface vs. bulk) and the strength of interaction (physisorption vs. chemisorption) are distinguished through sorption–desorption isotherms, enthalpy of sorption measurements, and reversibility tests under consistent operating conditions. For example, porous carbons and MOFs mainly operate via surface physisorption, while metal halides and borohydrides take up NH_3 into the bulk via chemisorptive absorption. Additionally, some composite sorbents, which combine adsorbent and absorbent, have also been developed. The solid materials mainly used for NH_3 sorption are outlined in Fig. 9.

Adsorbents. Some carbon-based materials such as active carbon and biochar have garnered significant attention for NH_3 adsorption due to their porous structure, high surface area and low cost. However, due to the lack of sufficient surface acidity of common active carbon, the NH_3 uptake is only driven by the weak H bonding or Lewis acid-based interactions, resulting in low NH_3 adsorption capability [205]. The adsorption typically follows the Type I (Langmuir-like) physisorption isotherms, favored by high pressure and low temperature [206]. The adsorption data can often be fitted using Langmuir or BET isotherm models, where the former assumes monolayer coverage and the latter accounts for multilayer adsorption. The NH_3 uptake capacity of normal active carbon reported in the range from 0.11 to 1.18 mmol/g at 23 °C and atmosphere pressure from a flow of 300 mL min^{-1} of air containing 1000 ppm of NH_3 [207,208]. Several modification approaches are normally used to improve the NH_3 uptake capacity of active carbon. For example, Zheng et al. have used nitric acid to oxidize the activated carbon fiber at room temperature, forming high-capacity adsorbent with up to 2.94 mmol/g NH_3 uptake ability at room temperature [209]. Zhang et al. reported a biochar adsorbent modified by cupric silicate that can adsorb 6.36 mmol/g at room temperature and pressure [210]. Another modification method is to improve the porous structure of the carbon materials, since its limited NH_3 capture ability is also partially due to its larger pore size (1–2 nm in average) compared to the NH_3 molecule size (0.3 nm) [205]. Qajar et al. have synthesized nano-porous carbons with nitric acid treatment, reducing the pore size to a minimum value of 0.5 nm. The highest tested NH_3 adsorption capacity is approximate 10 mmol/g at 25 °C and 1 bar [211]. The reported carbon-based adsorbents with different modifications are capable to uptake NH_3 in the range from tens μmol to several mmol per gram adsorbent, mostly at atmospheric pressure and room temperature and dominated by nanocarbons.

MOFs formed by metal-ligand interaction with high porosity and tunable pore size and structures have also been deployed for NH_3 adsorption [212]. The pore size of MOFs can be tuned to the molecule level for a targeted gas (0.3 nm for NH_3), largely enhancing its adsorption capability through the capillary condensation effect [213]. To date, many MOFs have been synthesized using different choices of metals and ligands for NH_3 removal. For instance, Jasuja et al. reported six variations of functional UiO-66 (Zr-based MOF) for NH_3 adsorption from air, exhibiting up to 5.69 mmol/g capacity under dry conditions [214]. Rieth et al. tested Mn-, Co- and Ni-based MOFs for NH_3 reversible uptake under standard temperature and pressure, which found that the capacities can reach 15.44, 11.98, and 12.00 mmol/g, respectively [215]. Moreover, a series of flexible MOFs with the form of $M(NA)_2$ (M = Zn, Co, Cu, Cd; NA = nicotinate) have been synthesized in Ref. [216], showing $Co(NA)_2$ is the best candidate with the highest adsorption ability of 17.47 mmol/g at room temperature and pressure. Notably, these materials can be effectively regenerated under vacuum and heating at 150 °C for 70 min, without any loss in performance. In general, MOFs' sorption ability is favored by increasing pressure. The sorption isotherm behavior of MOFs typically resembles Type I or IV, depending on their pore architecture. In mesoporous MOFs, capillary condensation at elevated pressures results in steep adsorption branches, thereby enhancing NH_3 uptake beyond monolayer coverage. For example, Lu et al. reported that at 298 K and pressures of 0.001/1.0 bar, the NH_3 uptake capacities were 4.8/12.8, 1.4/10.0, 0.47/9.0, and 0.07/3.0 mmol/g for MIL-160, CAU-10-H, Al-FUM, and MIL-53(Al), respectively [217]. The performances of NH_3 uptake for different types of MOFs from under low pressure (<2 mbar), normal pressure (1–2 bar) and high pressure (>5 bar) are reviewed in Ref. [212]. As novel material, MOFs exhibit exciting opportunities for high-quality NH_3 adsorption, particularly due to its pore size tunability. However, MOFs cannot withstand very high pressures (e.g., 30 MPa for UiO-66), as this may damage their structure and reduce porosity. Similarly, high temperatures can compromise their structural integrity, further limiting their applicability. The practical implementation of MOFs is significantly constrained by their limited thermal and moisture stability, as well as their high cost. Consequently, most relevant studies on MOFs remain confined to laboratory-scale investigations [51,218].

POPs formed by covalent bonds are the other groups of novel adsorptive material for NH_3 adsorption, featuring large surface area, tunable porosity and functionality. Barin et al. investigated the performance of series POPs with Brønsted acidic groups and two kinds of network structures, achieving NH_3 uptake capacity as high as 2 mmol/g under equilibrium pressure of 0.05 mbar [219]. A group of diamondoid POPs functionalized with carboxylic acids has been synthesized for low and normal pressure NH_3 adsorption. Among them, the best developed BPP-5, which is regulated <0.6 nm pore size, can capture 17.7 mmol/g at atmosphere pressure. For the larger pore size framework BPP-7, the NH_3 saturation capacity is limited to 3.15 mmol/g under low pressure and room temperature. Compared to MOF material, POP normally performs better in terms of stability due to its different synthesis method. The metal ions of POP are attached to its major framework instead of being connected in the framework like MOFs. Therefore, the interaction of adsorbed NH_3 with metal ions has no impact on POPs' major framework, avoiding the collapse problem after trapping NH_3 [220]. The representative POPs from recent studies for NH_3 uptake have been listed in the review paper [51].

Zeolites are also able to adsorb NH_3 due to their high porosity, abundant acidic sites and small pore size (comparable to NH_3 molecule level) [221]. Lucero et al. demonstrated a selective NH_3 adsorption process using a synthesized zeolite NaP, displaying high NH_3 sorption capacity of 8.47 mmol/g from N_2 and H_2 mixture [222]. Helminen et al. proved that the Langmuir-Freundlich isotherm model provides the most accurate fit for the two kinds of zeolite (13X and 4A), achieving 3.0–3.5 mmol/g capacity over the temperature range of 298–393 K [223]. Similar to zeolite, the other natural mineral bentonite is also capable of being used for NH_3 adsorption. For example, Cheng et al. proposed to use a modified bentonite for NH_3 removal from domestic wastewater, displaying 0.34 mmol/g saturated sorption capacity at low temperature [224]. Recently, Wang et al. prepared novel nanosheets with multi-layer structure from bulk BiI_3 powder, exhibiting up to 22.6 mmol/g NH_3 uptake at ambient conditions, which is approaching the maximum recorded value for NH_3 reversible adsorption [225]. The efforts on new material development for NH_3 adsorption are ongoing.

Absorbents. The most promising NH_3 absorbent is metal halide material due to its notable absorption capacity. In principle, the sorption of NH_3 is through the bulk interactions of NH_3 and absorbent forming ammine complexes. The general reaction of NH_3 absorption in metal halides can be written as follows [53].

$$MX_m + nNH_3 \rightleftarrows M(NH_3)_nX_m \quad (R2)$$

Where M denotes metal, for instance Mn, Ni, Mo; X denotes a halide such as F, Cl, I, Br. Liu et al. summarized the thermodynamic properties of

Table 4
Summary table of the reported sorption materials.

Sorbent Type	Pros.	Cons.
Carbon Based	- High surface area and porosity - Cost-effectiveness - Effective at room temperature and pressure	- Low NH_3 uptake capacity (1 mmol/g to over 10 mg/g) - Limited surface acidity
MOFs	- High tunability of pore size - High adsorption capacity (over 24 mmol/g) at lower temperature	- Thermal and moisture instability - High production costs - Limited applicability under high temperature and pressure
POPs	- Large surface area - Good stability under different conditions	- Limited commercial availability - Potentially slightly lower capacity than MOFs
Metal Halides	- High absorption capacity in wide temperature range (room temperature to 200 °C) - Effective chemisorption with reversibility - Simple regeneration process - Low cost	- Limited by stability in moisture - Potentially form HCl leading to corrosion - Structural instability caused by volume swings
Metal Borohydride	- High NH_3 uptake capability - Effective under various conditions	- Less stability - Limited reversibility - Complexity in handling and regeneration
Composite Sorbents	- Very high sorption capacity (over 50 mmol/g) - Enhanced performance characteristics - Improved mass and heat transfer	- Complexity in synthesis - Potentially higher costs

alkaline earth halides (such as $MgCl_2$, $CaCl_2$ and $CaBr_2$) in NH_3 separation procedure [226]. The sorption capacities and equilibrium pressures for a temperature swing of 298–473 K and pressure swing of 0–80 kPa, are also listed. The order of calculated equilibrium pressure at 298 K for the pure alkaline earth metal chlorides is $BaCl_2$ (187 kPa) > $SrCl_2$ (15.2 kPa) > $CaCl_2$ (1.36×10^{-3} kPa) > $MgCl_2$ (6.45×10^{-7} kPa). Moreover, among the same alkaline earth metals, the affinity to NH_3 of bromide is higher than that of chloride, whereas chlorides are more commonly used due to their better stability. The formation process of ammine complexes namely $Mg(NH_3)_6Cl_2$, $Mg(NH_3)_3Cl_2$ and $Mg(NH_3)Cl_2$ is investigated in Ref. [227], revealing the temperature impacts to the chemisorption process. In addition, the NH_3 desorption behaviors of metal (Mg, Mn, Ca and Ni) chlorides are studied in Ref. [228]. The mechanisms and impacts of heat transfer for the reversible absorption are elucidated, indicating the fast desorption kinetics for all steps. A recent review study on metal halides using as NH_3 absorbent has been reported in Ref. [229], listing the advanced material developments and ongoing mechanism investigations. $MgCl_2$ based sorbents are performed as the best candidate in terms of sorption capacity and rate. However, $MgCl_2$ is inherently hygroscopic, making the sorbent susceptible to moisture absorption when exposed to air [229]. The reaction with moisture generates hydrogen chloride (HCl), which poses a significant risk of corrosion to the reactor, thereby limiting its feasibility for practical applications.

Similar to metal halides, the general reaction of NH_3 uptake by solid-state metal borohydrides can be written as follows [230,231].

$$M(BH_4)_m + nNH_3 \rightleftarrows M(NH_3)_n(BH_4)_m \quad (R3)$$

The normally used metal borohydride based NH_3 absorbents are: $LiBH_4$, $NaBH_4$, KBH_4, $Mg(BH_4)_2$ and $Ca(BH_4)_2$ from previous studies, and the number of absorbed NH_3 molecule n can be 1, 2, 3, 4, 5 and 6 [53,232]. For instance, the maximum amount of NH_3 uptake is recorded as 5 mol per mol sorbent ($Mg(BH_4)_2$ or $Ca(BH_4)_2$) at room temperature, as reported by Ref. [230]. The NH_3 uptake performances for various metal borohydrides at different temperature and pressure were evaluated, as presented in the dataset of U.S. National Institute of Standards and Technology [53]. The results indicate that the overall tendency of equilibrium pressure at plateau follows the order of $P_{eq}(Na(NH_3)_2BH_4)$ > $P_{eq}(Li(NH_3)_2BH_4)$ > $P_{eq}(Ca(NH_3)_2BH_4)$ > $P_{eq}(Mg(NH_3)_2BH_4)$.

Different from forming ammine complex like metal halides or metal borohydrides, NH_3 storage in metal hydrides follows the reversible reaction below [53]:

$$MH + NH_3 \rightleftarrows MNH_2 + H_2 \quad (R4)$$

It is an indirect way of absorbing NH_3 with the formation of H_2, which is only used under specific purpose and more applied to NH_3 cracking for H_2 generation [233]. For instance, Yamamoto et al. investigated a series of recyclable MH samples for H_2 generation by absorbing NH_3 under 0.5 MPa and 300 °C. The results confirm that that the reactivities of MH with NH_3 follow the metal's atomic number on the periodic table, i.e., Li < Na < K [234].

Composite sorbents. Recently, composite sorbents combining adsorbents and absorbents have been investigated for improving the performance of NH_3 sorption in terms of capacity, rate and mass and heat transfer [202]. Porous adsorbents such as graphite and active carbon are usually used in combination with bulk sorption materials such as metal halides for composite sorbent development [235]. For example, in Ref. [236] a composite sorbent comprising $CaCl_2$ and multi-walled carbon nanotubes was developed, demonstrating a significantly enhanced sorption capacity of 50.49 mmol/g. Wang et al. have developed and analyzed five composite sorbents of NH_4Cl, NaBr, $BaCl_2$, $CaCl_2$ and $SrCl_2$ with ENG-TSA as matrix for NH_3 storage under temperature below 100 °C [237]. The results show that NH_4Cl-based sorbent has the highest NH_3 storage capacity under low pressure, while $CaCl_2$-based sorbent excels for its reasonable working pressure and lower cost. The metric and principles for the development of composite sorbents are reviewed in Ref. [202], along with the characteristics of the existing composite sorbents. Pros and cons for different types of sorbent materials are compared in Table 4. Generally, adsorbents, such as carbon-based materials and MOFs, are better suited for applications under mild conditions (e.g., room temperature and atmospheric pressure), offering benefits like cost-effectiveness and ease of regeneration. In contrast, absorbents and composite sorbents are more appropriate for high-temperature and high-pressure environments, making them particularly promising for in-situ sorption applications coupled with ammonia synthesis process.

4.1.2. Membrane preparation

Gas separation via membrane is based on the different permeabilities of gas molecules through a thin membrane. Two key factors, namely NH_3 permeance and selectivity over N_2 and H_2, are the main concerns of the membrane material design and development for NH_3 separation. An ideal membrane can selectively permeate NH_3 into one side of the membrane while retaining the unreacted N_2 and H_2 in the other side for system recycling [25]. Typically, membrane separation selectivity arises from molecular size or specific chemical interactions [54], resulting in two kinds of membrane: porous membrane and dense membrane. For porous membranes, the separation utilizes the molecular size-sieving effect of the thin membrane structure. Unfortunately, the molecular size of NH_3 lies between the two other species (H_2 and N_2), thus largely limiting the separation capability based on the size exclusion [51]. Some efforts have been attempted recently, for example, William et al. have

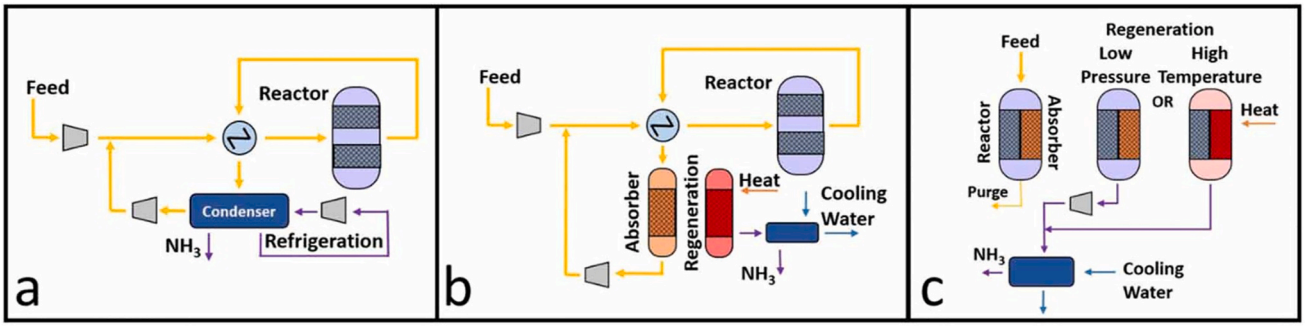

Fig. 10. Schematics of NH_3 synthesis processes using condensation (a), *ex situ* absorption (b), and *in situ* absorption separation (c). Reprinted from Ref. [246] with the permission from IOP Publishing.

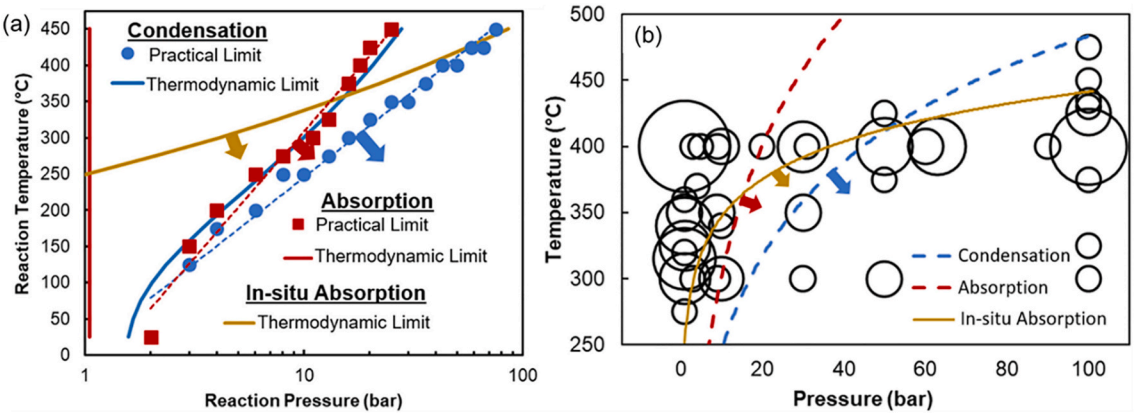

Fig. 11. Thermodynamic limits of NH_3 synthesis using different separation techniques (a), summary of synthesis conditions in previous studies relative to separation limitations (b), circle size indicates the number of studies at a particular system pressure and temperature. Reproduced from Ref. [247] with permission from Elsevier.

investigated NH_3-selective membranes using nanostructured sulfonated block copolymers at near ambient conditions. Membranes with polystyrene sulfonate domains of 7–23 nm were synthesized and tested, showing its NH_3 permeability is over 20.1 × 10^{-17} kmol m/(m^2 s Pa) (600 Barrers) at 25 °C and 2 bar with over 90 selectivity to a mixed gas feed containing NH_3 and N_2. The NH_3 permeance for a synthesized membrane with 500 nm thickness is thus 1200 gas permeance unit (GPU, 1 GPU = Barrer/μm (membrane thickness)). It also proves the block copolymer membranes exhibited high NH_3 selectivity, particularly under mixed gas conditions, compared to Nafion membranes, which lost selectivity due to swelling [238]. In practical application, a membrane must possess an NH_3 permeance over 100 GPU, as well as a selectivity of NH_3 towards hydrogen and nitrogen of no less than 10 [239]. Wei et al. have synthesized LTA type zeolitic imidazolate framework membranes (ZIF-21), successfully demonstrating the synthesis of continuous ZIF-21 membranes grown on alumina porous tubes [240]. The developed membranes exhibit a high NH_3 permeance of 1727 GPU, with 35 and 12 selectivities over N_2 and H_2, respectively. In Ref. [241], a set of high-performance NH_3-selective MFI nanosheet membranes have been prepared, exhibiting an NH_3/N_2 separation factor of 2236 GPU with NH_3 permeance of 1.1 × 10^{-6} mol m^{-2} s^{-1} Pa^{-1} at room temperature. At a higher temperature of 323 K, the separation factors are 191 GPU and 220 GPU at 3 and 7 bar, respectively. The results suggest that MFI membranes can potentially be used in separating NH_3 in NH_3 synthesis and utilization processes. In the two cases, the NH_3 separation is actually achieved mainly through the favored adsorption of NH_3 by ZIF-21 and MFI compared to that of N_2 and H_2.

For dense membranes, the gas permeation is mainly attributed to the

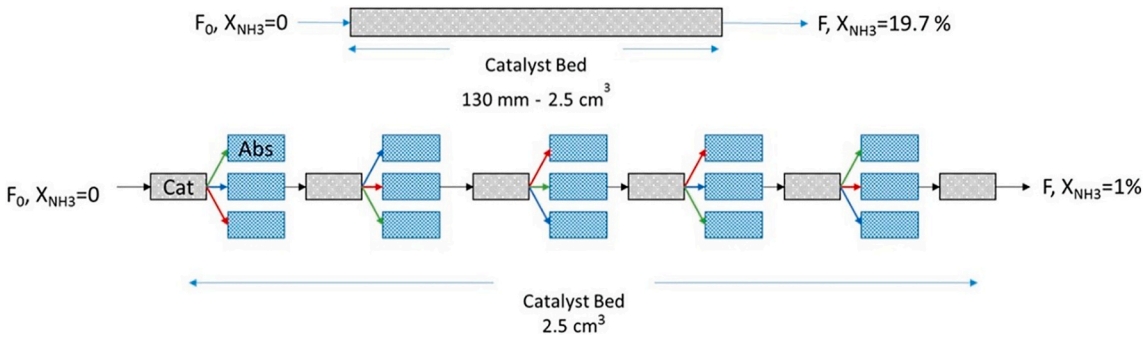

Fig. 12. Diagram of the conventional NH_3 synthesis reactor (top) and the conceptual reaction-absorption reactor (bottom). Reproduced from Ref. [248] with the permission from American Chemical Society.

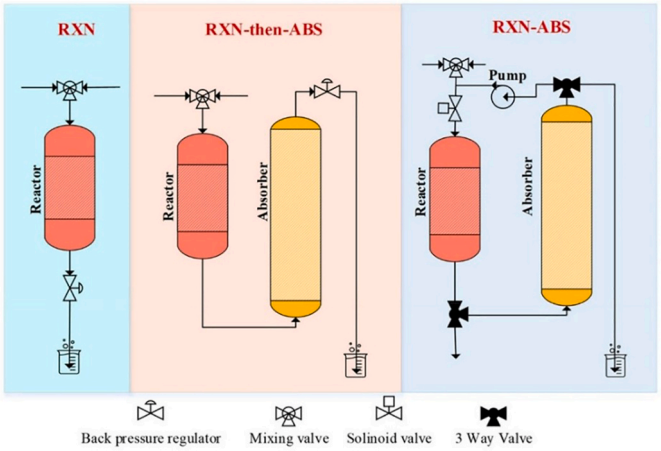

Fig. 13. Schemes of NH_3 synthesis process with and without absorption and recycling. Reproduced from Ref. [38] with the permission from American Chemical Society.

solution-diffusion mechanism, by which the permeance of the targeted gas is enhanced by the mass transport phenomenon [54]. In order to increase the selectivity of NH_3, active sites are introduced that selectively enable interaction with NH_3 into the matrix of dense membranes. For instance, Yang et al. integrated imidazolium-based protonated ionic liquids (ILs) into the Nexar membrane matrix, achieving an NH_3 permeability of 3565 Barrers, with ideal selectivities of 186 for NH_3/N_2 and 364 for NH_3/H_2 [242]. Moreover, immobilized NH_3 thiocyanate liquid membranes in porous nylon demonstrated an NH_3 permeance of 1900 GPU and an NH_3 selectivity of 8700 over N_2 at 23 °C and 268 kPa [25]. It is worth noting that most of the membranes developed work under 100 °C, which is not compatible with the NH_3 synthesis reactor normally used. To develop an NH_3 membrane that can work over 300 °C is a challenge and only inorganic membranes show the possibility due to their thermal stability [243]. Padinjarekutt et al. recently developed Na^+ -gated nanochannel membranes for efficient NH_3 separation from mixed gases containing H_2 and N_2 under high temperature and pressure. By optimizing synthesis parameters, such as seeding and gel aging, the membranes achieved NH_3/H_2 and NH_3/N_2 selectivities of 328 and 1106, respectively, at 200 °C and 21 bar [244]. The properties and working conditions (mostly under mild operation) for several membrane examples for separating NH_3 from H_2 and N_2 are summarized in Ref. [239]. More work needs to be done for the high-temperature tolerant membrane materials development, to enable the in-situ application of membranes for NH_3 synthesis.

4.2. Enhanced reactors

4.2.1. Sorption-enhanced reactors

The strategy of sorption-enhanced reactors is to use sorbents to separate the NH_3 produced instead of conventional condensation and thereby bringing the conversion rate near or even above the equilibrium limitation, intensifying the HB loop or reducing the severity of its operation conditions [42,245]. The sorption-enhanced reactors for NH_3 synthesis can be divided into two categories, i.e., ex-situ sorption reactor and in-situ sorption reactor. The former one always uses two reactors for loading catalyst and sorbent separately, and thus the NH_3 synthesis and absorption processes can work under different operating conditions, while the latter one normally loads catalyst and sorbent in a single vessel (layer by layer or fully mixed), hence the yield NH_3 from catalyst surface can be absorbed instantly by the nearby sorbent under the same working conditions. Fig. 10 shows the concept diagrams for NH_3 synthesis using traditional condensation, ex-situ sorption and in-situ sorption. The substantial difference between the ex-situ and in-situ sorption configurations lies in whether the catalyst and sorbent are housed in the same vessel. In the in-situ configuration, both are integrated within a single reactor, requiring them to operate under the same reaction conditions.

Compared to the typical condensation, the sorption enhanced processes (both ex-situ and in-situ) can break the practical thermodynamic limits of the HB process. Since it is possible to remove NH_3 under very low pressure (0.01 bar) using absorbents compared to conventional condensation (>1.5 bar), the boundary curves shift toward low pressure by implementing absorption as shown in Fig. 10(a) [247]. Theoretically, the ex-situ sorption enhanced process can remove NH_3 completely under its favored conditions, therefore it does not exhibit thermodynamic limitations (red line in Fig. 11(a)). However, the energy cost caused by un-reacted N_2 and H_2 recirculation and NH_3 desorption leads to practical limits in its implementation (represented by red markers in Fig. 11 (a)). On the other hand, in the case of the in-situ sorption reactor, where both the catalyst and absorbent operate isothermally, the thermodynamic limit is governed by the ammonia partial pressure required for

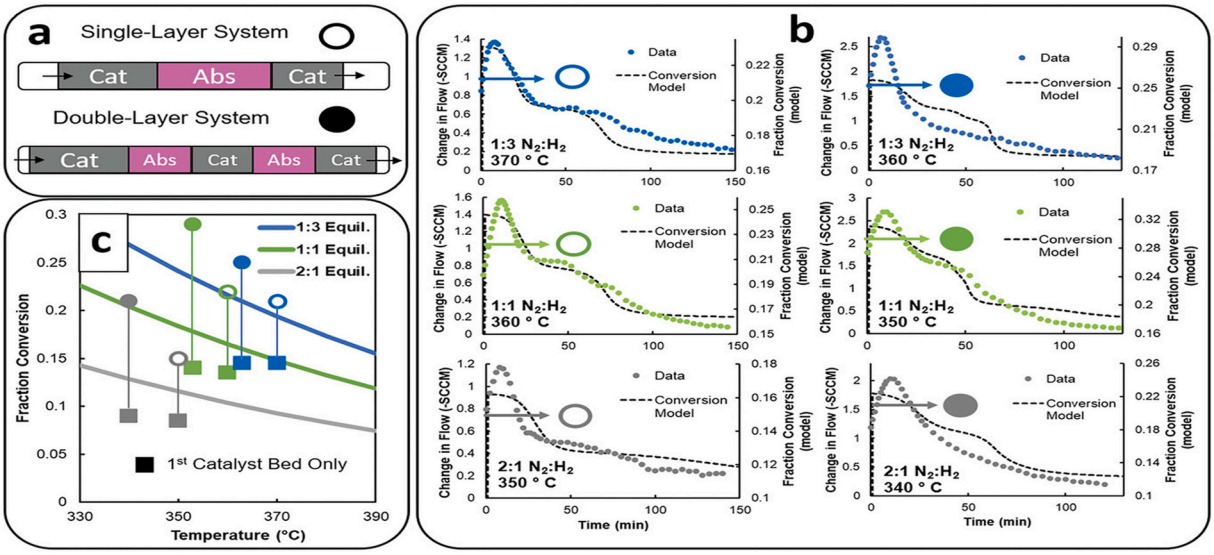

Fig. 14. Integrated catalyst-absorbent layer by layer system. (a) Configuration of two reactors with 3 layers and 5 layers, respectively. (b) Comparison of measured change in flow to that predicted by the self-developed model and the corresponding estimated fractional conversion by the self-developed model. (c) Summary of the first 30 min conversion compared to equilibrium. Reproduced by Ref. [55] with the permission from Wiley.

Table 5
Recent studies on sorption-enhanced NH_3 synthesis process.

Studies	Materials used	Operation conditions	Remarks	Source
1	Magnetite (Fe_3O_4) catalyst Anhydrous $MgCl_2$ sorbent	Ex-situ sorption mode. 80 bar and 400 °C for catalyst reactor, 200 °C for absorbent loading reactor. N_2 and H_2 molar supply ratio is 1:3	- NH_3 conversion can achieve over 95 % using $MgCl_2$ for selective absorption. - NH_3 synthesis rates over time with/without sorbent are compared, highlighting NH_3 diffusion impact in solid $MgCl_2$ to the overall kinetics. - Highlight the intricate balance between reaction kinetics and absorption equilibria in achieving high conversion.	[245]
2	Catalyst: Nonstoichiometric ferrous oxide catalyst (wustite) Sorbent: Anhydrous $CaCl_2$	Ex-situ sorption mode. Catalyst bed: 620–740 K. Absorbent bed: 460 K. Pressure swing: 20–90 bar. Flow rate: 0.7–3 mL/s	- Demonstrated the viability of NH_3 synthesis at significantly lower pressures with $CaCl_2$ enhanced production and separation of NH_3. - Temperature, pressure and gas transport impacts on NH_3 production rates for low pressure NH_3 synthesis. - $CaCl_2$ can work efficiently under the temperature close the synthesis temperature. - Larger recycle flow results in faster absorber breakthrough, leading to faster loading absorbents.	[248]
3	Wustite-based Fe catalyst Sorbent: $MgCl_2$ supported on silica	Two reactors: 15–30 bar, 400–500 °C for catalyst reactor. 100–200 °C for absorbent reactor	- Output a kinetic model for NH_3 sorption and desorption using $MgCl_2$ sorbent. - A dynamic model to explore optimal process designs across various scales (100 kg/h to 10,000 kg/h). - Scalability demonstration with a capacity exponent of 0.77, indicating favorable economics at smaller scales. - Desorption heating as the primary energy consumer, accounts for over 80 % of the total energy usage.	[249]
4	Catalyst: wustite-based Sorbent: $MgCl_2$ and $CaCl_2$	400 °C for synthesis, 100–450 °C for absorbents. Pressure from 10 to 100 bar	- Detailed analysis of how NH_3 synthesis rates are influenced by synthesis and absorption interactions. - Absorption significantly enhanced NH_3 production rate, potentially exceeding 1000 % with optimized recycle rates. - Optimizing the synthesis and absorption process separately by modeling methods. - Investigate the same conditions of catalyst bed and absorbent bed at constant temperature in a single vessel.	[250]
5	Catalyst: Ru-based catalyst ($Ru/Ce/CsO_2$) Sorbent: $MnCl_2/SiO_2$	Single reactor with catalyst and absorbent staggered layers. 250–400 °C, 20 bar	- Comparison of absorption-enhanced NH_3 conversion with equilibrium. - Layer by layer *in situ* sorption reactor that can exceed single-pass NH_3 synthesis equilibrium. - Feasible pathway of low-temperature (<300 °C) NH_3 synthesis using Ru-based catalyst and sorbent. - Develop and implement two kinetic models for NH_3 synthesis and absorption under same operation conditions. - Impacts of layer numbers to final conversion and required layer numbers to achieve 95 % conversion.	[55]
6	Catalyst:5 %Ru/10 %Ce/CsO_2, commercial KATALCO 74-1, KATALCO 35-8A from Johnson Matthey Absorbent: $MnCl_2/SiO_2$	Catalyst reactor and catalyst-absorbent reactor. 220–420 °C 20 bar	- Compared the performance of Ru-catalyst and the commercial catalysts under low temperature and pressure, showing the potential for utilizing existing catalysts in novel, renewable energy-driven processes. -Explores the integration of NH_3 synthesis with absorption separation in a single vessel, highlighting a shift towards lower pressures (<30 bar) and temperatures (<380 °C). - Indicates the viability of commercial, especially iron-based, catalysts for NH_3 synthesis under low-temperature and low-pressure conditions with presence of in-situ NH_3 absorption. - Commercial catalysts may offer a cost-effective and efficient alternative for NH_3 production.	[251]
7	Catalyst: Fe-based Sorbent: $NiCl_2$ and $MgCl_2$	Integrated reactor 400 °C and 27 bar, stoichiometric mixture of N_2 and H_2	- Demonstrates an integrated approach by combining NH_3 synthesis and separation in a single vessel at 400 °C, achieving comparable rate to traditional methods. - Explores the kinetics and thermodynamics of NH_3 absorption at 400 °C. - $NiCl_2$ exhibits substantial uptake even at lower NH_3 partial pressures compared to $MgCl_2$. - The integrated process can operate effectively at 27 bar, offering an energy and capital effective distributed NH_3 synthesis route.	[42]
8	Promoted Fe-based catalyst Anhydrous $CaCl_2$ sorbent	Double reactors, stoichiometric mixture of N_2 and H_2 380–475 °C <30 bar	- Highlighted the viability of NH_3 production at pressure as low as 30 bar, utilizing $CaCl_2$ as the absorbent. - Optimization of operating parameters in a reaction-absorption process, achieving NH_3 production rate up to 27 μmol/gcat/s. - Absorber temperature significantly influences NH_3 production, with optimal absorption observed at 25 °C. - The reaction-absorption process across multiple cycles with has no decay in absorber performance after short regeneration cycles, indicating the potential for continuous, efficient operation.	[38]
9	Fe-based catalyst sorbent: phosphate solution	600–1000 K 50–200 bar	- A system simulation for small-scale NH_3 synthesis at reduced pressures by integrating phosphate absorption.	[41]

(*continued on next page*)

Table 5 (*continued*)

Studies	Materials used	Operation conditions	Remarks	Source
			- Process efficiency is improved under moderate pressures by using phosphate absorption. -Importance of heat integration, specifically focusing on the efficient use of reaction exothermicity with operating cost reduction. - A detailed comparison with conventional HB synthesis, underlining the benefits of the intensified process in smaller scales.	
10	40 wt % $MgCl_2$ and 60 % SiO_2 as sorbent	Absorption: 50–275 °C Desorption: 50–500 °C	- $MgCl_2$ shows high cyclic stability and capacity for NH_3 absorption, with optimal performance at low absorption temperatures and high desorption temperatures. - The working capacity of sorbents improves at lower absorption (50 °C) and higher desorption temperatures (300 °C), with 3-min desorption being ideal for maximizing NH_3 production per hour. - Ammonia release from the sorbent is primarily limited by the rate of NH_3 diffusion out of the solid during desorption, rather than by heat transfer.	[43]
11	Iron and Ru catalysts $MgCl_2$ absorbent	250–500 °C 1–100 bar GHSV 5000− 45,000 h^{-1}	- Developed a Gibbs energy minimization model for simultaneous NH_3 synthesis and sorption equilibrium. - Higher sorbent ratios significantly shift equilibrium and enhance NH_3 formation rates. - Ru catalyst showed lower kinetic performance than Fe under tested conditions.	[252]

absorption and the ammonia partial pressure achieved during the reaction (yellow line in Fig. 11(a)). This behavior suggests that employing low-temperature (<300 °C) catalysis could enable a process operating at low to moderate pressures. Overall, the in-situ sorption performs best in terms of thermodynamic limitations compared to the other two methods, opening the avenue of low-temperature (<300 °C) and moderate pressure HB process [247]. Fig. 11(b) summarizes the operation conditions in previous studies for NH_3 thermal catalytic synthesis based on the three separation approaches. The results indicate that NH_3 synthesis with in-situ absorption has the potential of challenging the HB restrictive conditions.

For example, Malmali et al. designed and tested a conceptual reactor consisting of overlapping absorbent layers after each catalyst layer, which is able to produce 1.8 mol NH_3 per hour, as shown schematically in Fig. 12 [248]. The arrows from catalyst layers to absorbent layers with the color of green, blue and red represents the bed in process, transition and regeneration, respectively. Constrained by the target productivity (1.8 mol NH_3 per hour) and absorption performance (outlet mole fraction of NH_3 <1 %), the reactor is filled with 17 catalytic sections followed by absorption. The mole fraction of NH_3 drops significantly compared to the case without absorption, namely from 19.7 % to 1 %, and the mass balance is confirmed through monitoring the flow rate. The resulting data proves that the reaction-absorption reactor is capable of producing 1.8 mol NH_3 hourly under a pressure of 25 bar [248].

Similarly, Nowrin et al. have investigated absorption enhanced NH_3 synthesis process with two reactors with and without recycling, as depicted in Fig. 13 [38], where RXN denotes the reaction-only setup, RXN-then-ABS applies an absorber vessel after the reaction reactor in a single pass, RXN-ABS is a closed-loop system with gas recycling under approximately constant pressure. The recycling technique in the two-reactor system enables the in-situ separation of the yield NH_3, while allowing the absorber reactor to work under different thermal conditions. The results indicate that the reaction temperature predominantly governs the overall ammonia production rate, regardless of the absorption temperature, due to equilibrium limitations. Moreover, the recycling flow rate has a significant impact on the production rate, beyond the effects of the operating conditions alone. Under optimized conditions, a production rate exceeding 27 μmol g_{cat}^{-1} s^{-1} was achieved. The reaction–absorption process demonstrated stable performance over more than nine cycles, however, heat dissipation from both reactors contributes to the system's energy inefficiency.

Noticeably, Smith et al. have investigated in-situ sorption reactor with loading catalyst and absorbent layer by layer to exceed the thermodynamic limitations during NH_3 synthesis process, as shown in Fig. 14(a) [55]. A series of experiments have been conducted using $MnCl_2$ as the sorbent, including the temperature swings, changes in reactant ratios, and the impacts of layer numbers. The results show that the in-situ sorption enhanced synthesis can exceed the equilibrium limitation as shown in Fig. 14(c), and that a greater number of layers favors this behavior. Fig. 14(b) proves that the layer number increases would significantly raise the conversion, by comparing the left figures (single-layer system) to the right figures (double-layer system). The monitored change in flow verifies the NH_3 removed by the absorbents, demonstrating the effectiveness of this layer-to-layer catalyst and absorbent configuration. The calculation method for optimizing the layer number with a certain conversion rate is also demonstrated in this paper. Guided by the theoretical analysis of absorption-enhanced NH_3 synthesis process, many scientific investigations have been conducted. Table 5 summarizes the most relevant studies on sorption enhanced NH_3 synthesis.

Although many efforts have been devoted to sorption-enhanced NH_3 synthesis, challenges still remain. A key issue lies in the desorption process: NH_3 release from sorbents typically requires heating and/or fluid washing, both of which introduce additional energy costs. A modeling study [249] estimated desorption conditions of 500 °C and 13.4 bar for the absorbent vessel. Experimental work [43] demonstrated that efficient NH_3 desorption from supported $MgCl_2$ absorbents occurs within the range of 180–400 °C, which is significantly higher than the absorption working temperature of ~50 °C. More recently, it was reported that desorption at 200 °C under sufficiently low sweep gas flow enables $MgCl_2$ sorbent regeneration and yields NH_3 with 72 mol% purity [253]. This result is particularly significant, as it shows the feasibility of reducing the energy penalty of sorption-enhanced ammonia synthesis. Nevertheless, these studies all employ separate reactors for the absorbent and catalyst, and the desorption behavior in integrated catalyst–sorbent reactor systems remains largely unexplored. In in-situ configurations, sorbent regeneration at elevated temperatures may inadvertently promote NH_3 decomposition within adjacent catalytic zones, thereby diminishing the overall collection efficiency. In addition, the application of purge gases to facilitate desorption introduces the risk of NH_3 dilution, which complicates downstream separation and reduces product purity. The issue of NH_3 desorption during sorbent regeneration makes in-situ sorption-enhanced ammonia synthesis practically unviable, underscoring the need for substantial advances in both regeneration strategies and reactor design.

In summary, recent advances in sorption-enhanced reactors for NH_3 synthesis have demonstrated significant potential to overcome the

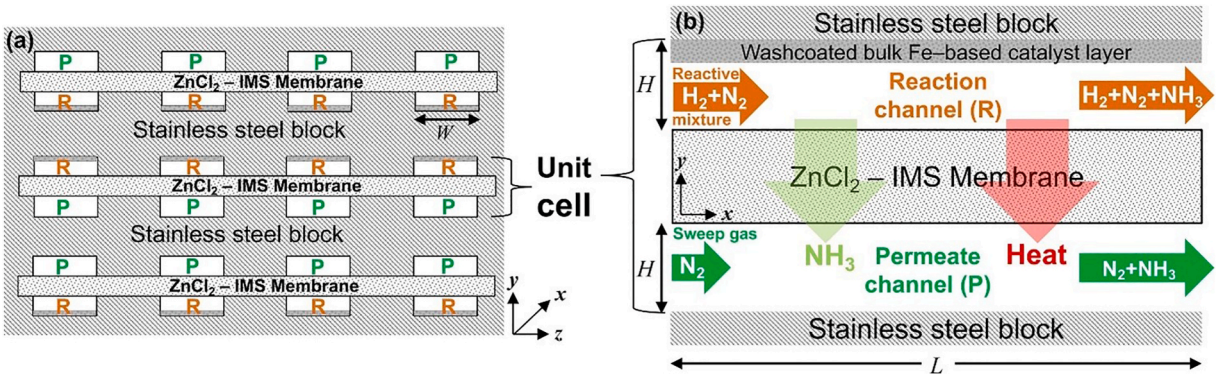

Fig. 15. Proposed cooling integrated microchannel membrane reactor (a), and the characteristic repeating unit of the multichannel (b) in two dimensions. (R: rectangular reaction, P: permeate) Reproduced by Ref. [255] with permission from Elsevier.

thermodynamic limitations of conventional Haber-Bosch process. Innovations such as in-situ sorption reactors, which integrate catalyst and absorbent layers, have shown promising results in achieving high NH_3 conversion rates at lower temperatures and pressures. Studies have highlighted the efficiency of various sorbents, including metal halides and supported analogues, in enhancing NH_3 absorption and simultaneously optimizing operational conditions. However, challenges remain, particularly in the scalability of these systems and the economic feasibility of implementing advanced sorbents in industrial applications. The performance of absorbent at high temperatures such as 300 °C is still at a low level for most of the currently developed materials, resulting in difficulties in integration of catalyst and sorbent for in-situ sorption process. Additionally, cyclic tests are necessary to be conducted due to partial agglomeration caused by volume changes during repeated absorption/desorption cycles [229]. Challenges related to sorbent stability, sensitivity to moisture, regeneration efficiency, and the energy costs associated with reactant recycling must be resolved to fully unlock the potential of sorption-enhanced technologies for NH_3 production.

4.2.2. *Membrane reactors*

Few experimental studies have been reported regarding membrane reactors for synthesizing and separating NH_3 in a single unit, while modeling works are leading the progress. Zhang et al. have designed the requirements and evaluated the operation conditions for a catalytic membrane reactor through a computational approach, aiming to intensify moderate NH_3 synthesis through an NH_3-permeant membrane [254]. The results indicate that the efficiencies of NH_3 synthesis and separation are dictated by the NH_3 permeance. The NH_3 permeance is ideally in the range of 100–1000 GPU, where values lower than 100 do not efficiently separate NH_3, while values higher than 1000 show diminishing returns due to the saturation phenomenon in the reactor. The ideal NH_3 selectivity over N_2 and H_2 should be above 10, while in any scenario, it should be no less than 4. This work is meaningful for membrane NH_3 synthesis reactor design, guiding the development of membranes and their implementation.

Another modeling study, recently reported in Ref. [255], numerically investigates a proposed micro–structured membrane reactor comprising NH_3 synthesis, cooling and separation in the same volume, as illustrated in Fig. 15. The reactor block mainly comprises rectangular reaction and permeate channels with cross-sectional dimensions of 3×10^{-4} m and 6×10^{-4} m, respectively, and an identical length of 0.15 m. The modeling results show that integrating NH_3-selective membrane separation with in-situ cooling enables N_2 conversion up to 47 %, surpassing the thermodynamic limit at 613 K and 50 bar. The membrane reactor achieves approximately 3.5 times higher NH_3 yield than the non-membrane case and exhibits strong sensitivity to temperature, pressure, feed composition, and space velocity.

Recently, a modeling study on NH_3 membrane reactor has been reported in Ref. [239], aiming at analyzing a larger scale reactor with multi-tubular fixed bed structure. As shown in Fig. 16, the reactor consists of an inner membrane tube and an outer shell containing the catalyst (Ru-based for this case), referred as the permeate and retentate sides. A 1D steady-state model, describing the catalytic and membrane-separation processes, considering both mass and energy balances, has been developed based on Aspen Plus. The modeling results confirm that the conversion and NH_3 recovery are mostly independent of the membrane's selectivity, when it exceeds the threshold of 10–20 towards H_2. However, a much higher selectivity (>1000 towards H_2) is necessary for yielding pure NH_3 permeate. Moreover, the model has been integrated into a Power-to-Ammonia (PtA) system, indicating that the membrane reactor can raise the system efficiency by around 8 % and up to15 % for SOEC-based PtA process.

Another interesting experimental work has been reported recently in Ref. [256], using separate vessels for NH_3 synthesis and membrane separation, allowing independent temperature control. This idea is similar to ex-situ sorption NH_3 synthesis. The schematic diagram for the experimental setup is illustrated in Fig. 17. Compared to the conventional HB process, the condenser is replaced by a membrane module, which can separate trace amounts of NH_3. Thereby, the NH_3 synthesis reactor can be operated under mild conditions (300–400 °C, 20–60 bar in this study), still with efficient NH_3 separation owing to the membrane separator. The performance of ceramic composite and sulfonated (3-mercaptopropyl) trimethoxysilane membranes for extracting the upstream synthesized NH_3 from feed side to permeate side has been tested, showing an impressive increase of NH_3 fraction from 0.01 of equilibrium state to 0.1–0.45 in permeate stream in a temperature swing of 20–100 °C. Further system parametric analysis has been conducted together with a plug-flow modeling study, offering valuable insights for designing membrane-enhanced NH_3 synthesis systems.

Overall, investigations of membrane reactors for promoting NH_3 synthesis remain a nascent and promising field, with a growing need for further studies are desired in reactor and system level, particularly with experimental work.

4.3. *Macroscopic models in reactor scale*

Modeling investigations at the macroscale are essential for reactor design and optimization, especially for implementing and validating new technologies, such as enhanced NH_3 synthesis processes using sorbents or membrane techniques. This section reviews two types of macroscopic modeling approaches: global kinetic modeling and differential equation-based reactor modeling. The former emphasizes the latest kinetic models for NH_3 synthesis and absorptions, while the latter provides an overview of comprehensive reactor models that include mass and heat transfer phenomena, covering computational fluid dynamics (CFD) modeling studies.

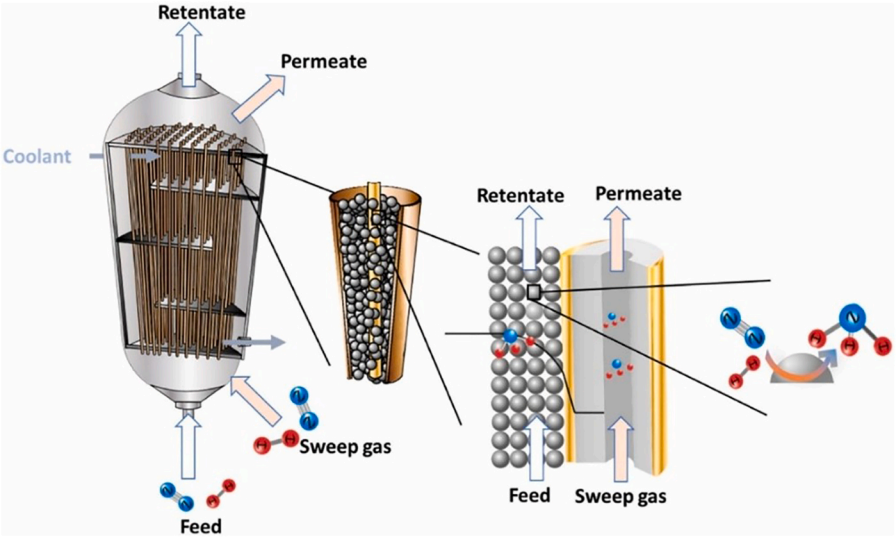

Fig. 16. Design of a multi-tubular packed bed membrane reactor favored for its manufacturing simplicity, scalable design and efficient heat exchange. Reproduced by Ref. [239] with permission from Elsevier.

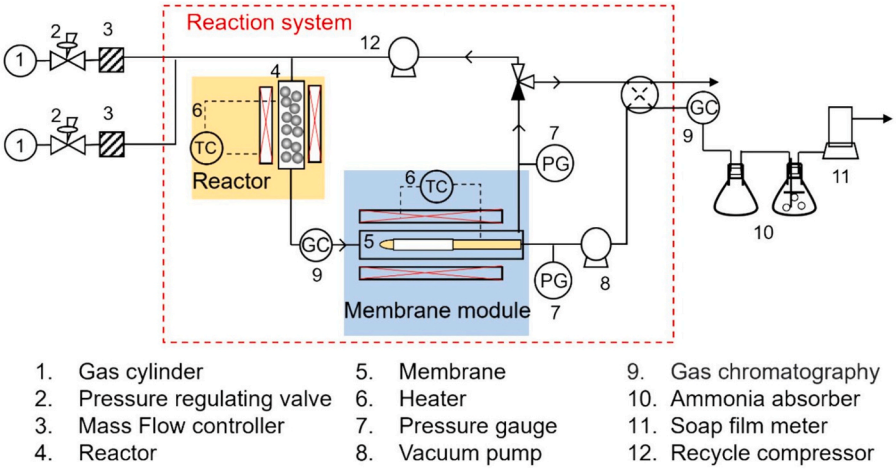

Fig. 17. Experimental apparatus schematic diagram of the recycle membrane reactor for NH_3 production. Reproduced from Ref. [256] with permission from Elsevier.

4.3.1. Macroscopic kinetic models

4.3.1.1. Ammonia synthesis model. Even though several microscopic kinetic models have been developed, detailing the fundamental mechanisms or reaction pathways of NH_3 catalytic synthesis process. However, most of the models are too complicated and time-consuming to be used for describing the large number of reactions in a practical reactor. Therefore, macroscopic/global kinetic models considering only one-step reaction for NH_3 synthesis process has been developed. Commonly used global kinetic expressions for estimating the NH_3 synthesis rate are summarized in Table 6. It is important to note that the estimated kinetic parameters can vary significantly across different studies and catalysts (as referenced accordingly), even when the same kinetic expressions are used.

4.3.1.2. Ammonia absorption model. Apart from kinetic modeling for NH_3 synthesis, several kinetic models describing NH_3 absorption have also been developed, establishing the basis of numerical studies on sorption-enhanced reactors. For example, Matthew et al. have developed a global kinetic model to predict the absorption (temperature range from 100 to 200 °C) and desorption (500 °C) rates of NH_3 into silica supported $MgCl_2$ absorber [249]. The global rates for sorption and desorption are governed by Eqs. (1) and (2).

$$r_{abs} = \begin{cases} \dfrac{k_{abs}\left(p_{NH_3} - p_{eq}\right)^7}{K_{abs} + \left(p_{NH_3} - p_{eq}\right)^6}, & p_{NH_3} > p_{eq},\ q_{NH_3} < q_{NH_3}^{max} \\ 0, & p_{NH_3} > p_{eq},\ q_{NH_3} = q_{NH_3}^{max} \end{cases} \quad (1)$$

$$r_{des} = \begin{cases} k_{des}\left(p_{eq} - p_{NH_3}\right), & p_{NH_3} < p_{eq},\ q_{NH_3} > 0 \\ 0, & p_{NH_3} < p_{eq},\ q_{NH_3} = 0 \end{cases} \quad (2)$$

Where p_{NH_3} and p_{eq} denote NH_3 partial pressure and sorbent equilibrium pressure, respectively. $q_{NH_3}^{max}$ indicates the maximum sorption capacity in terms of mol/kg_{abs}, e.g., 10.5 mol NH_3/kg_{MgCl2} has been used in the original study. The absorption kinetic constant k_{abs} and the desorption kinetic constant k_{des} are estimated as 0.4668 and 7.002 × 10^{-3} mol/(s kg_{abs} bar), respectively, as reported in Ref. [249]. The net absorption rate is then:

$$\frac{dq_{NH_3}}{dt} = r_{abs} - r_{des} \quad (3)$$

Another kinetic model for $MgCl_2$-based NH_3 absorption has been reported in Ref. [250], accounting for three exothermic steps of NH_3 reacting with $MgCl_2$:

$$NH_3 + MgCl_2 \leftrightarrow MgCl_2 \bullet NH_3 \quad (R5)$$

$$NH_3 + MgCl_2 \bullet NH_3 \leftrightarrow MgCl_2 \bullet (NH_3)_2 \quad (R6)$$

$$4NH_3 + MgCl_2 \bullet (NH_3)_2 \leftrightarrow MgCl_2 \bullet (NH_3)_6 \quad (R7)$$

The absorption rate is governed by Eq. (4).

$$r_{abs} = \begin{cases} k_{a1} e^{k_{a2}\left(p_{NH_3} - p_{eq}\right)}, & p_{NH_3} - p_{eq} < 1\ bar \\ k_{a3} e^{\left(p_{NH_3} - p_{eq}\right)^2}, & p_{NH_3} - p_{eq} > 1\ bar \end{cases} \quad (4)$$

The kinetic rate constants k_{a1}, k_{a2} and k_{a3} are estimated by fitting with experimental data with the values of 1.6×10^{-4} μmol/(s g_{abs}), 9.0×10^{-2} kPa^{-1} and 3.8×10^{-6} μmol/(s g_{abs} kPa^2), respectively. This study also proved that $MgCl_2$ sorbent performs better than $CaCl_2$ for high-temperature (205 °C) NH_3 absorption.

A further study from the same author has been presented in Ref. [55], modeling NH_3 absorption rate with another metal halide, that is $MnCl_2$. The model also considers three steps of NH_3 absorption by $MnCl_2$ absorber, i.e., physical adsorption and two chemisorption steps as listed.

$$0.5\ NH_3 + MnCl_2 \leftrightarrow MnCl_2 \bullet 0.5\ NH_3 \quad (R8)$$

$$0.5\ NH_3 + MnCl_2 \bullet 0.5\ NH_3 \leftrightarrow MnCl_2 \bullet NH_3 \quad (R9)$$

The overall sorption rate in terms of mol/(g_{MnCl2} min) is determined from Eq. (5),

$$\begin{aligned} r_{abs} = {} & 3 \times 10^{-4}\left(p_{NH_3} - 0.05\right)\left(1 - X_A^1\right) + 2 \\ & \times 10^{-2}\left(p_{NH_3} - p_{eq1}\right)^4\left(1 - X_A^2\right)^4 + 2.5 \\ & \times 10^{-2}\left(p_{NH_3} - p_{eq2}\right)^4\left(1 - X_A^3\right)^6 \end{aligned} \quad (5)$$

in which the three parts in the right side sequentially describes the physisorption rate and the two reaction steps' rates. Different from the above two models, there are two equilibrium pressures p_{eq1} and p_{eq2} are introduced for the steps in Eqs. (6) and (7), respectively, which can be obtained by the reciprocal of the equilibrium constants K_{eq1} and K_{eq2}.

$$\ln K_{eq1} = -\frac{42100}{8.314}\left(\frac{1}{T} - \frac{1}{650}\right) \quad (6)$$

$$\ln K_{eq2} = -\frac{42100}{8.314}\left(\frac{1}{T} - \frac{1}{610}\right) \quad (7)$$

The coefficients X_A^i indicates the saturation index of ith step with the experimental data fitted value of 0.13, 0.35 and 0.35 for the order of i = 1, 2 and 3, respectively. In practice, it indicates the capacity of each step in terms of $MnCl_2$ molar equivalent based NH_3 removal. This model has been implemented for predicting an in-situ sorption enhanced NH_3 synthesis reactor under higher temperatures up to 420 °C, showing its capability of modeling high-temperature sorption process. Further work regarding desorption is highly encouraged, to prove the reversibility of the high-temperature sorption process along with experimental studies.

4.3.2. Differential equation-based and CFD models

The kinetic models have successfully described the chemical reaction process of NH_3 synthesis and absorption. However, the other physical phenomena such as mass transport and heat transfer due to fluid flow are also important, which have not been considered in kinetic models. The differential equation-based models including CFD models, incorporating the chemical reactions and corresponding kinetic models into the mass and heat transport governing equations, provide a more accurate way to simulate NH_3 synthesis reactors. Several relevant models have been reported in previous studies.

For instance, a steady-state, one-dimensional mathematical model for a gas-flowing solids-fixed bed reactor has been developed in Ref. [264], intricately incorporates the NH_3 catalytic equilibrium reaction and NH_3 adsorption processes. The ordinary differential equations (ODEs) have been introduced to detail several key features: material balances for both the gas and solids phases, energy balances, conversion rates and pressure loss. The model framework consists of six ODEs are summarized in Table 7 together with their specifications, covering mass and energy balance and the flow pressure loss through the packed bed. This comprehensive modeling framework allows for accurate simulation of the synthesis-adsorption reactor's performance, offering a useful tool for investigating the adsorption enhanced NH_3 synthesis process.

Nikzad et al. reported a comprehensive CFD analysis of three conceptual spherical radial flow reactor configurations for NH_3 synthesis, attempting to improve the NH_3 synthesis through reactor design [265].

Table 6
Summary of commonly used global kinetic expressions for ammonia synthesis.

Name	Ammonia synthesis rate expression	Remarks	Ref.
The Temkin-Pyzhev expression	$k_1 p_{N_2}\left(\frac{p_{H_2}^3}{p_{NH_3}^2}\right)^{\alpha} - k_2\left(\frac{p_{NH_3}^2}{p_{H_2}^3}\right)^{1-\alpha}$	• Invented for promoted iron catalyst at high temperature and pressure in 1940 • The model considers non-equilibrium adsorption of species (nonuniform surface) • The dissociative adsorption of N_2 is considered as the rate-determining step • The empirical exponent α adjusts the influence of NH_3 inhibition, $0 \le \alpha \le 1$ • The model captures the effects of partial pressures and temperature • The model is semi-empirical, the formulation was derived from extensive experimental data fitting • Good fit to experimental data with simple parameters, but lacks mechanistic foundation	[257] [258]
The extended Temkin expression	$\frac{k_1\left(K_a^2 a_{N_2} - a_{NH_3}{}^2/a_{H_2}{}^3\right)}{\left(1 + K_{NH_3} a_{NH_3}/a_{H_2}{}^{\omega}\right)^{2\alpha}}$	• Derived from the Temkin model by replacing partial pressures by activities defined by fugacities • Broader temperature range 330–495 °C for iron catalysts • More fitting parameters	[259, 260]
The modified Temkin expression	$2k\left(K_a^2 a_{N_2}\left[\frac{(a_{H_2})^3}{(a_{NH_3})^3}\right]^{\alpha} - \left[\frac{(a_{NH_3})^2}{(a_{H_2})^3}\right]^{1-\alpha}\right)\eta$	• Embedding diffusion corrections by the effectiveness factor • Maintaining model simplicity • Avoided pressure dependence of rate constant	[261]
Rossetti's model	$k\lambda(q)\gamma\frac{(a_{N_2})^{0.5}\left[\frac{(a_{H_2})^{0.375}}{(a_{NH_3})^{0.25}}\right] - \frac{1}{K_a}\left[\frac{(a_{NH_3})^{0.75}}{(a_{H_2})^{1.125}}\right]}{1 + K_{H_2}(a_{H_2})^{0.3} + K_{NH_3}(a_{NH_3})^{0.2}}$	• Investigated for Ru/C catalysts under 370–460 °C, 50–100 bar • More mechanistic via LHHW approach • Introduces an additional term accounting for the competitive adsorption of H_2 • The activation energy was 23 kcal/mol, much lower than Fe-based catalysts. • The N_2/H_2 feeding ratio can vary as 1:3 or 2:3 by changing λ(q) • Effectiveness factor is not considered due to small and diluted particles used	[262, 263]
Smith's model	$k_1 p_{N_2} - k_{-1} p_{NH_3}^{1.3} p_{H_2}^{-2.5}$	• Developed for Ru-catalysts under low operational conditions, 220–420 °C • Implemented in the study together with absorbents	[55]

The study develops a 2D pseudo-homogeneous model, which incorporates the extended Temkin kinetic model for quantifying NH_3 catalytic synthesis rate under the CFD model framework. Three novel spherical reactor configurations (as shown in Fig. 18) are simulated by the model and compared with the typical tubular reactor, including various feed inlets. The proposed configurations offer advantages such as the ability to operate at higher flow rates with reduced pressure drop compared to the tubular design. Simulation results indicate that the spherical configuration with four inlets (Fig. 18(c)) achieves the highest nitrogen conversion, i.e., 20.96 %, among the three configurations, likely due to its minimal pressure loss, particularly at high flow scale-up ratios. This model has been further employed to evaluate and compare NH_3 production performances in different types of reactors, i.e., spherical radical flow (SRF), spherical axial flow (SAF) and tubular reactors (TR) [266]. Fig. 19 presents the simulated nitrogen conversion, temperature contours, and velocity fields, revealing markedly different distributions of these key parameters; notably, SAF exhibits superior temperature uniformity. Overall, nitrogen conversion in SAF and SRF increased by 32.2 % and 26 %, respectively, compared to TR. While, the construction simplicity of SAF makes it more practical than SRF among the spherical designs. This study demonstrates the great potential of CFD modeling for visualization and optimization of NH_3 synthesis reactor configurations.

In 2023, Tyrański et al. developed a two-dimensional CFD model to investigate ammonia synthesis in an industrial axial-radial Topsoe converter, where a circular flow pattern is established, using magnetite-based catalysts under high pressure (220 atm) and moderate temperature (342 °C) [267]. By implementing an extended Temkin-Pyzhev kinetic model with diffusion correction [259], they systematically analyzed the effects of catalyst particle diameter (ranging from 1 to 10 mm), bed porosity, and geometric configurations on flow behavior, reaction distribution, and ammonia formation rates. The simulations showed that smaller catalyst particles enhance local reaction rates but may result in unused bed volumes due to early equilibrium, while optimized bed geometries can substantially reduce catalyst volume without compromising conversion. This work highlights the applicability of CFD as a powerful tool for reactor design and optimization in large-scale ammonia production.

In the same year, a 3D steady-state CFD model for Ru-based catalytic NH_3 synthesis has been developed, numerically tackling decentralized NH_3 synthesis over advanced catalysts [268]. The modified Temkin kinetic model, as aforementioned, specifically for Ru catalysts has firstly been implemented in CFD simulation for synthesizing NH_3 in the temperature and pressure ranges of 350–430 °C and 50–100 bar, respectively. The application of this updated kinetic model highlights its potential and suitability for simulating thermocatalytic NH_3 synthesis over advanced Ru-based catalysts. Except the kinetic model and the computational dimension, other fluid dynamic models and numerical methods employed, such as the SST k–ω turbulence model, porous zone modelling approach, and the SIMPLE algorithm for pressure–velocity coupling, are consistent with those used in Ref. [267]. The model has been validated through comparison with experimental data under various isothermal conditions, while varying pressure, space velocity and reactants ratio. Then, it has been deployed to numerically optimize the operating conditions, outputting the best space velocity in terms of NH_3 productivity. However, the inlet and outlet boundary conditions employed in Ref. [268] are debatable. For high-pressure reactor simulations with a specified inlet volumetric flow rate, the use of velocity inlet and outflow outlet conditions is generally considered more appropriate.

Another NH_3 synthesis unit has been simulated using CFD in Ref. [269], focusing on process flexibility under varying production loads. The reactor under different production loads from 30 % to 100 % as well as parameter sensitivity analysis in terms of temperature, pressure and catalyst size, has been studied. The key findings reveal that reduced loads may cause operational challenges, such as gas dead spaces and backflow zones, reducing catalyst productivity, thermal efficiency, and exergy efficiency (dropping from 51 % to 34 %). The study highlights that 3D CFD modeling provides critical insights into the operation of NH_3 reactors under flexible, renewable energy-driven synthesis conditions. While operational flexibility is achievable, it entails trade-offs in production yield, catalyst efficiency, and energy losses, particularly at lower production loads. Overall, CFD modeling is less common in NH_3 synthesis research compared to kinetic modeling, especially for mildly operated reactors. Fewer than 35 publications were identified in the Web of Science database using the keywords “ammonia synthesis” AND “CFD” (or “ammonia synthesis” AND “computational fluid dynamics”). Comprehensive CFD simulations for sorbent- or membrane-separation-enhanced reactors remain unexplored. We speculate one of the main reasons is that NH_3 synthesis, which matured in the early 20th century, many decades before CFD modeling had been widely applied. Significant expansion of CFD implementation came only after the development of advanced algorithms like SIMPLE (1970) and Rhie & Chow interpolation (1983) in the latter half of the 20th century [270]. For advancing NH_3 reactors beyond current limits, CFD modeling will play an increasingly crucial role and warrants greater attention moving forward.

In summary, this chapter reviews the latest advancements in thermocatalytic NH_3 synthesis technologies, with a focus on solid sorption-enhanced and membrane-based processes. It highlights the development of advanced solid sorbents and membranes, showcasing both state-of-the-art achievements and ongoing challenges. Additionally, it summarizes studies on intensified NH_3 synthesis using sorption and membrane-enhanced techniques, including prototypes and unit-scale modeling efforts. The insights underscore the potential of these technologies and emphasizes the need in reactor scale to address existing challenges and explore NH_3 production beyond conventional Haber-Bosch process.

Table 7
Governing equations for the reactor model developed in Ref. [264].

Items	Equations	Specifications
Material balances	$F_{0,N_2}\frac{dZ}{dx} = 0.5R_{NH_3}\eta\dot{\varepsilon}A$ $\frac{dF_{NH_3}}{dx} = R_{NH_3}\eta\dot{\varepsilon}A - k_g a_s \rho_s (q_e - q)\dot{\varepsilon}A$ $u_s\frac{dq}{dx} = k_g a_s (q_e - q)$	F_{0,N_2} is inlet molar flow rate, Z is N_2 conversion. The NH_3 synthesis rate is determined by the Temkin equation with a correction factor η. q_e denotes the NH_3 equilibrium concentration on the Cu–Y zeolite.
Energy balances	$\dot{u_g}\rho_g Cp_g\frac{dT_g}{dx} = -\Delta H_r R_{NH_3}\eta - ha_s\rho_s(T_g - T_s)$ $u_s\rho_s Cp_s\frac{dT_s}{dx} = -\Delta H_{ads} S a_s (q_e - q) + ha_s\rho_s(T_g - T_s)$	Non-thermal equilibrium model. The heat transfer coefficient h is calculated by Ranz–Marshall correlation.
Pressure loss	$\frac{dp}{dx} = -\left(\frac{150}{Re_p} + 1.75\right)\frac{u_g^2\rho_g}{d_{eq}}\frac{(1-\dot{\varepsilon})}{\dot{\varepsilon}^3} - \frac{3}{4}\frac{C_d\beta_d\rho_g u_r^2}{d_s\dot{\varepsilon}}$	Modified Ergun equation for resistance of the packed bed. Drag force due to the co-current flow.

5. Green ammonia system integration and assessments

In present, existing large-scale Haber-Bosch plants produce up to 3300 tNH_3/day, requiring substantial H_2 supplies that often exceed the capacity of current water electrolysis technologies. To enable integration with water electrolysis systems and thereby establish the Gen. 2 NH_3 production route (refer to Fig. 2), NH_3 production units must be downscaled to capacities of 3–60 tNH_3/day [27]. System-level investigations focusing on the integration of advanced thermocatalytic NH_3 synthesis with water electrolysis are gaining significant attention. This chapter reviews the advances, challenges, and adaptation strategies associated with this integration, along with practical case studies. The key aspects of this green ammonia system integration route are depicted

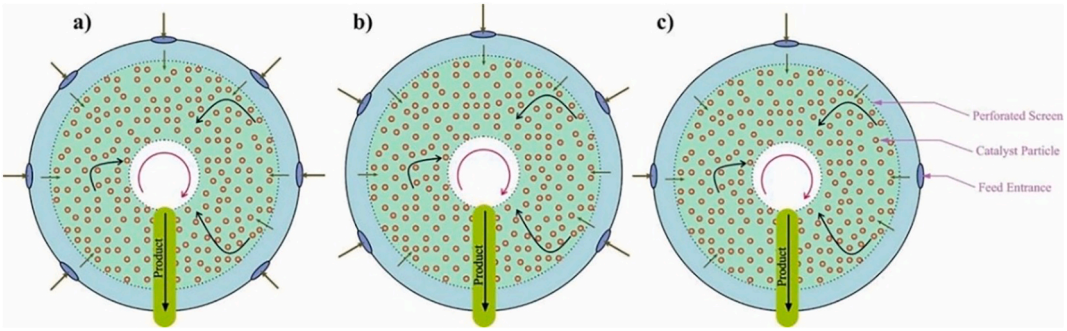

Fig. 18. Conceptual schematics of spherical radial flow reactors (a) eight feed inlet, (b) six feed inlet, (c) four feed inlet. Reproduced from Ref. [265] with permission from Elsevier.

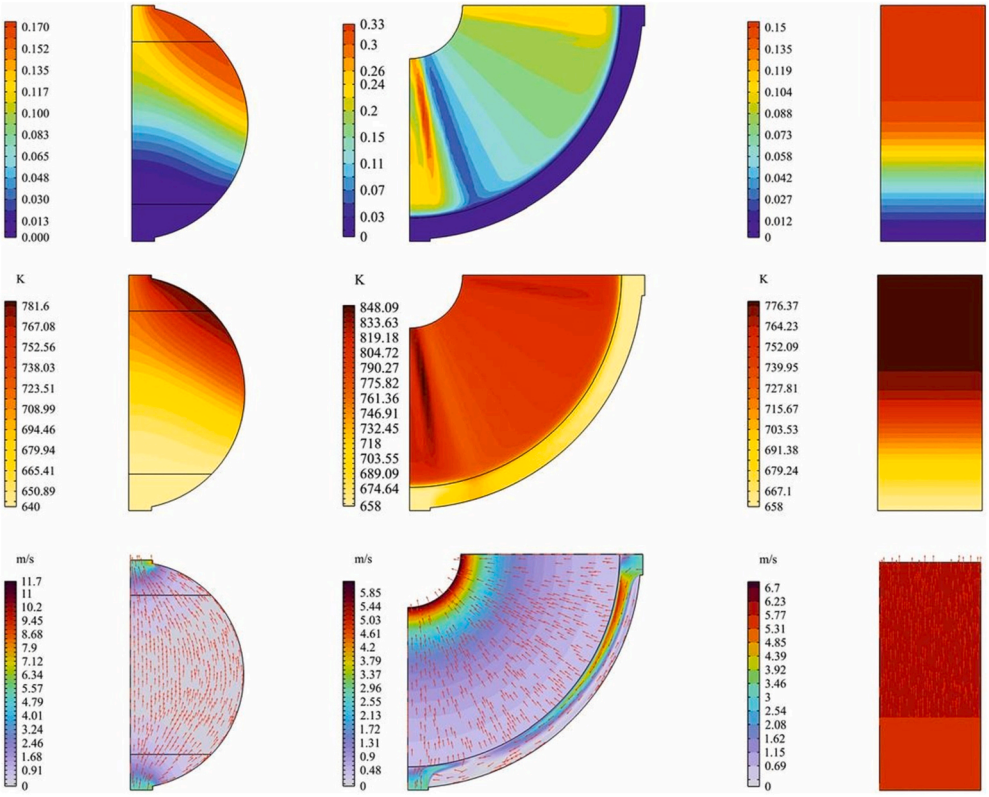

Fig. 19. Contours of N_2 conversion, temperature and velocity field for the SAF, SRF and tubular packed bed reactor. Reproduced from Ref. [266] with permission from Elsevier.

in Fig. 20 and structurally elaborated in the subsequent sections.

5.1. System integration challenges

5.1.1. Pressure compatibility

The first critical challenge in process integration is the compatibility of operating conditions of water-splitting H_2 production and NH_3 synthesis. The operation conditions of an HB reactor are not directly compatible with water electrolysis units. For instance, the current water electrolysis process is usually operated under 30 bar (PEM electrolysis cell can be higher to 100 bar), creating specific requirements for the HB operating pressure, which many enhanced HB processes have yet to achieve [271]. A compressor is therefore required to increase the H_2 flow pressure in such cases, resulting in additional capital investment and energy consumption. The *Techno-Economics of Hydrogen Compression* Technical Brief highlights the challenges and costs associated with H_2 compression, reporting energy requirements ranging from 1.7 to 6.4 kWh/kg H_2 depending on inlet/outlet pressures and compressor efficiency [272]. This underscores the necessity of integrating with moderate-pressure NH_3 synthesis processes, which do not require compressing H_2 to extremely high levels. For example, Ishaq et al. presented a modeling study of a Power-to-NH_3 system that included a compressor raising electrolytic H_2 to 70 bar to supply a cascaded NH_3 synthesis unit [273]. In their analysis, the compressor's energy demand constituted only a minor fraction of the total energy consumption, which was dominated by the electrolyzer. However, the actual energy consumption in practical applications is likely to be higher than the values estimated in this modeling study.

Alkaline (ALK) water electrolysis, as a more mature H_2 production technology, has also been attempted to integrate with NH_3 synthesis unit. Zhang et al. studied a NH_3 synthesis process integrated with ALK water electrolysis cells powered by photovoltaic panels [274]. The study highlights improvements in energy efficiency, achieving over 60 % efficiency by optimizing ALK electrolysis operation conditions. The energy

efficiency peaks at a current density of 0.2 A/cm^2. Higher operating temperatures further improve efficiency, while lower pressures slightly enhance performance. The techno-economic analysis shows that increasing the current density reduces the cost of NH_3 production, despite higher power demands. The use of ALK electrolysis cells makes PtA pathway even more feasible. However, the absence of H_2 compressor data renders this conclusion somewhat optimistic, as alkaline electrolyzers typically operate at pressures around 30 bar, significantly lower than the requirements of downstream NH_3 synthesis processes. In fact, accurately estimating the cost of ALK electrolyzers remains challenging due to the wide variability in reported data and the lack of transparency regarding which components are included such as compressors and storage tanks, as pointed in Ref. [275].

5.1.2. Heat integration

Similar to pressure inconsistency, a heater or chiller is required for the H_2 flow converted from water electrolysis process before it enters the NH_3 synthesis process, because ALK and PEM electrolysis typically operate at temperatures below 100 °C, while the SOEC process usually operates at high temperature (600–900 °C) [276]. The strengths, weaknesses, opportunities and risks analysis for the three types of water electrolysis were reviewed in Ref. [277], highlighting the potential and limitations of the three major water electrolysis technologies in PtA applications. System heat integration is also necessary for PtA systems design and optimization. Overall efficiency, complexity, robustness and economic feasibility are the key concerns. In 2020, a SOEC-based PtA process with heat integration using a three-pressure-level steam cycle has been designed and compared with biomass-to-NH_3 (BtA) and methane-to-NH_3 (MtA) processes [278]. The study highlights the efficiency benefits of using SOEC due to its high electrical efficiency and the potential for heat integration. The PtA process achieves the highest system efficiency, exceeding 74 % compared with the BtA and MtA processes, while the economic cost is also the highest. The results forecast that H_2 production from SOEC and increased availability of low-cost renewable electricity could reduce payback times to below five years, making SOEC-based PtA competitive with conventional NH_3 production methods.

In addition, the PEM electrolysis-based PtA process and SOEC-based PtA process have been demonstrated and compared in Ref. [279], in terms of energy efficiency and resource utilization. The results indicate that PEM-based PtA achieves H_2 and N_2 utilization efficiencies of 92.64 % and 90.56 %, respectively, which are slightly higher than those achieved by SOEC-based PtA. However, SOEC-based PtA demonstrates higher energy efficiency, reaching up to 75.08 %, compared to 65.40 % for the PEM-based system. Moreover, the study also highlighted the impacts of using different heat integration strategies, i.e., direct heat integration versus indirect heat integration, as compared in Fig. 21. The indirect method, PEM-PtA, focuses on waste heat recovery through steam which produces 63.6 MW of heat, still requiring 3 MW heat from external sources. The direct method, PEM-PtA, optimizes internal heat exchange, reducing utility consumption and producing 36.1 MW of high-pressure steam for electricity generation. For SOEC-based PtA, the indirect integration (SOEC-PtA) recovers heat similarly, generating excess heat (63.62 MW) but requiring better optimization. In direct integration (SOEC-PtA), the process recovers heat through a Rankine cycle, using surplus heat for electricity generation and service steam extraction. SOEC's higher operational temperature leads to greater heat recovery, improving efficiency but increasing system complexity.

Furthermore, an advanced small-scale NH_3 production system, integrating absorption-enhanced NH_3 synthesis units with ALK electrolysis stacks, has been proposed and modeled using Aspen Plus and MATLAB [280]. The NH_3 production configuration, illustrated in Fig. 22, incorporates multiple ruthenium-based catalyst beds and $MgCl_2$ sorbent beds in separate reactors to facilitate NH_3 synthesis and separation, enabling the process to surpass equilibrium limitations. The predicted results indicate that this innovative approach achieves over 90 % conversion of H_2 to NH_3 in a single pass, without the need for high-pressure reactors or chillers.

On the H_2 production side, a unique direct-contact water cooling method for the electrolyte has been employed, significantly reducing parasitic power consumption and improving system efficiency by 13.27 %. The overall system configuration is detailed in Fig. 23, which outlines the process flow for H_2 and O_2 production via ALK electrolysis, alongside a novel method for cooling the electrolyte within a cooling tower. The system modeling results demonstrate 46.2 % reduction in power consumption compared to the conventional HB process, which uses a vapor compression refrigeration cycle to condense and purify NH_3. It was also shown that the utilization of the novel cooling system for H_2 production may result in a 19 % reduction in NH_3 production costs, owing to substantial savings in electricity costs of H_2 production. This process eliminates the need for NH_3 condensation at low temperatures, thereby improving both its energy efficiency and economic viability. In addition, challenges related to sorption material capacity for large-scale applications have been identified, as well as the sensitivity of catalyst and sorbent layer design to space velocity. This study provides meaningful insights into the potential of sorption enhanced NH_3 production process on a system level, showing valuable reference results for guiding the process design and optimization.

5.1.3. Hydrogen impurity

Another critical challenge is H_2 impurity. In the upstream water electrolysis process, the yield H_2 may contain impurities, which would poison the catalyst in the NH_3 reactor [46]. For NH_3 synthesis, H_2 supplied from the water electrolysis unit shows significantly reduced

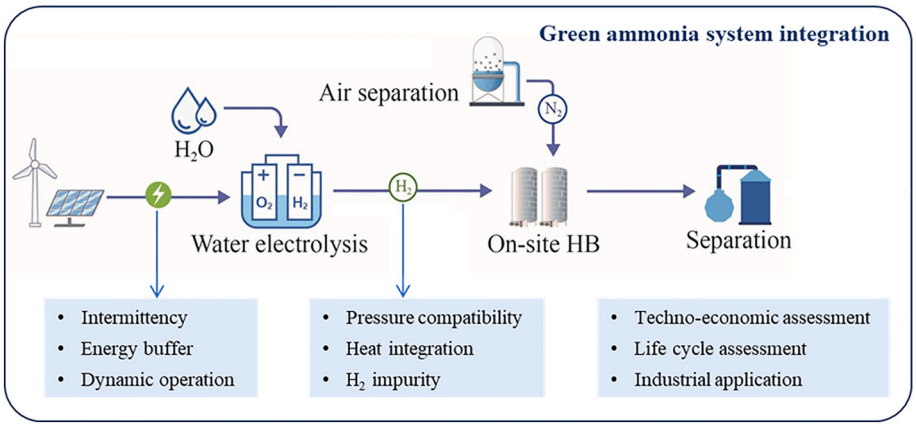

Fig. 20. Key points of the system integration for green ammonia via Gen. 2 route. (For interpretation of the references to color in this figure legend, the reader is referred to the Web version of this article.)

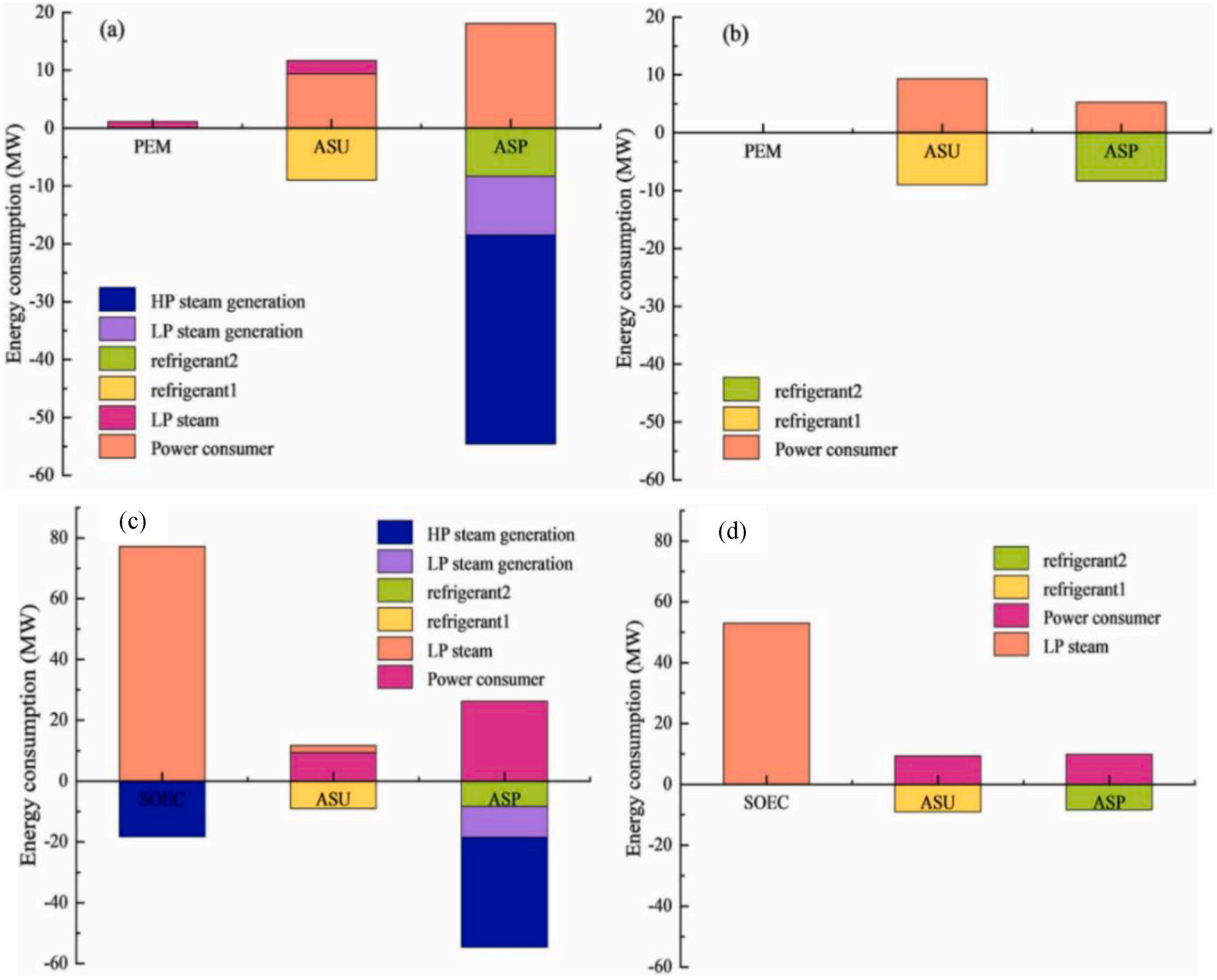

Fig. 21. Energy consumption distribution for PEM-based PtA (a) before heat integration; (b) after heat integration; SOEC-based PtA (c) before heat integration; (d) after heat integration (ASU: Air separation unit, ASP: Ammonia synthesis plant). Reproduced from Ref. [279] with the permission from Elsevier.

impurities compared to the steam reforming process typically used for conventional HB plants, offering a clear advantage for integration. However, small amounts of impurities, such as moisture and O_2, may still persist [281]. Oxygen and water can poison NH_3 synthesis catalysts by forming oxide layers on the catalyst surface, blocking active sites and halting NH_3 production. Initially, NH_3 production spikes due to rapid

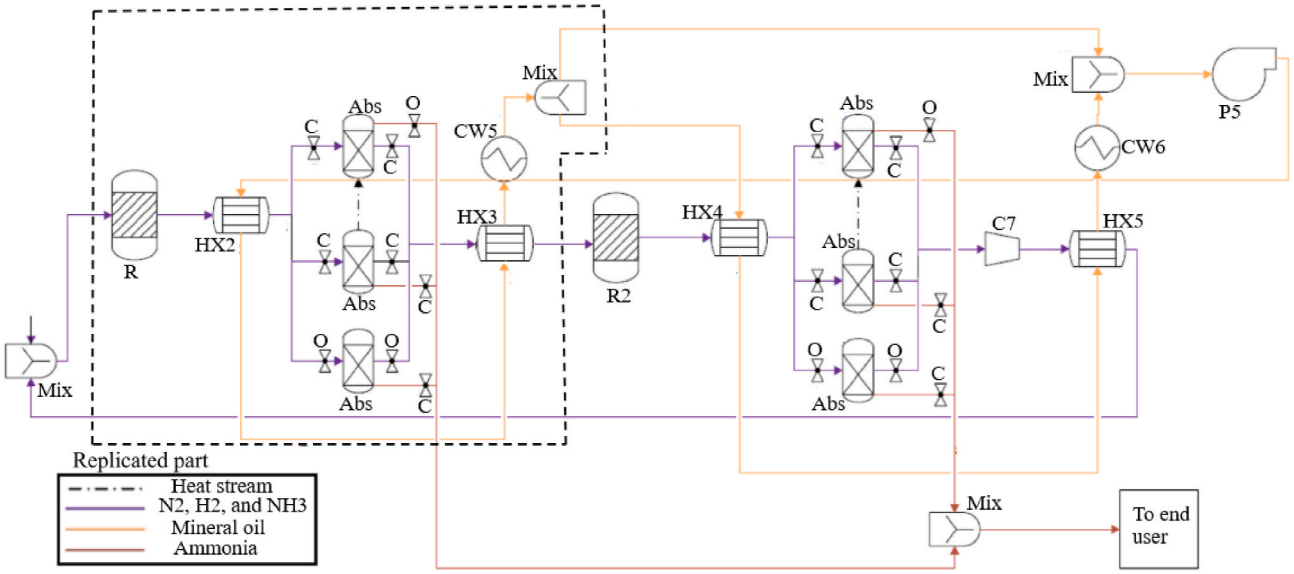

Fig. 22. Diagram of sorption enhanced NH_3 production process flow (Abs: Absorption, R: Reactor, O: Open, °C: Closed, HX: Heat exchangers). Reproduced from Ref. [280] with permission from Elsevier.

surface reorganization, but prolonged exposure results in complete poisoning. Ammonia synthesis typically requires >99.999 mol% pure H_2 and N_2 reactants for safe operation [282], although H_2 from water electrolysis units may fall short of this standard. For instance, Huag et al. observed O_2 impurities in H_2 from ALK electrolyzers ranging from 0.132 mol% to 0.478 mol%, depending on variables such as current density, electrolyte flow rate, and temperature [283]. Bacquart et al. reported that temperature swing adsorption purification in PEM electrolysis systems lowered O_2 impurities to 0.5–2 μmol/mol and water impurities to below 3 μmol/mol [284]. Simulation results in Ref. [285] also indicate that catalyst activity varies significantly with feed gas composition, even at extremely low water content levels below 10 ppm. In addition, moisture also poses a risk to other materials, such as sorbents, if sorption-intensified NH_3 reactors are used in the PtA process. As aforementioned, metal halide-based absorbents are vulnerable to moisture with risk of releasing HCl. Developing catalysts with a high impurity tolerance for NH_3 synthesis remains ongoing; thus, H_2 purification is essential when integrating water electrolysis with NH_3 synthesis processes, and cryogenic ASU is preferred for producing high-purity N_2.

To summarize, the integration of water-splitting H_2 production and NH_3 synthesis presents challenges due to the differing operational conditions of the involved processes. Heat integration, purification, pressure management, and temperature control are critical for optimizing system efficiency and ensuring economic feasibility. Advanced heat recovery and integration are key to improving the overall process, providing significant opportunities for process optimization. Increasing the availability of low-cost renewable energy, along with further optimization of electrolyzer technologies, will be crucial in making NH_3 production more competitive and scalable, offering significant potential for cost reduction and improving energy efficiency.

5.2. System intermittency and dynamic operation

The second critical challenge of the PtA process arises from fluctuations in renewable electricity inputs, which significantly affects the operation of key components in the PtA chain, such as the water electrolysis unit, air separation unit (ASU), and NH_3 production reactor. These effects can be categorized into two aspects: 1) reactor start-up and shutdown, and 2) load variation during operation, depending on the different fluctuation modes of renewable electricity [59]. The frequent start-stop and load-varying operation will result in system inefficiency, longevity and safety problems for PtA processes.

If the PtA process is fully powered by off-grid renewable energy, frequent start-ups and shutdowns may occur. However, the required response times for these operations vary in orders of magnitude across different units. For example, the start-up time for a PEM electrolyzer is on the scale of minutes [286], while for a cryogenic ASU, it is of the order of hours (also differs from cold start-up and warm start-up). In general, although a mildly operated NH_3 reactor has relatively short response time for start-up, it still requires several tens of hours due to pressurization and purification pretreatments. In addition, water electrolysis cells are sensitive to the shutdown and idle phases, which may accelerate their degradation [287]. Consequently, under highly intermittent renewable electricity, the PtA process might never fully start up if it must shut down before all reactors are operational. In this case, the PtX process imposes specific requirements on the intermittency of renewable energy, implying that not all sources can be directly coupled to PtX processes. If the process is (partially) powered by grid electricity, a much faster response time is required to meet the grid demand, typically on the millisecond to second scale. It is particularly important for large-scale PtA process deployment. Currently, achieving such rapid

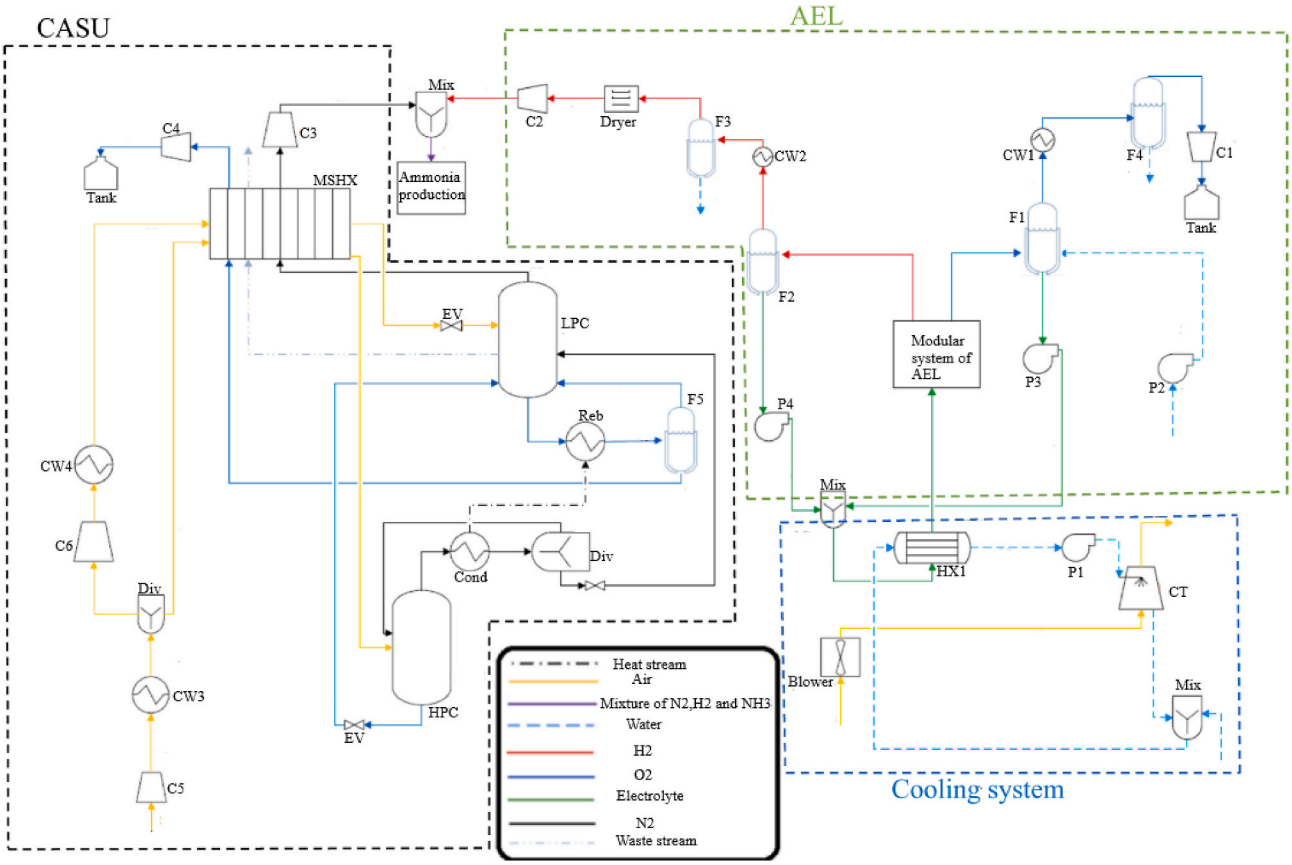

Fig. 23. Diagram of overall NH_3 production process flow (AEL: Alkaline electrolysis, CASU: Cryogenic air separation unit, F: Flash, CT: Cooling tower, HPC: High pressure column, LPC: Low pressure column, C: Compressor, Reb: Reboiler, Cond: Condenser, EV: Expansion valve, MSHX: Multi-stream heat exchanger, CW: Cooling water, HX: Heat exchanger, P: Pump, Mix: Mixer, Div: Divider). Reproduced from Ref. [280] with permission from Elsevier.

response times remains a significant challenge, which sets demands of efforts from the control and optimization side for multi-energy or hybrid energy PtA systems [288].

On the other hand, the key components in PtX systems must dynamically respond to load variations from renewable sources. Each unit generally operates within a defined load range to maintain safe and efficient performance. Amongst, electrolyzers demonstrate significant flexibility in load-varying operations. For example, PEM electrolyzer can operate across a broad load range from 0 % to 160 % of its nominal capacity [59]. Advanced NH_3 reactors can function from as low as 10 %–100 % of nominal load [289]; however, sustained operation at very low loads is generally avoided to prevent efficiency losses and potential catalyst degradation. By comparison, ASUs are limited to a narrower load range of 60 %–100 % of nominal capacity, primarily due to the operational stability required in cryogenic processes. Another important factor in dynamic operation is the ramping rate, as high-pressure and extreme thermal conditions necessitate careful control to prevent stress on reactors. PEM electrolyzers exhibit rapid ramp rates, up to 3.3 % per second and as high as 10 % per second of the standard load in some industrial applications [286], making them highly responsive to fluctuations in renewable energy input. Conversely, NH_3 production units operate with slower ramp rates, typically around 20 % per hour [290], due to the thermal inertia and sensitivity of the catalytic processes involved. From a flexibility standpoint, PEM electrolyzers are superior, outperforming ALK and SOE electrolyzers, and are promising for PtA processes. Effective control strategies are essential to achieve a reliable and efficient PtA process under load-varying conditions, underscoring the importance of integrated dynamic control in flexible Power-to-X applications.

5.2.1. Energy buffer system

To address the dynamic behavior due to renewable energy inputs, two strategies can be implemented: (1) mitigating fluctuations through intermediate energy buffers (e.g., batteries and/or H_2 storage), or (2) developing fully flexible reactors for both H_2 production and NH_3 synthesis that can adapt to varying electricity inputs. Implementing these strategies yields three types of PtA processes, as depicted in Fig. 24.

Generally, storing renewable electricity in batteries or liquid H_2 buffer vessels is costly, significantly increasing the production cost of NH_3, and it is limited by the storage capacity of the buffer. Fig. 25 illustrates three types of energy buffers applicable in PtX systems, contrasts H_2 storage buffers with two types of battery systems, i.e., lithium-ion and Carnot batteries, in terms of energy storage characteristics [291].

In a battery-assisted system, fluctuations in renewable energy can be effectively mitigated at the outset, enabling the entire PtA process to operate in a static or smooth mode [292]. This approach benefits from a high overall efficiency of approximately 95 %, rapid response times, and flexibility in power supply, making it ideal for scenarios that require swift adjustments to energy output. However, significant drawbacks for large-scale applications include limited storage capacity, higher costs, and environmental impacts such as manufacturing emissions and hazardous material leakage in the end-of-life management. Conversely, the H_2 buffer-plugged system, potentially complemented by a N_2 buffer, necessitates that the electrolysis unit operates in tandem with electricity fluctuations, while the downstream NH_3 reactor can function steadily [293]. This 'partially flexible' system is highly feasible, owing to the rapid dynamic behavior of electrolysis stacks. It is inherently suited for larger-scale processes that require substantial energy buffering over relatively longer durations. The study reported in Ref. [275] projects that by 2040, H_2 storage will account for approximately 7 % of the total CAPEX of a NH_3 production system. Nevertheless, it is important to note that this system remains challenges related to safety risks and lower energy utilization efficiency. Overall, the introduction of additional energy buffers facilitates stable system operation, broadening PtA applicability across diverse renewable energy sources and simplifying control processes. While this approach shows promise in specific cases, such as isolated PtA systems exclusively relying on renewable energy, its implementation for large-scale e-NH_3 production is constrained by buffer limitations, high costs and safety risks.

5.2.2. Dynamic operation

An alternative approach involves dynamically operating all major system components in response to intermittent energy inputs, eliminating the need for energy buffers. This approach is the most economical, avoiding additional costs associated with batteries or H_2 buffers, and is particularly advantageous for large-scale NH_3 production. However, fully flexible operation may reduce the capacity factor, lower the efficiency, affect product quality, or increase wear on critical units. This mode of operation imposes constraints on heat and mass integration at the process scale, potentially compromising system robustness and reliability. Thus, fully flexible operation is feasible only under specific conditions, for instance, it requires a relatively stable energy supply with limited fluctuations, ideally avoiding the shutdown of essential PtA components. In some cases, connection to the grid as a backup energy source can stabilize operations. Moreover, real-time control and monitoring systems must be implemented to adjust unit loads precisely with variations in multi-energy input. Highly customized design with complicated control strategies is the unique factor for fully dynamic NH_3 production. Given these challenges, research on the development of fully flexible PtA systems remains limited.

Currently, a hybrid approach, combining operational flexibility with energy buffering, displays an effective solution: optimizing the balance between operational flexibility and energy storage capacity. In this approach, NH_3 production is maximized within a dynamic system, while reliance on batteries or H_2 buffers is minimized. The research in Ref. [294] show that H_2 storage costs account for up to 19 % of total production costs when the conventional Haber-Bosch process operates with flexibility constraints during prolonged periods of insufficient energy supply (10-day intervals). Ex-situ and in-situ sorption enhanced NH_3 synthesis units, i.e., sorption-enhanced and single-vessel reactors, have been implemented in a dynamic PtA system, as illustrated in Fig. 26.

The results show that the single-vessel system and absorption-enhanced system with flexible operation achieves superior economic efficiency with minimal storage requirements, especially under high seasonal fluctuations. At smaller scales (100 kW), production costs increase significantly due to the higher relative cost of electrolyzers and storage. The research underscores a critical transition from maximizing energy efficiency to minimizing costs in renewable-powered systems, highlighting the need for varying scales and energy dynamics NH_3 production processes designed for low-pressure operation, agility, and reduced capital costs.

5.3. Assessments

To ultimately achieve green NH_3 production through the integration of thermocatalytic NH_3 synthesis with water electrolysis, a techno-economic assessment (TEA) and life cycle assessment (LCA), must be conducted. This necessitates the incorporation of diverse impact categories in TEA and LCA. For instance, while solar or wind energy systems effectively reduce greenhouse gas (GHG) emissions, they may also lead to other environmental issues, highlighting the importance of holistic assessment strategies. The rapid advancements in H_2 production with renewable energy technologies result in frequent updates to cost and efficiency data, leading to significant variability in TEA and LCA results for NH_3 production and PtA processes over short time frames. Consequently, this paper focuses exclusively on work recently published, primarily within the past five years. And it presents and compares advanced assessment methods, standards, results, and conclusions, followed by a summary of the current status.

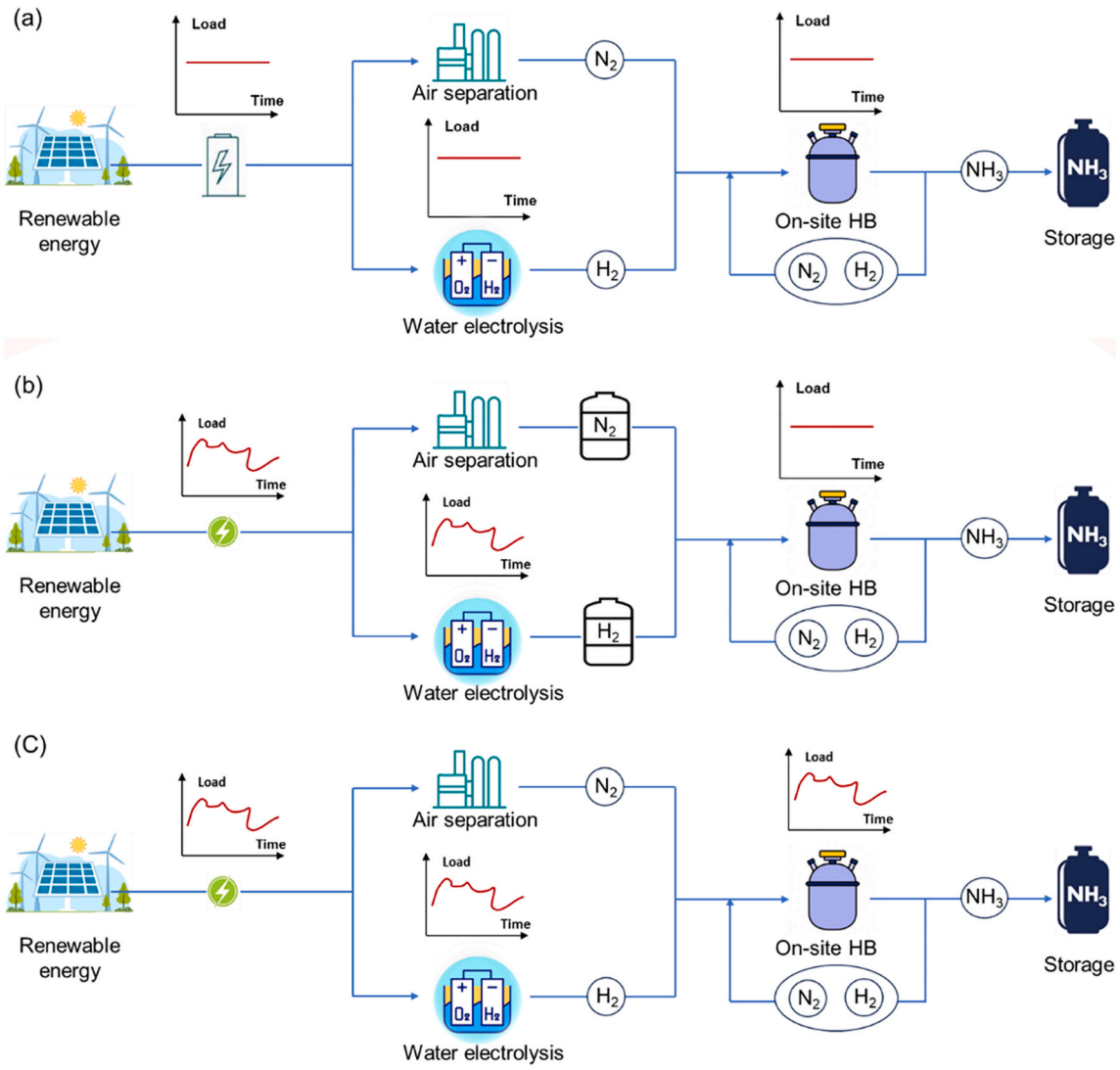

Fig. 24. System types of NH_3 synthesis integrating with intermittent renewable energy.

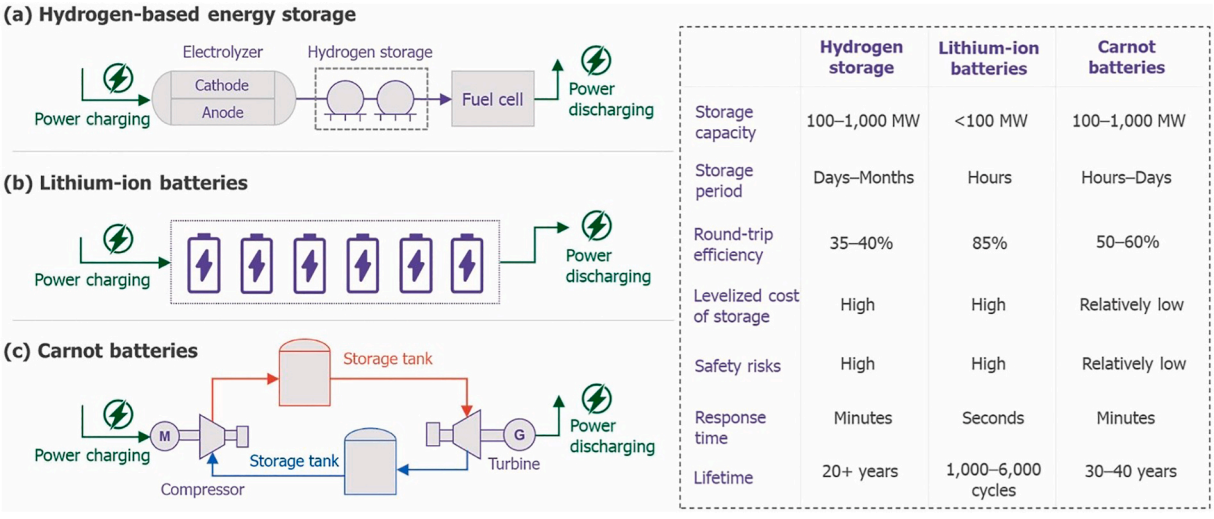

	Hydrogen storage	Lithium-ion batteries	Carnot batteries
Storage capacity	100–1,000 MW	<100 MW	100–1,000 MW
Storage period	Days–Months	Hours	Hours–Days
Round-trip efficiency	35–40%	85%	50–60%
Levelized cost of storage	High	High	Relatively low
Safety risks	High	High	Relatively low
Response time	Minutes	Seconds	Minutes
Lifetime	20+ years	1,000–6,000 cycles	30–40 years

Fig. 25. Three types of energy buffers that can be used in PtA processes. Reproduced from Ref. [291] with permission from Elsevier.

5.3.1. Techno-economic assessment

In general, TEA for NH_3 production and PtA plants can be divided into two categories based on the different assessment approaches employed [295]: process modeling and economic analysis (PM) [296], and individual plant models with local energy system integration (ESI) [282]. The first category relies on a process model that accounts in detail for components, integration and mass and heat balances, typically assuming a fixed electricity supply with a constant price. As a result, these plants are evaluated under steady-state operating conditions [297]. In contrast, the second category addresses the intermittency and price variations of energy supply, leading to an assessment of plants operating in a flexible mode with intermediate energy buffers, such as batteries or H_2 tanks [290]. Both types of TEA for NH_3 production have specific applicable scenarios, fostering the further development of PtA technologies. For the PM-type assessment, Zhang et al. developed a multi-objective techno-economic optimization method using the OSMOSE platform to analyze the performance of PtA and compare it with biomass-to-NH_3 (BtA) and traditional methane-to-NH_3 (MtA) processes [278]. All systems are assumed to have a fixed production scale of 50 kton of NH_3 per year, with additional cost assumptions detailed in the paper. The analysis considers system efficiency, levelized cost of NH_3 (LCOA), and investment payback time. Results indicate a trade-off between system efficiency and NH_3 production cost; increasing system efficiency correlates with higher production costs. For PtA, the system achieves the highest efficiency of 75 % but incurs the highest production cost of over $550/ton, with a payback period of five years. Fig. 27 compares the investment (a), operational costs (positive values) and revenues (negative values) (b) across all cases. The results show that PtA process performs best in revenue and lowers investment than BtA process, highlighting the future competitiveness of the PtA process.

In [298], a TEA of the energy supply chain utilizing NH_3 has been conducted, incorporating Aspen Plus process simulations that include ASU, NH_3 synthesis, and water electrolysis. Three scenarios, i.e., current, near future, and sustainable future, were evaluated, revealing that 11.044 to 9.349 MWh of renewable electricity will be required in exporting countries to produce 1 ton of NH_3. The detailed costs for the future scenario are illustrated in Fig. 28, based on an assumed electricity price of $15/MWh.

Another optimistic TEA study for future PtA systems based on PEM or SOE technologies have been reported in Ref. [279]. The projected NH_3 production costs in future will decrease to $359.7/t NH_3 and $343.5/t for PEM-PtA and SOEC-PtA processes, respectively, assuming the implementation of carbon tax and renewable electricity price down to 0.014 $/kWh. By comparison, conventional HB processes yield production costs ranging from $403.1 to $514.7/t NH_3, highlighting the significant economic advantages of these emerging methods and their promising potential for further development. The performance of different NH_3 synthesis processes, current versus future, are shown in Fig. 29. The PEM- and SOEC-based ammonia synthesis routes are recognized as equally promising technologies based on the key performance metrics: element utilization rate, energy efficiency, capital investment, and carbon emission.

Moreover, the assessment in Ref. [277] reveals the sensitivity of e-NH_3 production costs to electricity prices. Specifically, it shows that electricity prices below $12.50/MWh would render e-NH_3 production economically viable. Alternatively, to make e-NH_3 production comparable to the benchmark Haber-Bosch process, a carbon tax of $210.80 per ton of CO_2 or a charge of $135.80 per ton of carbon emissions on the fossil fuel-based Haber-Bosch process would be necessary. Nonetheless, these studies are conducted within the PM framework, which does not account for the dynamic behavior of the PtA process, where an energy storage buffer (battery or H_2 tank) may be necessary. Hence, the resulted conclusions in terms of LCOA and efficiency are interpreted as optimistic results.

On the other hand, there are assessment investigations that consider the intermittency of integrated energy systems, specifically EIS-type TEA. For example, Bouaboula et al. developed a techno-economic model for a pilot-scale (4 t/d) NH_3 plant that includes an energy storage system comprising batteries and thermal energy storage (TES) [292]. To manage the load of the Haber-Bosch unit, the model applied a

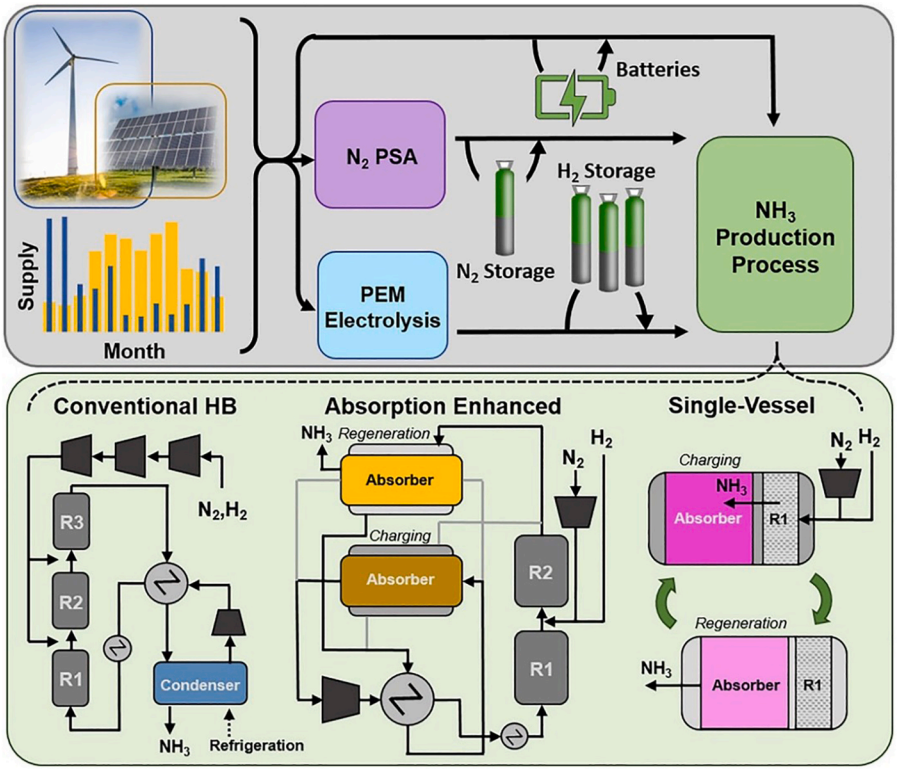

Fig. 26. Schematic of NH_3 production from solar and wind energy. Reproduced from Ref. [294] with permission from Elsevier.

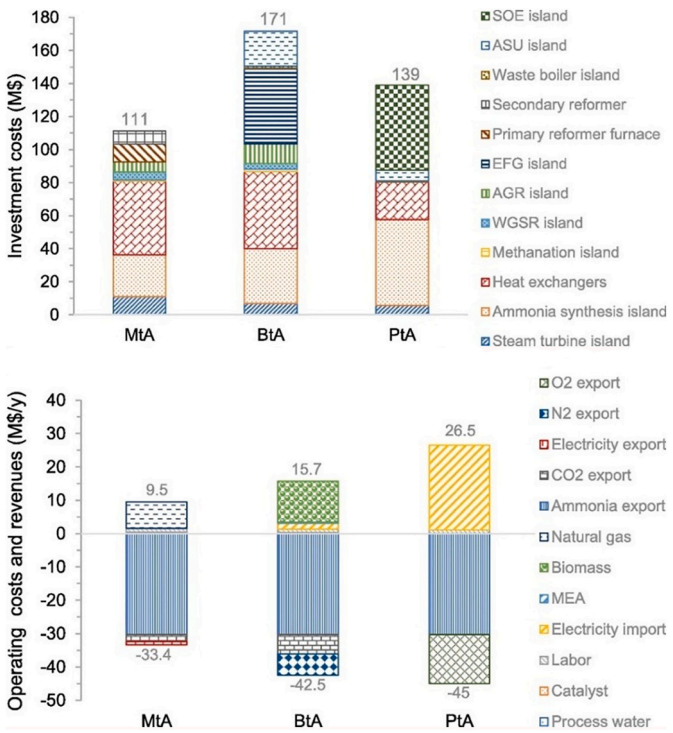

Fig. 27. Comparison of investment (a), operational cost (positive value) and revenues (negative value) (b) for MtA, BtA and PtA systems. Reproduced from Ref. [278] with permission from Elsevier.

novel Energy Management Strategy (EMS) to optimize renewable power allocation for charging and discharging the Energy Storage Systems (ESS).

The results indicate that the cost of NH_3 production in this scenario is \$774/t NH_3, with the major contributors being batteries, photovoltaics (PV), and electrolyzers contributing 39 %, 33 %, and 22 % of the cost, respectively. However, the LCOA is could decrease in the future, reaching \$250/t NH_3 by 2050, as shown in Fig. 30, based on the economic assumptions listed in Table 8 for the major components PV panel, battery and electrolyzer stack. The study also recommends the use of advanced Haber-Bosch processes as alternatives to conventional methods, enhancing the system's flexibility to accommodate the intermittent nature of renewable sources.

Similarly, Wang et al. conducted a TEA case study for evaluating the economic viability for partially flexible NH_3 production in Australia [299]. The system utilizes off-grid power, specifically wind and solar, along with batteries and H_2 buffers to address the intermittency of wind and solar electricity. As illustrated in Fig. 31, the study compares the LCOA across different scenarios: powered solely by wind, solely by solar, and utilizing a hybrid of both resources. The results demonstrate the

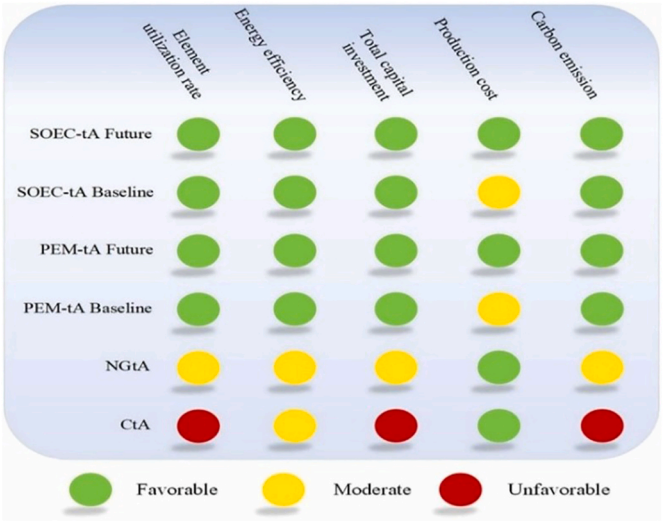

Fig. 29. Comparison of the comprehensive performances for different NH_3 synthesis. Reproduced from Ref. [279] with permission from Elsevier.

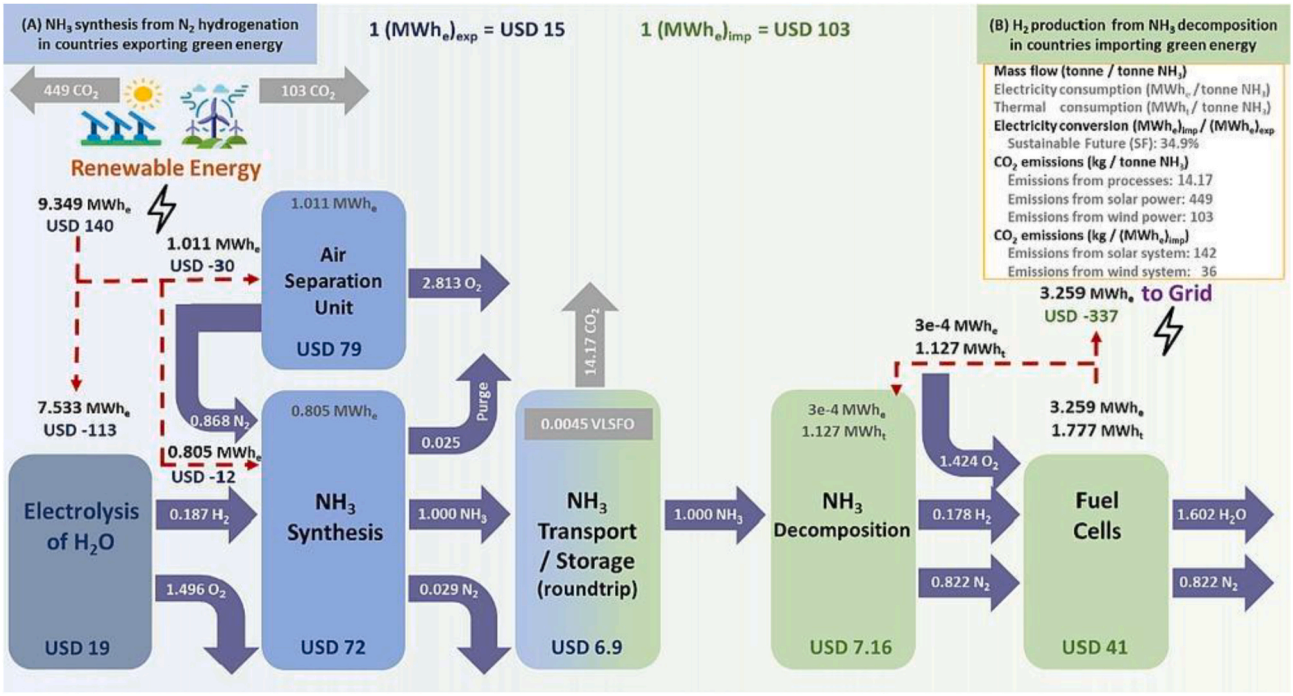

Fig. 28. Comprehensive analysis of economic evaluation, material balance, and energy consumption of NH_3 energy supply chain in sustainable future scenario. Reproduced from Ref. [298] with permission from Elsevier.

advantages of integrating wind and solar sources and employing a flexible operational strategy. The investigation reports the LCOA for 2025 and 2030 as AU$756/ton ($500/ton) and AU$659/ton ($436/ton), respectively. By 2030, this would be economically competitive with grey NH_3, assuming a natural gas price exceeding AU $14/MBtu and a carbon price of at least AU$123/ton.

Campion et al. developed an open-source TEA model tailored for dynamic PtX plants, optimizing investment and operational costs based on varying power profiles and hourly grid electricity price [295]. The modeling results indicate that a combination of local energy and a grid connection (semi-islanded setup) is the most cost-effective option, achieving a cost reduction of up to 23 % compared to off-grid systems, though it results in GHG emissions. The model also demonstrates that a flexible NH_3 plant significantly reduces fuel costs. For fully off-grid systems, estimating costs using the levelized cost of electricity and capacity factors to derive operational hours can lead to cost overestimations of up to 30 % compared to optimization methods, as potential savings from complementary power sources or intermediate storage are not accounted for. The most economical off-grid configuration achieves production costs of €842/ton ($996/ton), whereas the prices for grey NH_3 were €250/ton ($296/ton) in January 2021 and €1500/ton ($1775/ton) in April 2022 in Western Europe. A comparison of NH_3 production costs is presented in Fig. 32, detailing the costs for different modes NH_3 production located in Chile, Denmark, and Australia.

In addition, Osman et al. reported a methodology for the design, cost estimation, and optimization of an industrial scale NH_3 production plant (1840 t/d) in the UAE, powered exclusively by renewable energy [301]. The plant employs batteries and thermal storage to continuously supply the N_2 and H_2 required for NH_3 synthesis, with H_2 generated via seawater desalination followed by electrolysis. Aspen Plus and the Python-based Gurobi Optimizer were utilized to develop the working flow. The cost-optimal configuration includes 3.5 GW of PV capacity and 0.24 GWh of battery storage, achieving approximately 37 % energy efficiency under UAE operating conditions. The estimated LCOA for this base case is $718/ton NH_3, with further reductions anticipated due to expected technical advancements, potentially lowering the cost to $450/ton. According to the IEA's 2021 prediction [6], the levelised cost of PtA is expected to be around $600/ton considering low cost of energy storge solution, although it varies regionally due to the variation of electricity price, as seen in Fig. 33.

In summary, various studies illustrate the current economic status of

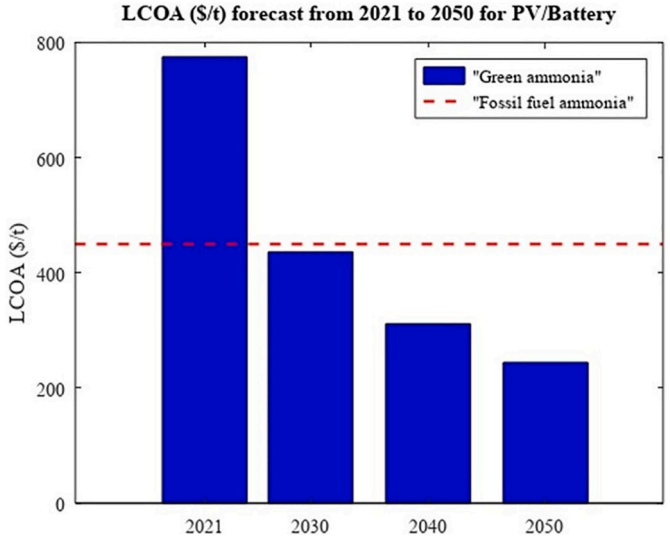

Fig. 30. Forecast of flexible NH_3 production cost. Reproduced from Ref. [292] with permission from Elsevier.

Table 8
Economic assumptions for PV, battery and electrolyzer [300].

Component	Cost	Year			
		2021	2030	2040	2050
PV	CAPEX ($/kW)	590	380	260	205
Battery	CAPEX ($/kW)	132	62	41	34
	CAPEX ($/kW)	264	124	86	34
Electrolyzer	CAPEX ($/kW)	770	540	435	380

NH_3 production under different scenarios that (partially) integrate sustainable energy sources, demonstrating its promising cost-competitiveness compared to conventional Haber-Bosch plants. Flexible operations that incorporate energy storage systems can significantly reduce the levelized cost of NH_3 over time. These findings emphasize the economic potential of advanced NH_3 production, especially with the impending carbon tax, despite current e-NH_3 price being higher than those of grey NH_3. Continued research is essential to address dynamic operational challenges and enhance competitiveness against conventional NH_3 synthesis processes.

5.3.2. *Life cycle assessment*

A comprehensive evaluation of environmental impacts in NH_3 synthesis is essential to avoid inadvertently shifting burdens onto human health and ecosystems. However, literature on LCAs that encompass the entire cradle-to-gate or cradle-to-grave spectrum of NH_3 synthesis remains limited. A mini-review presented in Ref. [302] summarizes methodologies and recent advancements in life cycle studies across all existing NH_3 production processes, providing valuable insights into their environmental sustainability. The mini-review underscores the critical balance between technological innovation, economic viability, and environmental impact. The recent investigations focusing on renewable energy-powered thermocatalytic NH_3 synthesis, which are not covered in the mini-review [302], are as follows.

Bicer et al. conducted an LCA study for a NH_3 production system that integrates a water electrolyzer with the Haber-Bosch process, utilizing various renewable energy sources, including hydropower, nuclear energy, biomass, and municipal waste [303]. The CML 2001 and Eco-Indicator 99 methods were employed to identify and quantify environmental impacts in categories such as global warming potential, human toxicity, and abiotic depletion. The results show that hydropower-based NH_3 synthesis offers the most environmentally favorable option, exhibiting the highest energy efficiency (42.7 %) and an exergy efficiency (46.4 %), along with the lowest GHG emissions of 0.38 kg CO_2-eq per kg of NH_3. In contrast, biomass and nuclear pathways showed higher emissions of 0.85 kg CO_2-eq and 0.84 kg CO_2-eq, respectively, highlighting the need for technological improvements. Notably, municipal waste incineration not only reduces waste but also serves as a sustainable alternative with the lowest global warming potential of 0.34 kg CO_2-eq per kg of NH_3. In a related study by the same author indicates that the nuclear electrolysis-based NH_3 generation method results in the lowest global warming and climate change impacts, whereas coal-based electrolysis options led to significantly greater environmental issues [304]. The greenhouse gas emissions associated with nuclear-based electrolysis are calculated at 0.48 kg CO_2 equivalent, in stark contrast to 13.6 kg CO_2 per kg of NH_3 produced using the coal-based electrolysis method. Moreover, the GHG emissions from various NH_3 production pathways, i.e., based on ALK electrolysis, PEM electrolysis, and SOE integrated with the HB process, have been compared to those of the conventional HB process, in Ref. [305]. According to Fig. 34, the corresponding CO_2 emission ranges for NH_3 production using ALK, PEM, and SOE water electrolysis are 0.83–0.93, 0.82–0.99, and 0.69–0.72 kg CO_2/kg NH_3, respectively, depending on the efficiency range from worst-to best-case scenarios. These represent average reductions of 2.46 × , 2.42 × , and 3.07 × times compared to the conventional HB process. The potential of SOEC-integrated NH_3

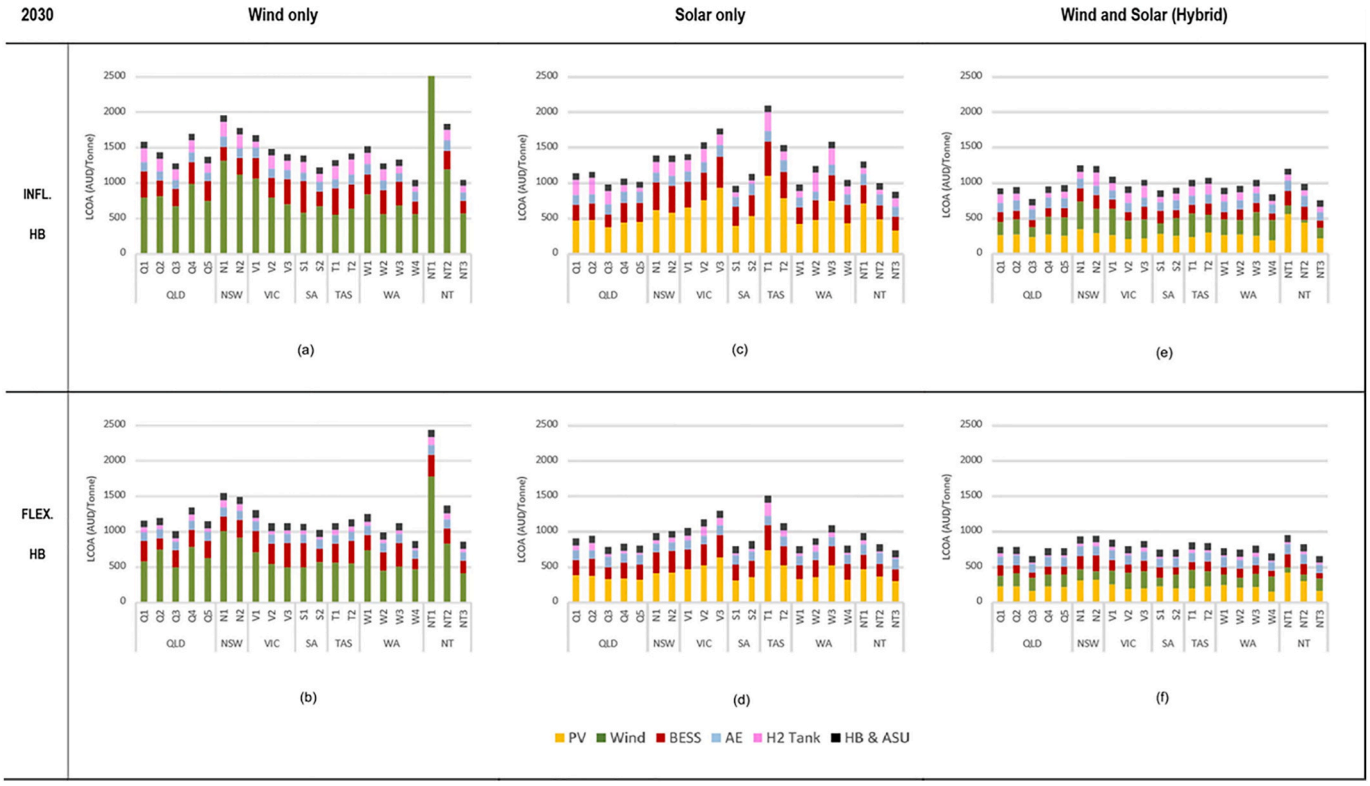

Fig. 31. LCOA based on the CAPEX assumptions in 2030 for scenarios with wind, solar and a hybrid wind and solar system (Horizontal axial abbreviations represent states of Australia). Reproduced from Ref. [299] with permission from Elsevier.

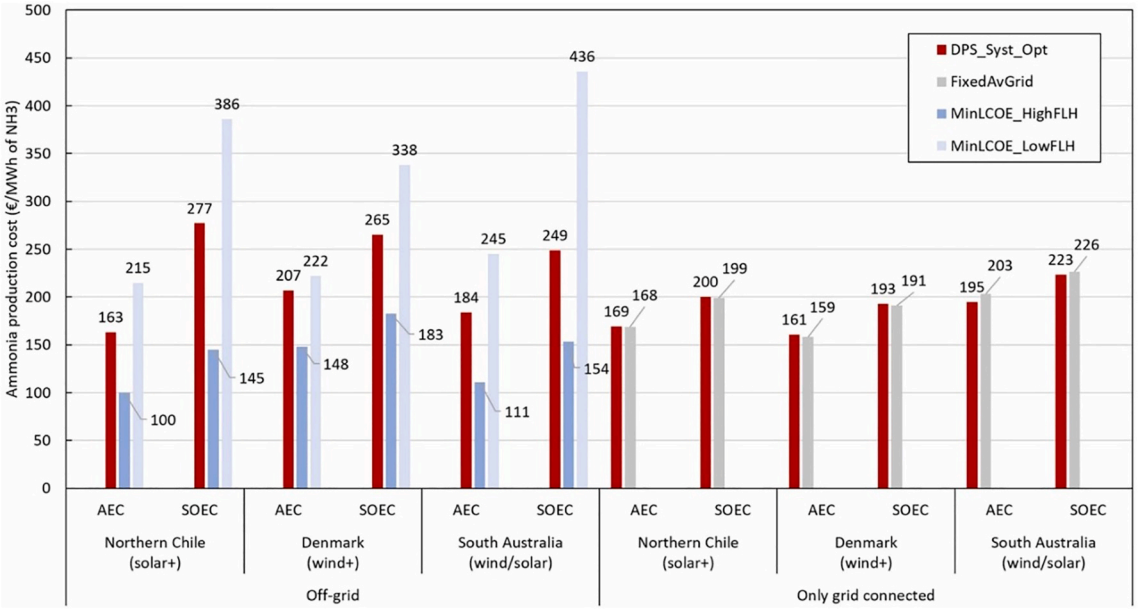

Fig. 32. Ammonia production costs comparison: only grid connected vs. off-grid scenarios. Reproduced from Ref. [295] with permission from Elsevier.

synthesis is further emphasized in LCA, highlighting its relatively lower carbon footprint.

Chisalita et al. conducted an environmental assessment of conventional and emerging H_2 production routes integrated with NH_3 synthesis in Europe, employing the ReCiPe impact assessment method [306]. Mass and energy data from the process model were used as inputs for the analysis. The results indicate that the NH_3 synthesis route achieves a Global Warming Potential (GWP) reduction exceeding 85 % compared to the conventional method. Furthermore, by replacing the H_2 supply chain, the environmental burden of NH_3 production can be reduced by approximately 40 % of total emissions, along with a 15 % reduction in total energy consumption. In Ref. [307], various NH_3 production pathways have been evaluated addressing their cradle-to-plant-gate fossil energy use and GHG emissions. Among the alternative pathways, souring N_2 via cryogenic distillation and H_2 from low-temperature electrolysis powered by renewable electricity results in the lowest

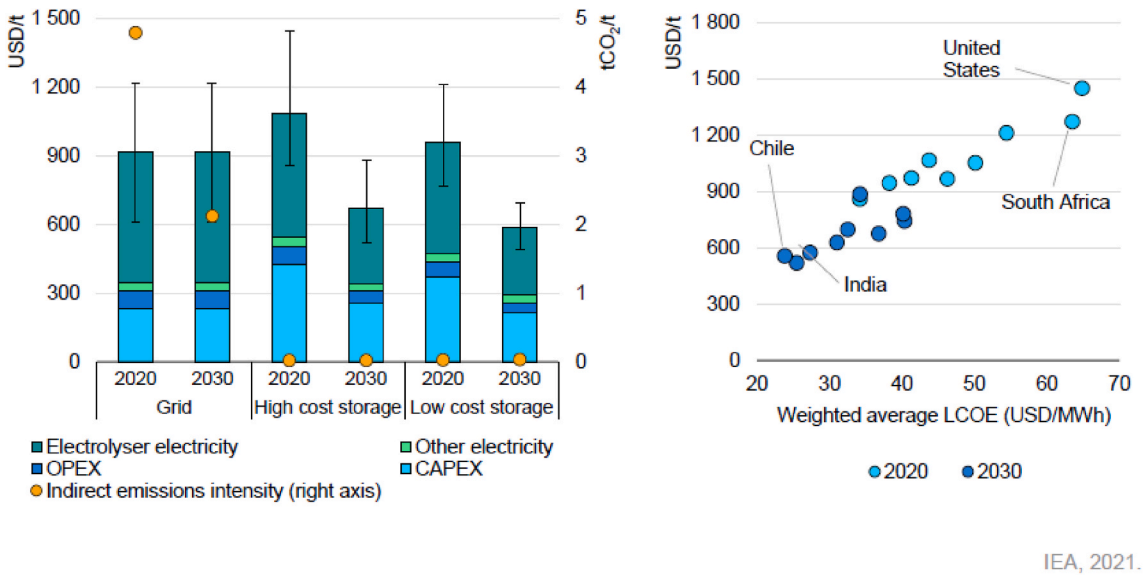

Fig. 33. Levelised cost of electrolytic NH_3 and electricity production. Reproduced from Ref. [6] with permission from International Energy Agency.

cradle-to-plant-gate GHG emissions, representing a 91 % reduction compared to the conventional steam methane reforming. However, integration of energy storage solutions to mitigate the intermittency of renewable electricity may negatively impact the economic feasibility of low-carbon NH_3 production, highlighting the critical importance of flexible operations once again. Lee et al. also compare the NH_3 production route with carbon capture in the United States, achieving a 55–70 % reduction in GHG emissions [308]. However, the effectiveness of NH_3 production depends on various regional factors, including market demands and the availability of renewable energy. Therefore, a regional analysis is recommended to accurately assess the life cycle emissions of different NH_3 production technologies. The most recent LCA study on PtX has highlighted the potential of NH_3 as the terminal electro-fuel, reporting the highest negative GWP of −7.55 kg CO_2-eq compared to methanol, methane and liquid H_2 [309].

To sum up, many existing studies have utilized a cradle-to-gate system boundary, focusing solely on the manufacturing phase of NH_3 production. There is a strong incentive for LCAs with broader boundaries, such as cradle-to-grave analyses, to engage comparisons across various NH_3 production processes. Additionally, challenges arise from data quality and allocation rules in LCA, which involve distributing responsibility for resource consumption, emissions, and waste streams. The IEA report [6] forecasts future CO_2 emissions and energy consumption for various production routes, as illustrated in Fig. 35. To ultimately achieve net-zero emissions, more comprehensive LCA research with a thorough uncertainty analysis is essential, particularly for the water electrolysis-based processes.

5.4. *On-going green ammonia projects*

Beyond academic efforts, industrial progress is also remarkable, leading to the launch of several PtA projects coordinated by industrial stakeholders. There has been a rapid increase in the number of announced PtA projects in recent years. The existing and announced projects for near-zero-emission NH_3 production until 2021 have been statistically summarized by IEA in terms of production capacity (metric tons), as displayed in Fig. 36. The figure illustrates both on-going and planned projects for near-zero-emission NH_3 production, focusing on two main technologies: electrolysis and carbon capture and storage (CCS). From 2015 to 2025, there has been a significant increase in projects announced, especially in electrolysis, with a projection of up to 4 million tons of NH_3 by 2030, indicating a high potential in green NH_3 production. Overall, the data reveal a promising trajectory in the development of NH_3 production methods, highlighting the shift towards renewable energy sources and innovative production techniques.

In the past few years, NH_3 projects have surged globally, advancing the commercialization of renewable NH_3 synthesis. Europe and China are the leading players in this sector, conducting a substantial number of

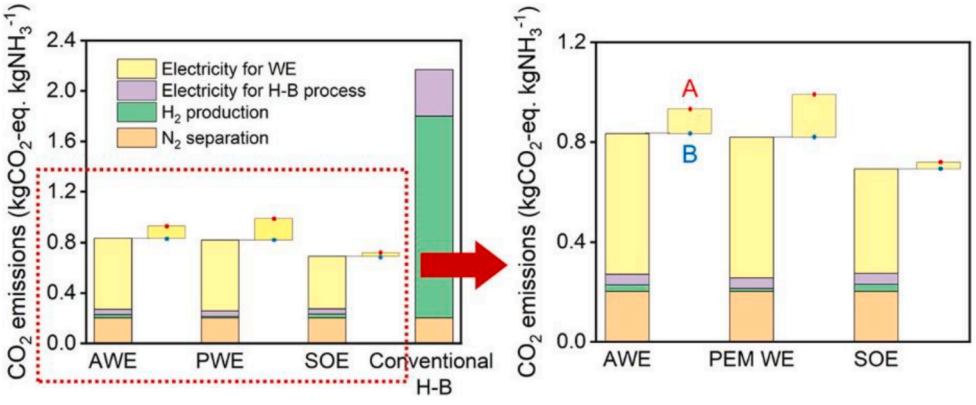

Fig. 34. CO_2 emissions of NH_3 synthesis for various production pathways: water electrolysis HB process using ALK, PEM, and SOE, and conventional HB process. Reproduced from Ref. [305]with permission from American Chemical Society.

projects and production capacities ranging from 5000 t/y to 1.6 million t/y. The primary energy sources for these projects are solar and wind, with one project utilizing hydropower. Recent initiatives have increasingly emphasized dynamic behavior and flexible operation, particularly in smaller-scale plants. Most of the projects announced are currently under construction, warranting continued monitoring of their progress and implementation status. Table 9 summarizes the key features of the newly released green NH_3 projects since 2021, thanks to the information reported by Ammonia Energy Association. All listed projects are water electrolysis-based ammonia plants; however, their energy sources are not exclusively from renewables, as some projects are grid-connected.

The recently announced NH_3 projects signify a substantial shift toward sustainable NH_3 production, primarily powered by renewable energy sources like solar and wind. These initiatives showcase a growing trend in decarbonization and process innovation within the NH_3 sector. However, achieving full sustainability and net-zero emissions requires progress across several critical technological milestones, as outlined in Table 10. Current bottlenecks include advancements in water electrolyzer capacity, H_2 production scalability, and carbon capture technologies, which need to be expanded in future to support this transition effectively. Continued investment, research and upscaling in these areas will be essential for overcoming these challenges and fully realize the goals of SDS and NZE.

6. Challenges and opportunities

While promising advancements in NH_3 synthesis via advanced thermocatalytic technology are underway, these efforts remain insufficient. Greater contributions are needed from a wide range of stakeholders worldwide to enable NH_3 producers to significantly reduce CO_2 emission and a transition to renewable energy. The major obstacles and opportunities to sustainable NH_3 production from both technological and societal perspectives, are outlined in this chapter.

6.1. Technical challenges and opportunities

To make NH_3 synthesis more sustainable, achieve higher production rates, and ensure compatibility with renewable energy sources, several key technical areas require further research and innovation. Advancements in any of these areas could significantly impact the NH_3 industry by lowering energy requirements, enabling flexible production, and increasing compatibility with variable renewable energy. The following areas represent priority research fronts.

- *Catalysts.* The development of novel catalysts capable of reducing the pressure and temperature requirements for NH_3 synthesis is a critical area of research, given the substantial energy demands of the process. Such advances form the foundation of scalable NH_3 synthesis units, improving their feasibility and efficiency when integrated with renewable power sources. Continuous efforts to invent super active catalysts, e.g., synthesizing NH_3 at temperatures as low as 300 °C and pressures of 50 bar with good production rate, are essential. Supports and promoters play an instrumental role in enabling NH_3 synthesis under these milder conditions. While precious metals like ruthenium demonstrate increased activity at reduced temperatures, their high cost poses challenges for practical application. Consequently, the discovery of alternative materials or solutions that minimize the use of noble metals is essential to achieving stable and economically viable catalysts [325]. Emerging catalysts incorporating materials such as electrides, hydrides, amides, nitrides, oxynitride hydrides, and oxide-supported compounds offer promising alternatives. Furthermore, to facilitate the Haber–Bosch process in localized, small-scale NH_3 production, the development of oxygenate-tolerant catalysts is highly desirable to streamline the PtA process and enhance overall efficiency [40], therefore insight into the catalyst during the reaction is sought after. Modern operando techniques provide experimental input, and it is highly recommended to combine them with computational approaches, capturing the live changes of catalyst and reactor conditions during the process. Sintering of catalyst particles, nitride-based third-generation catalysts bleed N_2 atoms from the bulk, high-temperature and high-pressure surface reconstructions and similar effects require models that can account for changes in the kinetics and surface properties on-the-fly.
- *Process intensification.* Beyond catalyst development, implementing chemical or physical intensifications of reactors, serving as compensatory measures for mild synthesis conditions, is a promising approach to enhancing NH_3 production. Technologies such as sorption-enhanced reactors and catalytic membrane reactors, which intensify the synthesis process by separating product yields, demonstrate significant potential. However, both remain at low TRL, undergoing small-scale to pilot-scale investigations due to several technical challenges [25]. For instance, in-situ sorption-enhanced reactors face a trade-off between the optimal operating temperatures of the catalyst and sorbent, along with material poisoning issues when co-loaded in a single vessel. The development of high-temperature-tolerant absorbents (above 300 °C) that can operate effectively with catalysts is a key step forward. Moreover,

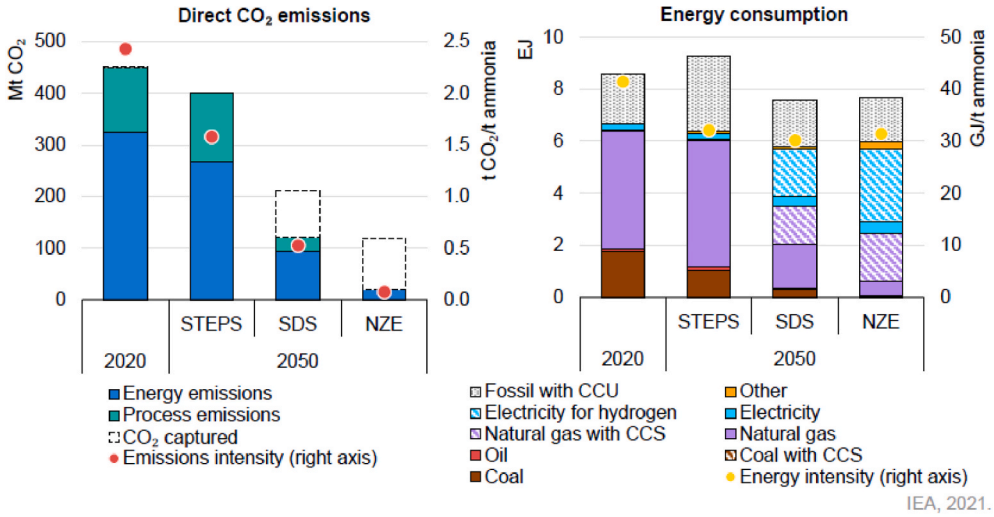

Fig. 35. Direct CO_2 emissions and energy consumption for NH_3 production by scenario. Reproduced from Ref. [6] with permission from International Energy Agency.

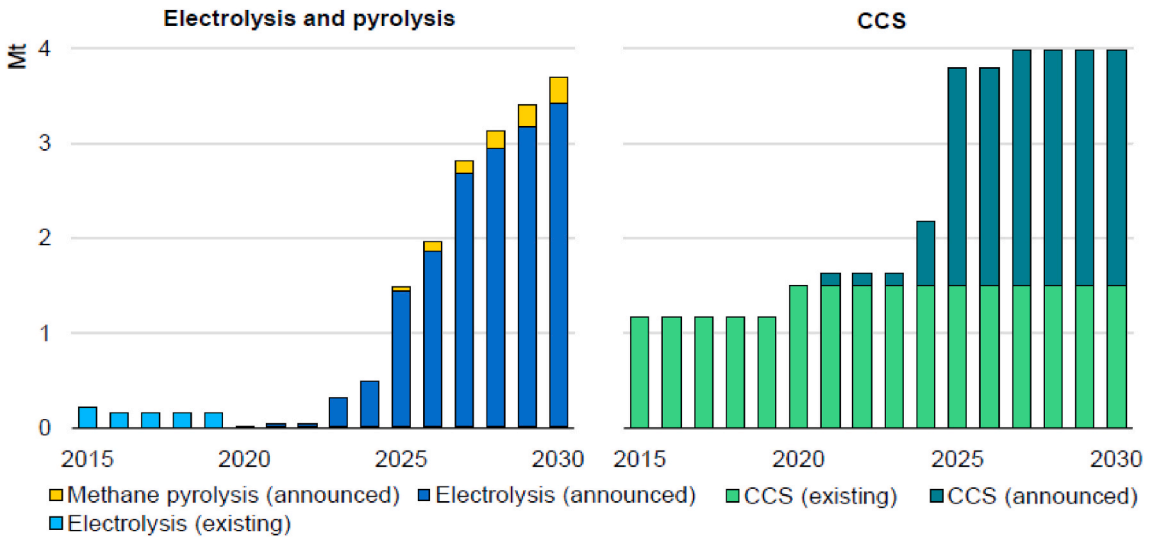

Fig. 36. Current and announced projects for near-zero-emission NH_3 production summarized in 2021. Reproduced from Ref. [6] with permission from IEA.

engineering challenges, such as corrosion caused by using metal halide sorbents, should also be addressed. Consequently, the development of more robust sorbents (or support materials) suitable for practical applications is required. Similarly, high-selectivity membranes that perform under elevated temperatures, while maintaining cost-effectiveness, merit further exploration. To achieve continuous production, efficient desorption processes such as zero-flush NH_3 collection and sorbent recycling, must also be developed. Additionally, heat and mass transfer within the reactor significantly impact catalytic reactions. Macroscopic modeling studies that integrate catalytic reactions, intensification processes, and transport phenomena should be prioritized. Customized reactor design and optimizations need to be conducted based on the models, potentially enhancing mass transfer and increasing residence time. Currently, comprehensive models that bridge atomic-level reactions with macroscale reactor dynamics remain underdeveloped and are an essential avenue for advancing reactor design.

- *Scalability and flexibility.* Traditionally, the NH_3 industry has been dominated by large, centralized plants. However, relocating production units closer to renewable energy sources would reduce dependence on fossil fuel-based NH_3 and support regions where large-scale infrastructure is impractical. Scalability is therefore essential for NH_3 production units that can be integrated with local renewable power systems, further reducing transportation costs. Efficiency and cost are the primary metrics for evaluating NH_3 units across different scales. Heat integration between water electrolysis and NH_3 reactors is believed to be effective to enhance efficiency. On the other hand, to synchronize with renewable energy sources, NH_3 synthesis systems must also operate dynamically to accommodate the intermittent nature of renewables. Batteries and H_2 buffers are effective for stabilizing system fluctuations, though they often come at the cost of economic efficiency. Flexible operation guidelines, derived from high-fidelity simulation, should be created, to 1) maximize NH_3 production and energy utilization, and 2) minimize dependence on energy buffers. Mild operating conditions, with their lower energy requirements, inherently support scalability and flexibility. Thus, focus should be placed on advancing reactor design, system control, real-time simulation, and plant configurations that can adapt to frequent startup and shutdown, load variations, and align with grid and market conditions. Alternatively, the gap between green hydrogen implementation and expectations also hinders the development of NH_3 production [326]. A reliable and cost-effective renewable H_2 source is a fundamental prerequisite for the success of sustainable NH_3 production.

6.2. Societal support

Ammonia synthesis has been developed for over a century, predominantly serving the fertilizer industry. With the advancement of solar and wind energy, NH_3 is expected to play an increasingly vital role in the energy sector, necessitating a shift in production methods. However, at present, NH_3 from renewables is not yet competitive in current markets, which poses challenges to scaling up to industrial production. Societal supports and collaborations are crucial drivers for enhancing the market competitiveness of green NH_3 production. Key focus areas include:

- *Broad collaboration.* The future of NH_3 production depends on collaborative efforts among diverse stakeholders, including policymakers, producers, consumers, technology suppliers, financial institutions, researchers, non-governmental organizations, and others [6]. Timely communication is essential to synchronize research, technological advancements, market needs, and policymaking. Cross-regional cooperation can expedite progress, facilitating necessary technical, economic, and regulatory developments for a sustainable transition in NH_3 production.
- *Renewable energy cost and carbon taxation.* Policymakers shall establish a stable, long-term policy framework to facilitate energy transition and emission reduction. Reducing renewable energy cost is vital for PtA systems, alongside setting standards for electricity quality and integration. Government should also support the establishment of grid connections for NH_3 production plants in specific regions. Additionally, implementing carbon emissions taxes is an effective method to encourage a shift from grey or blue NH_3 production to green. Before this, clear standards for defining 'green' NH_3 should be established [299].
- *Nitrogen use efficiency.* Policies should also elevate the efficiency of N_2 utilization, as the global N_2 cycle is projected to expand significantly. Supportive measures should include ensuring a level playing field for global producers, developing necessary infrastructure, and enhancing data collection and reporting. These efforts will ensure more ecologically responsible use of NH_3-based fertilizers, thereby mitigating the environmental impacts associated with NH_3 consumption.

7. Concluding remarks

Exploring advanced ammonia (NH_3) synthesis under moderate conditions, while maintaining high productivity, is essential for

Table 9
Summary of the recently released Power-to-Ammonia projects.

Project name	Construction Period	Location	Power/H_2 input	Production Capacity	Status	Remarks	Ref.
Unigel's Electrolytic Hydrogen & Ammonia Project	2023–2025	Camaçari, Brazil	3 × 20 MW electrolyser	60,000 tons/year	First phase was operated	- Brazil's first industrial-scale electrolytic H_2 and NH_3 project, with a total investment of $120 million. - Capacity is expected to quadruple to 240,000 tons/year by 2025	[310]
REDDAP Dynamic Renewable Ammonia Plant	2021–2023	Ramme, Denmark	50 MW PV panels & 12 MW wind turbines	50000 tons/year	Inaugurated in August 2024	- Dynamic operation by integrating alkaline electrolysis with renewable energy sources, designed for variable load operation between 10 % and 100 %, with a ramp rate of at least 3 % per minute. - Prevent approximately 8200 tons of CO2 emissions annually.	[311]
Envision Group Renewable Ammonia Project	2023–2029	Chifeng, Inner Mongolia	N.A.	1.5 million tons/year	Initial phase operated	- Flexible renewable NH_3 production facility with direct integration of electrolysers to NH_3 reactor. - Phase 0: pilot plant of 20,000 tons/year, operational by September 2023. - Phase 1: 300,000 tons/y, operational by December 2024. - Phase 2&3: 600,000 tons/y, operational by 2026 and 2029.	[312]
HØST PtX Esbjerg Hydrogen Plant	2021–2029	Esbjerg, Denmark	10 GW offshore wind power	100,000 tons H_2/year and 600,000 tons NH_3/year	All environmental permits have been approved in Q4 2024	- The flexible operation of the plant will adapt to the power supply, utilizing gigawatt-level electrolysis technology. - Waste heat will be harnessed for district heating, benefiting around 15,000 households.	[313]
Oman Project	2023–2027	Karnataka India	5.5 GW solar PV plant	1–1.2 million tons/year	Shipments of equipment began in June 2025	- Th largest facility in terms of green NH_3 production in India.	[314]
Hive Hydrogen and Linde Ammonia Facility	2021–2027	Nelson Mandela Bay, South Africa	N.A.	780,000 tons of NH_3 annually	Solar PV Plant Development Phase was completed in 2025	- Solar energy driven H_2 production with batteries. - First phase will be finished in 2025.	[315]
Mintal Hydrogen Renewable Ammonia Plant	2023–2025	Baotou, China	N.A.	390,000 tons per year	Under construction	- Topsoe's electrolyser plant directly connected to renewable energy generation - Utilizing the region's substantial wind and solar resources.	[316]
Offshore Floating Ammonia Project	2023–2029	Off the coast of Southern Europe	300 MW PEM electrolyzer	300,000 tons annually	Nearing final design in 2025	- Mobile unit, use offshore floating energy. - Products will be used to fuel multiple oceangoing vessels.	[317]
ACWA Power's Project in Uzbekistan	2023–2024	Uzbekistan	N.A.	500,000 tons per year.	Begin producing green hydrogen in 2025	- First Green Ammonia Pilot Project in Uzbekistan. - Utilize H_2 at an existing plant operated by state-owned Uzkimyosanoat	[318]
Green and Low-carbon Advanced Technology Demonstration Projects	2024-	Jilin Province, China	N.A.	600,000 tons per year	Commences operation in 2025	– 1000Nm^3/h ALK electrolyser used. - Produce also e-methanol.	[319]
Project Nujio'qonik	2022-	Newfoundland, Canada	4 GW wind power	1.6 million tons of NH_3	Released from Environmental Assessment in 2024	- Grid connection that enhances the utilization rate of the electrolyzers to 75 %. - FID and Financial Close for Phase 1 in 2025.	[320]
Castellón Green Ammonia and Hydrogen Project	2024–2031	Castellón, Spain	N.A.	800,000 tons of renewable NH_3 annually	Begin Construction in 2025	- More than 2 million tons of CO2 emissions will be avoided. - Facilitate NH_3 storage at the port, with plans to ship the product.	[321]
ATOME's Villeta Project	2023–2026	Paraguay	120 MW electrolyzer	100,000 tons annually	Completion of the environmental and social impact assessment	- Leverage surplus hydroelectric power from the Itaipu dam, grid-connected.	[322]
Hygenco's Green Ammonia Project	2024–2027	Gopalpur, Odisha, India	N.A.	750 tons per day	Received the renewable fuel of non-biological	- Supported by Topsoe's dynamic NH_3 technology, DynAMMO™.	[323]

(*continued on next page*)

Table 9 (*continued*)

Project name	Construction Period	Location	Power/H_2 input	Production Capacity	Status	Remarks	Ref.
CEEC's Songyuan Project	2025–2027	Songyuan, China	3 GW solar and wind energy	600,000 tons annually	origin (RFNBO) pre-certification in 2025 Phase I into the commissioning stage	- Phase one is expected to be in operation by 2027. - China's first gigawatt-scale green hydrogen project - Phase I Project is planned to be put into operation in the second half of 2025, with an annual output of 200,000 tons ammonia. - At end of June 2025, the first phase has reached an overall completion rate of 80 %. - Mainly powered by off-grid electricity, supported by batteries and hydrogen buffer.	[324]

Table 10
Technology milestones of global NH_3 industry for achieving SDS and NZE targets by 2050. Reproduced from Ref. [6] with permission from IEA.

Technology	2020	2030		2050	
		SDS	NZE	SDS	NZE
Reduction in direct CO_2 emissions relative to 2020	–	21 %	25 %	73 %	96 %
Share of production via near-zero emissions route	0.4 %	10 %	12 %	50 %	73 %
Share of production with CO_2 utilized for urea synthesis	23 %	27 %	27 %	25 %	21 %
Hydrogen demand in Mt H_2	33	37	37	41	41
On-site electrolyser capacity in GW	0	29	29	112	171
CO_2 capture for storage in Mt CO_2	2	15	24	91	101
CO_2 capture for utilization in Mt CO_2	130	139	139	107	92

transitioning NH_3 production to be sustainable and positioning it as an energy storage solution. This review provides a comprehensive overview of advanced thermocatalytic NH_3 synthesis approaches beyond the conventional Haber-Bosch process, addressing the major challenges of high energy consumption, carbon emissions, and scalability limitations inherent in the conventional method, and illustrating a vision for NH_3 production in the future. Through a thorough examination of novel catalysts, reaction pathways, reactor intensifications, and renewable system integration, this work highlights the progress and achievements in mild-condition NH_3 thermocatalytic synthesis across various scales, conducting meta-analysis on the specific themes reviewed. The most up-to-date advances are systematically discussed in three primary aspects: catalyst development, reactor intensification, and system integration with sustainable energy sources.

In catalyst development, the foremost innovation lies in the design of new materials capable of effectively operating at reduced temperatures and pressures. Advances in catalyst design leverage the Sabatier principle and computational methods, identifying materials that achieve an optimal balance between N_2 activation and NH_3 desorption. By addressing the rate-limiting nitrogen activation step, recently developed catalysts, including transition metals, non-noble metals, and other innovative materials, are summarized. The effects of supports and promoters are also discussed, amongst which these catalysts exhibit enhanced adsorption and activation properties for N_2 and H_2, creating the possibility of efficiently synthesizing NH_3 under moderate conditions. Additionally, implementation of computational methods such as DFT calculations, microkinetic modeling, and machine learning are summarized alongside the derived mechanisms, reaction pathways, and step conversion rates.

Referring to reactor intensification, this review examines the key obstacles and compensatory techniques for mild NH_3 synthesis reactors, addressing the low production rates and inefficient separation. Emerging separation technologies, such as solid sorption and membrane-based separation, offer energy-efficient alternatives that align well with milder conditions. Solid sorption materials, including physio-sorbents (e.g., MOFs) and chemi-sorbents (e.g., metal halides), as well as NH_3-selective membrane materials, are discussed. Sorption-enhanced reactors and catalytic membrane reactors are presented to highlight the potential of in-situ separation-intensified reactors to accelerate reaction rates by surpassing equilibrium limitations. Reactor-scale modeling studies, including global kinetic models and CFD simulations, are discussed as well, providing predictive tools for optimization of reactor design and performance.

Regarding process integration, this review summarizes the challenges and mitigation strategies associated with integrating NH_3 synthesis and water electrolysis, emphasizing the potential of ammonia as a clean energy carrier. Advanced thermocatalytic processes compatible with H_2 from water electrolysis allow for on-site NH_3 production. Often termed 'Power-to-Ammonia', this integration decouples NH_3 production from fossil fuels, reduces CO_2 emissions, and provides an effective path for utilizing intermittent renewable energy sources. Major challenges, including operational compatibility, heat integration, impurity effects, and fluctuations, are extensively discussed. Mitigation strategies, case studies and comparative analyses are presented along with TEA and LCA, demonstrating PtA's feasibility and impact within Sustainable Development and Net-Zero Emissions scenarios. In addition, recently initiated NH_3 projects are summarized, underscoring industrial efforts to promote technological maturity, scalability, market readiness, and economic viability of NH_3 production.

This review anticipates that the second-generation of NH_3 production, that is incorporating moderate thermocatalytic synthesis and water electrolysis, will become increasingly viable in the coming decades. The advances presented provide a roadmap for transitioning from the high-energy, emission-intensive HB model to more environmentally friendly and efficient processes. Foundational research on catalyst preparation, reaction mechanisms, and process integration establishes the basis for decentralized zero-emission NH_3 production. Addressing key challenges, such as nitrogen activation and NH_3 separation, underscores the transformative potential of advanced thermocatalytic NH_3 synthesis beyond conventional HB paradigm. Further innovations, such as the development of super catalysts, scalability solutions, and operational flexibility, are essential to utilize NH_3 as a clean fuel in the energy sector. Support from policymakers, stakeholders and society will play a crucial role to drive this transformation.

CRediT authorship contribution statement

Tianbao Gu: Writing – review & editing, Writing – original draft, Visualization, Investigation, Formal analysis, Data curation, Conceptualization. **Matej Huš:** Writing – review & editing, Writing – original

draft, Visualization. **Samuel Simon Araya:** Writing – review & editing, Writing – original draft. **Blaž Likozar:** Writing – review & editing, Supervision. **Fausto Gallucci:** Writing – review & editing, Supervision. **Vincenzo Liso:** Writing – review & editing, Writing – original draft, Project administration, Funding acquisition, Conceptualization.

Declaration of competing interest

The authors declare that they have no known competing financial interests or personal relationships that could have appeared to influence the work reported in this paper.

Acknowledgements

This work was supported by the European Union – Horizon Europe [101058643], HySTrAm: Hydrogen Storage and Transport using Ammonia. Matej Huš also appreciates funding from the Slovenian Research and Innovation Agency (ARIS) through project funding N1-0303 and infrastructure funding I0-0039. Blaž Likozar acknowledges support from ARIS core funding P2-0152 and project N2-0291.

The authors would like to express their sincere gratitude to Associate Professor Thomas Condra at Aalborg University for his assistance in thoroughly reviewing and proofreading this paper, which greatly improved its clarity and quality. Special thanks are extended to Ms. Aleksandra Zamljen and Ms. Taja Žibert from the National Institute of Chemistry for reviewing Chapter 4 and proofreading Chapter 3, respectively.

Data availability

The authors are unable or have chosen not to specify which data has been used.

References

[1] Monge-Palacios M, Zhang X, Morlanes N, Nakamura H, Pezzella G, Sarathy SM. Ammonia pyrolysis and oxidation chemistry. Prog Energy Combust Sci 2024;105:101177. https://doi.org/10.1016/J.PECS.2024.101177.

[2] Valera-Medina A, Xiao H, Owen-Jones M, David WIF, Bowen PJ. Ammonia for power. Prog Energy Combust Sci 2018;69:63–102. https://doi.org/10.1016/j.pecs.2018.07.001.

[3] Hermesmann M, Müller TE. Green, turquoise, blue, or grey? Environmentally friendly hydrogen production in transforming energy systems. Prog Energy Combust Sci 2022;90:100996. https://doi.org/10.1016/j.pecs.2022.100996.

[4] Chehade G, Dincer I. Progress in green ammonia production as potential carbon-free fuel. Fuel 2021;299:120845. https://doi.org/10.1016/j.fuel.2021.120845.

[5] Zhang M, Wei X, An Z, Okafor EC, Guiberti TF, Wang J, et al. Flame stabilization and emission characteristics of ammonia combustion in lab-scale gas turbine combustors: recent progress and prospects. Prog Energy Combust Sci 2025;106:101193. https://doi.org/10.1016/j.pecs.2024.101193.

[6] International Energy Agency. Ammonia technology roadmap: towards more sustainable nitrogen fertiliser production. France; 2021.

[7] El-Shafie M, Kambara S. Recent advances in ammonia synthesis technologies: toward future zero carbon emissions. Int J Hydrogen Energy 2023;48:11237–73. https://doi.org/10.1016/J.IJHYDENE.2022.09.061.

[8] Wang M, Khan MA, Mohsin I, Wicks J, Ip AH, Sumon KZ, et al. Can sustainable ammonia synthesis pathways compete with fossil-fuel based haber-bosch processes? Energy Environ Sci 2021;14:2535–48. https://doi.org/10.1039/d0ee03808c.

[9] Wang B, Li T, Gong F, Othman MHD, Xiao R. Ammonia as a green energy carrier: electrochemical synthesis and direct ammonia fuel cell - a comprehensive review. Fuel Process Technol 2022;235:107380. https://doi.org/10.1016/J.FUPROC.2022.107380.

[10] Vu MH, Sakar M, Do TO. Insights into the recent progress and advanced materials for photocatalytic nitrogen fixation for ammonia (NH_3) production. Catalysts 2018;8:621. https://doi.org/10.3390/catal8120621.

[11] Hosseini H. Dielectric barrier discharge plasma catalysis as an alternative approach for the synthesis of ammonia: a review. RSC Adv 2023;13:28211–23. https://doi.org/10.1039/d3ra05580a.

[12] Zhang Y, Niu J, Chen S, Chen Y, Chen H, Fan X. Ammonia synthesis by nonthermal plasma catalysis: a review on recent research progress. J Phys D Appl Phys 2024;57. https://doi.org/10.1088/1361-6463/ad4717.

[13] Bicer Y, Dincer I. Electrochemical synthesis of ammonia in molten salt electrolyte using hydrogen and nitrogen at ambient pressure. J Electrochem Soc 2017;164:H5036–42. https://doi.org/10.1149/2.0091708jes.

[14] Xu G, Liu R, Wang J. Electrochemical synthesis of ammonia using a cell with a nafion membrane and SmFe0.7Cu0.3-x Ni x O3 (X = 0-0.3) cathode at atmospheric pressure and lower temperature. Sci China B Chem 2009;52:1171–5. https://doi.org/10.1007/s11426-009-0135-7.

[15] Duan G, Chen Y, Tang Y, Gasem KAM, Wan P, Ding D, et al. Advances in electrocatalytic ammonia synthesis under mild conditions. Prog Energy Combust Sci 2020;81:100860. https://doi.org/10.1016/J.PECS.2020.100860.

[16] Izelaar B, Ramdin M, Vlierboom A, Pérez-Fortes M, van der Slikke D, Sajeev Kumar A, et al. Techno-economic assessment of different small-scale electrochemical NH3 production plants. Energy Environ Sci 2024. https://doi.org/10.1039/d4ee03299c.

[17] Peng P, Chen P, Schiappacasse C, Zhou N, Anderson E, Chen D, et al. A review on the non-thermal plasma-assisted ammonia synthesis technologies. J Clean Prod 2018;177:597–609. https://doi.org/10.1016/j.jclepro.2017.12.229.

[18] Zhang J, Li X, Zheng J, Du M, Wu X, Song J, et al. Non-thermal plasma-assisted ammonia production: a review. Energy Convers Manag 2023;293:117482. https://doi.org/10.1016/J.ENCONMAN.2023.117482.

[19] Zhang S, Zhao Y, Shi R, Waterhouse GIN, Zhang T. Photocatalytic ammonia synthesis: recent progress and future. Energy 2019;1:100013. https://doi.org/10.1016/j.enchem.2019.100013.

[20] Wang Q, Guo J, Chen P. Recent progress towards mild-condition ammonia synthesis. J Energy Chem 2019;36:25–36. https://doi.org/10.1016/j.jechem.2019.01.027.

[21] Tian F, Zhou N, Chen W, Zhan J, Tang L, Wu M. Progress in green ammonia synthesis technology: catalytic behavior of ammonia synthesis catalysts. Adv Sustain Syst 2024;8:2300618. https://doi.org/10.1002/adsu.202300618.

[22] Sun J, Alam D, Daiyan R, Masood H, Zhang T, Zhou R, et al. A hybrid plasma electrocatalytic process for sustainable ammonia production. Energy Environ Sci 2021;14:865–72. https://doi.org/10.1039/D0EE03769A.

[23] Liu W, Xia M, Zhao C, Chong B, Chen J, Li H, et al. Efficient ammonia synthesis from the air using tandem non-thermal plasma and electrocatalysis at ambient conditions. Nat Commun 2024;15:3524. https://doi.org/10.1038/s41467-024-47765-9.

[24] Salmon N, Bañares-Alcántara R. Impact of process flexibility and imperfect forecasting on the operation and design of haber–bosch green ammonia. RSC Sustain 2023;1:923–37. https://doi.org/10.1039/D3SU00067B.

[25] Lin B, Nowrin FH, Rosenthal JJ, Bhown AS, Malmali M. Perspective on intensification of haber−bosch to enable ammonia production under milder conditions. ACS Sustainable Chem Eng 2023;11:9880–99. https://doi.org/10.1021/acssuschemeng.2c06711.

[26] Smith C, Hill AK, Torrente-Murciano L. Current and future role of haber-bosch ammonia in a carbon-free energy landscape. Energy Environ Sci 2020;13:331–44. https://doi.org/10.1039/c9ee02873k.

[27] Rouwenhorst KHR, Engelmann Y, Van 'T Veer K, Postma RS, Bogaerts A, Lefferts L. Plasma-driven catalysis: green ammonia synthesis with intermittent electricity. Green Chem 2020;22:6258–87. https://doi.org/10.1039/d0gc02058c.

[28] Parkinson B, Balcombe P, Speirs JF, Hawkes AD, Hellgardt K. Levelized cost of CO2 mitigation from hydrogen production routes. Energy Environ Sci 2019;12:19–40. https://doi.org/10.1039/c8ee02079e.

[29] Bui M, Adjiman CS, Bardow A, Anthony EJ, Boston A, Brown S, et al. Carbon capture and storage (CCS): the way forward. Energy Environ Sci 2018;11:1062–176. https://doi.org/10.1039/c7ee02342a.

[30] MacFarlane DR, Cherepanov PV, Choi J, Suryanto BHR, Hodgetts RY, Bakker JM, et al. A roadmap to the ammonia economy. Joule 2020;4:1186–205. https://doi.org/10.1016/j.joule.2020.04.004.

[31] Malmali M, Reese M, McCormick AV, Cussler EL. Converting wind energy to ammonia at lower pressure. ACS Sustainable Chem Eng 2018;6:827–34. https://doi.org/10.1021/acssuschemeng.7b03159.

[32] Rouwenhorst KHR, Van der Ham AGJ, Mul G, Kersten SRA. Islanded ammonia power systems: technology review & conceptual process design. Renew Sustain Energy Rev 2019;114. https://doi.org/10.1016/j.rser.2019.109339.

[33] Westhead O, Barrio J, Bagger A, Murray JW, Rossmeisl J, Titirici MM, et al. Near ambient N2 fixation on solid electrodes versus enzymes and homogeneous catalysts. Nat Rev Chem 2023;7:184–201. https://doi.org/10.1038/s41570-023-00462-5.

[34] Chen H, Yuan D, Wu A, Lin X, Li X. Review of low-temperature plasma nitrogen fixation technology. Waste Dispos Sustain Energy 2021;3:201–17. https://doi.org/10.1007/s42768-021-00074-z.

[35] Smart K. Review of recent progress in green ammonia synthesis: decarbonisation of fertiliser and fuels via green synthesis. Johnson Matthey Technol Rev 2022;66:230–44. https://doi.org/10.1595/205651322X16334238659301.

[36] Olabi AG, Abdelkareem MA, Al-Murisi M, Shehata N, Alami AH, Radwan A, et al. Recent progress in green ammonia: production, applications, assessment; barriers, and its role in achieving the sustainable development goals. Energy Convers Manag 2023;277. https://doi.org/10.1016/j.enconman.2022.116594.

[37] Movick WJ, Kishimoto F, Takanabe K. Dynamic surface-coverage alteration based on microkinetic analysis for enhanced ammonia synthesis over ruthenium catalysts at low temperatures. Chem Eng J 2023;452. https://doi.org/10.1016/j.cej.2022.139525.

[38] Nowrin FH, Malmali M. Optimizing reaction-absorption process for lower pressure ammonia production. ACS Sustainable Chem Eng 2022;10:12319–28. https://doi.org/10.1021/acssuschemeng.2c03554.

[39] Humphreys J, Tao S. Advancements in green ammonia production and utilisation technologies. Johnson Matthey Technol Rev 2024;68:280–92. https://doi.org/10.1595/205651324X16946999404542.

[40] Humphreys J, Lan R, Tao S. Development and recent progress on ammonia synthesis catalysts for haber–bosch process. Adv Energy Sustain Res 2021;2. https://doi.org/10.1002/aesr.202000043.
[41] Spatolisano E, Pellegrini LA. Haber-bosch process intensification: a first step towards small-scale distributed ammonia production. Chem Eng Res Des 2023; 195:651–61. https://doi.org/10.1016/j.cherd.2023.06.031.
[42] Ojha DK, Kale MJ, McCormick AV, Reese M, Malmali M, Dauenhauer P, et al. Integrated ammonia synthesis and separation. ACS Sustainable Chem Eng 2019;7: 18785–92. https://doi.org/10.1021/acssuschemeng.9b03050.
[43] Kale MJ, Ojha DK, Biswas S, Militti JI, Mccormick AV, Schott JH, et al. Optimizing ammonia separation via reactive absorption for sustainable ammonia synthesis. ACS Appl Energy Mater 2020;3:2576–84. https://doi.org/10.1021/acsaem.9b02278.
[44] Hattori M, Iijima S, Nakao T, Hosono H, Hara M. Solid solution for catalytic ammonia synthesis from nitrogen and hydrogen gases at 50 °C. Nat Commun 2020;11. https://doi.org/10.1038/s41467-020-15868-8.
[45] Shipman MA, Symes MD. Recent progress towards the electrosynthesis of ammonia from sustainable resources. Catal Today 2017;286:57–68. https://doi.org/10.1016/j.cattod.2016.05.008.
[46] Jennings JR. Catalytic ammonia synthesis fundamentals and practice. New York: Plenum Press; 1991.
[47] Medford AJ, Vojvodic A, Hummelshøj JS, Voss J, Abild-Pedersen F, Studt F, et al. From the sabatier principle to a predictive theory of transition-metal heterogeneous catalysis. J Catal 2015;328:36–42. https://doi.org/10.1016/j.jcat.2014.12.033.
[48] Jacobsen CJH, Dahl S, Clausen BGS, Bahn S, Logadottir A, Nørskov JK. Catalyst design by interpolation in the periodic table: bimetallic ammonia synthesis catalysts [2]. J Am Chem Soc 2001;123:8404–5. https://doi.org/10.1021/ja010963d.
[49] Liu H. Ammonia synthesis catalyst 100 years: practice, enlightenment and challenge. Chin J Catal 2014;35:1619–40. https://doi.org/10.1016/S1872-2067(14)60118-2.
[50] Altenburg K, Bosch H, Van Ommen JG, Gellings PJ. The role of potassium as a promoter in iron catalysts for ammonia synthesis. J Catal 1980;66:326–34. https://doi.org/10.1016/0021-9517(80)90037-8.
[51] Zhang J, Zheng L, Ma Y, Cai Z, Cao Y, Huang K, et al. A mini-review on NH3Separation technologies: recent advances and future directions. Energy Fuels 2022;36:14516–33. https://doi.org/10.1021/acs.energyfuels.2c02511.
[52] Liu Huazhang. Ammonia synthesis catalysts innovation and practice. World Scientific Publishing; 2013.
[53] Zhang T, Miyaoka H, Miyaoka H, Ichikawa T, Kojima Y. Review on ammonia absorption materials: metal hydrides, halides, and borohydrides. ACS Appl Energy Mater 2018;1:232–42. https://doi.org/10.1021/acsaem.7b00111.
[54] Bernardo P, Drioli E, Golemme G. Membrane gas separation: a review/state of the art. Ind Eng Chem Res 2009;48:4638–63. https://doi.org/10.1021/ie8019032.
[55] Smith C, Torrente-Murciano L. Exceeding single-pass equilibrium with integrated absorption separation for ammonia synthesis using renewable energy—redefining the haber-bosch loop. Adv Energy Mater 2021;11. https://doi.org/10.1002/aenm.202003845.
[56] Joseph Sekhar S, Said Ahmed Al-Shahri A, Glivin G, Le THT, Mathimani T. A critical review of the state-of-the-art green ammonia production technologies-mechanism, advancement, challenges, and future potential. Fuel 2024;358. https://doi.org/10.1016/j.fuel.2023.130307.
[57] Varanasi SA, Fernández CA, Hatzell MC. Energy management and economic considerations of intermittent photovoltaic-driven electrochemical ammonia production. Energy Fuels 2023;37:15222–30. https://doi.org/10.1021/acs.energyfuels.3c02123.
[58] Kalz KF, Kraehnert R, Dvoyashkin M, Dittmeyer R, Gläser R, Krewer U, et al. Future challenges in heterogeneous catalysis: understanding catalysts under dynamic reaction conditions. ChemCatChem 2017;9:17–29. https://doi.org/10.1002/cctc.201600996.
[59] Mucci S, Mitsos A, Bongartz D. Power-to-X processes based on PEM water electrolyzers: a review of process integration and flexible operation. Comput Chem Eng 2023;175. https://doi.org/10.1016/j.compchemeng.2023.108260.
[60] Liu J-C, Ma X-L, Li Y, Wang Y-G, Xiao H, Li J. Heterogeneous Fe3 single-cluster catalyst for ammonia synthesis via an associative mechanism. Nat Commun 2018; 9:1610. https://doi.org/10.1038/s41467-018-03795-8.
[61] Garden AL, Skúlason E. The mechanism of industrial ammonia synthesis revisited: calculations of the role of the associative mechanism. J Phys Chem C 2015;119: 26554–9. https://doi.org/10.1021/acs.jpcc.5b08508.
[62] Vojvodic A, Medford AJ, Studt F, Abild-Pedersen F, Khan TS, Bligaard T, et al. Exploring the limits: a low-pressure, low-temperature haber-bosch process. Chem Phys Lett 2014;598:108–12. https://doi.org/10.1016/j.cplett.2014.03.003.
[63] Liu H-Z, Li X-N, Hu Z-N. APPLI ED CATALYSI S development of novel low temperature and low pressure ammonia synthesis catalyst, vol. 142; 1996.
[64] Bielawa H, Hinrichsen O, Birkner A, Muhler M. The ammonia-synthesis catalyst of the next generation: barium-promoted oxide-supported ruthenium. Angew Chem Int Ed 2001;40:1061–3. https://doi.org/10.1002/1521-3773(20010316)40:6<1061::AID-ANIE10610>3.0.CO;2-B.
[65] Kojima R, Aika K-I. Molybdenum nitride and carbide catalysts for ammonia synthesis, vol 219; 2001.
[66] Kojima R, Aika K-I. Rhenium containing binary catalysts for ammonia synthesis, vol 209; 2001.
[67] Asscher M, Somorjai GA, Haase G, Kojima R, Aika K, Zhong Z, et al. Chemistry letters 2000 913, vol. 98. Springer-Verlag; 1986.
[68] Sudo M, Ichikawa M, Soma M, Onishi T, Tamaru K. Catalytic synthesis of ammonia over the electron donor-acceptor complexes of alkali metals with graphite or phthalocyanines. J Phys Chem 1969;73:1174–5. https://doi.org/10.1021/j100724a082.
[69] Strongin DR, Carrazza J, Bare SR, Somorjai GA. The importance of C7 sites and surface roughness in the ammonia synthesis reaction over iron. J Catal 1987;103: 213–5. https://doi.org/10.1016/0021-9517(87)90109-6.
[70] Aika KI, Ozaki A. Kinetics and isotope effect of ammonia synthesis over an unpromoted iron catalyst. J Catal 1969;13:232–7. https://doi.org/10.1016/0021-9517(69)90396-0.
[71] Smith PJ, Taylor DW, Dowden DA, Kemball C, Taylor D. Ammonia synthesis and related reactions over iron-cobalt and iron-nickel alloy catalysts: part II. catalysts reduced above 853 K. Appl Catal 1982;3:303–14. https://doi.org/10.1016/0166-9834(82)80265-0.
[72] Taylor DW, Smith PJ, Dowden DA, Kemball C, Whan DA. Ammonia synthesis and related reactions over iron-cobalt and iron-nickel alloy catalysts. Part I. Catalysts reduced at 853 K. Appl Catal 1982;3:161–76. https://doi.org/10.1016/0166-9834(82)80089-4.
[73] Baiker A, Schlogl R, Armbruster E, Güntherodt HJ. Ammonia synthesis over supported iron catalyst prepared from amorphous iron-zirconium precursor: I. Bulk structural and surface chemical changes of precursor during its transition to the active catalyst. J Catal 1987;107:221–31. https://doi.org/10.1016/0021-9517(87)90287-9.
[74] Han W, Huang S, Cheng T, Tang H, Li Y, Liu H. Promotion of Nb2O5 on the wustite-based iron catalyst for ammonia synthesis. Appl Surf Sci 2015;353:17–23. https://doi.org/10.1016/J.APSUSC.2015.06.049.
[75] Wang P, Chang F, Gao W, Guo J, Wu G, He T, et al. Breaking scaling relations to achieve low-temperature ammonia synthesis through LiH-mediated nitrogen transfer and hydrogenation. Nat Chem 2017;9:64–70. https://doi.org/10.1038/nchem.2595.
[76] Tang Y, Kobayashi Y, Masuda N, Uchida Y, Okamoto H, Kageyama T, et al. Metal-dependent support effects of oxyhydride-supported Ru, Fe, Co catalysts for ammonia synthesis. Adv Energy Mater 2018;8. https://doi.org/10.1002/aenm.201801772.
[77] Kitano M, Kujirai J, Ogasawara K, Matsuishi S, Tada T, Abe H, et al. Low-temperature synthesis of perovskite oxynitride-hydrides as ammonia synthesis catalysts. J Am Chem Soc 2019;141:20344–53. https://doi.org/10.1021/jacs.9b10726.
[78] Wang X, Peng X, Ran H, Lin B, Ni J, Lin J, et al. Influence of Ru substitution on the properties of LaCoO 3 catalysts for ammonia synthesis: XAFS and XPS studies. Ind Eng Chem Res 2018;57:17375–83. https://doi.org/10.1021/acs.iecr.8b04915.
[79] Kobayashi Y, Tang Y, Kageyama T, Yamashita H, Masuda N, Hosokawa S, et al. Titanium-based hydrides as heterogeneous catalysts for ammonia synthesis. J Am Chem Soc 2017;139:18240–6. https://doi.org/10.1021/jacs.7b08891.
[80] Hattori M, Mori T, Arai T, Inoue Y, Sasase M, Tada T, et al. Enhanced catalytic ammonia synthesis with transformed BaO. ACS Catal 2018;8:10977–84. https://doi.org/10.1021/acscatal.8b02839.
[81] Lin B, Guo Y, Cao C, Ni J, Lin J, Jiang L. Carbon support surface effects in the catalytic performance of Ba-promoted Ru catalyst for ammonia synthesis. Catal Today 2018;316:230–6. https://doi.org/10.1016/J.CATTOD.2018.01.008.
[82] Inoue Y, Kitano M, Kim SW, Yokoyama T, Hara M, Hosono H. Highly dispersed ru on electride [Ca24Al28O 64]4+(e-)4 as a catalyst for ammonia synthesis. ACS Catal 2014;4:674–80. https://doi.org/10.1021/cs401044a.
[83] Ogawa T, Kobayashi Y, Mizoguchi H, Kitano M, Abe H, Tada T, et al. High electron density on Ru in intermetallic YRu2: the application to catalyst for ammonia synthesis. J Phys Chem C 2018;122:10468–75. https://doi.org/10.1021/acs.jpcc.8b02128.
[84] Marakatti VS, Gaigneaux EM. Recent advances in heterogeneous catalysis for ammonia synthesis. ChemCatChem 2020;12:5838–57. https://doi.org/10.1002/cctc.202001141.
[85] Kitano M, Kanbara S, Inoue Y, Kuganathan N, Sushko PV, Yokoyama T, et al. Electride support boosts nitrogen dissociation over ruthenium catalyst and shifts the bottleneck in ammonia synthesis. Nat Commun 2015;6. https://doi.org/10.1038/ncomms7731.
[86] Kitano M, Inoue Y, Yamazaki Y, Hayashi F, Kanbara S, Matsuishi S, et al. Ammonia synthesis using a stable electride as an electron donor and reversible hydrogen Store. Nat Chem 2012;4:934–40. https://doi.org/10.1038/nchem.1476.
[87] Lu Y, Li J, Tada T, Toda Y, Ueda S, Yokoyama T, et al. Water durable electride Y5Si3: electronic structure and catalytic activity for ammonia synthesis. J Am Chem Soc 2016;138:3970–3. https://doi.org/10.1021/jacs.6b00124.
[88] Wu J, Gong Y, Inoshita T, Fredrickson DC, Wang J, Lu Y, et al. Tiered electron anions in multiple voids of LaScSi and their applications to ammonia synthesis. Adv Mater 2017;29. https://doi.org/10.1002/adma.201700924.
[89] Wu J, Li J, Gong Y, Kitano M, Inoshita T, Hosono H. Intermetallic electride catalyst as a platform for ammonia synthesis. Angew Chem 2019;131:835–9. https://doi.org/10.1002/ange.201812131.
[90] Matar SF. Intermetallic hydrides: a review with ab initio aspects. Prog Solid State Chem 2010;38:1–37. https://doi.org/10.1016/J.PROGSOLIDSTCHEM.2010.08.003.
[91] Chang F, Guan Y, Chang X, Guo J, Wang P, Gao W, et al. Alkali and alkaline Earth hydrides-driven N2 activation and transformation over Mn nitride catalyst. J Am Chem Soc 2018;140:14799–806. https://doi.org/10.1021/jacs.8b08334.
[92] Wang P, Xie H, Guo J, Zhao Z, Kong X, Gao W, et al. The formation of surface lithium–iron ternary hydride and its function on catalytic ammonia synthesis at

low temperatures. Angew Chem 2017;129:8842–6. https://doi.org/10.1002/ange.201703695.
[93] Hargreaves JSJ. Heterogeneous catalysis with metal nitrides. Coord Chem Rev 2013;257:2015–31. https://doi.org/10.1016/J.CCR.2012.10.005.
[94] Kojima R, Aika KI. Cobalt molybdenum bimetallic nitride catalysts for ammonia synthesis: part 2. Kinetic study. Appl Catal Gen 2001;218:121–8. https://doi.org/10.1016/S0926-860X(01)00626-3.
[95] Daisley A, Hargreaves JSJ. The role of interstitial species upon the ammonia synthesis activity of ternary Fe–Mo–C(N) and Ni–Mo–C(N) phases. J Energy Chem 2019;39:170–5. https://doi.org/10.1016/J.JECHEM.2019.01.026.
[96] Ye TN, Park SW, Lu Y, Li J, Sasase M, Kitano M, et al. Vacancy-enabled N2 activation for ammonia synthesis on an Ni-loaded catalyst. Nature 2020;583:391–5. https://doi.org/10.1038/s41586-020-2464-9.
[97] Ma XL, Liu JC, Xiao H, Li J. Surface single-cluster catalyst for N 2 -to-NH 3 thermal conversion. J Am Chem Soc 2018;140:46–9. https://doi.org/10.1021/jacs.7b10354.
[98] Niwa Y, Aika KI. The effect of lanthanide oxides as a support for ruthenium catalysts in ammonia synthesis. J Catal 1996;162:138–42. https://doi.org/10.1006/JCAT.1996.0268.
[99] Ma Z, Xiong X, Song C, Hu B, Zhang W. Electronic metal-support interactions enhance the ammonia synthesis activity over ruthenium supported on Zr-modified CeO2 catalysts. RSC Adv 2016;6:51106–10. https://doi.org/10.1039/c6ra10540h.
[100] Wu Y, Li C, Fang B, Wang X, Ni J, Lin B, et al. Enhanced ammonia synthesis performance of ceria-supported Ru catalysts: via introduction of titanium. Chem Commun 2020;56:1141–4. https://doi.org/10.1039/c9cc07385j.
[101] Ogura Y, Sato K, Miyahara SI, Kawano Y, Toriyama T, Yamamoto T, et al. Efficient ammonia synthesis over a Ru/La0.5Ce0.5O1.75 catalyst pre-reduced at high temperature. Chem Sci 2018;9:2230–7. https://doi.org/10.1039/c7sc05343f.
[102] Kosaka F, Nakamura T, Oikawa A, Otomo J. Electrochemical acceleration of ammonia synthesis on Fe-Based alkali-promoted electrocatalyst with proton conducting solid electrolyte. ACS Sustainable Chem Eng 2017;5:10439–46. https://doi.org/10.1021/acssuschemeng.7b02469.
[103] Horiuchi Y, Kamei G, Saito M, Matsuoka M. Development of ruthenium-loaded alkaline-earth titanates as catalysts for ammonia synthesis. Chem Lett 2013;42:1282–4. https://doi.org/10.1246/cl.130574.
[104] Yoshida M, Ogawa T, Imamura Y, Ishihara KN. Economies of scale in ammonia synthesis loops embedded with iron- and ruthenium-based catalysts. Int J Hydrogen Energy 2021;46:28840–54. https://doi.org/10.1016/j.ijhydene.2020.12.081.
[105] Singh AR, Montoya JH, Rohr BA, Tsai C, Vojvodic A, Nørskov JK. Computational design of active site structures with improved transition-state scaling for ammonia synthesis. ACS Catal 2018;8:4017–24. https://doi.org/10.1021/acscatal.8b00106.
[106] Irena AEA. Innovation outlook : renewable ammonia. Int Renew Energy Agency 2022. Ammonia Energy Association.
[107] Lee K, Yoon HC, Kim SH, Shim J, Kim JH, Kim TS. Key engineering criteria for developing next-generation catalysts in advanced Haber–Bosch ammonia synthesis process: from laboratory studies to commercialization. Mol Catal 2025;572. https://doi.org/10.1016/j.mcat.2024.114781.
[108] Chen Z, Ye Y, Peng T, Wu C, Li H, Pan X, et al. Iron-single sites confined by graphene lattice for ammonia synthesis under mild conditions. ACS Catal 2023;13:14385–94. https://doi.org/10.1021/acscatal.3c03108.
[109] Zhou Y, Liang L, Wang C, Sun F, Zheng L, Qi H, et al. Precious-metal-free Mo-MXene catalyst enabling facile ammonia synthesis via dual sites bridged by H-Spillover. J Am Chem Soc 2024;146:23054–66. https://doi.org/10.1021/jacs.4c03998.
[110] Chang F, Tezsevin I, de Rijk JW, Meeldijk JD, Hofmann JP, Er S, et al. Potassium hydride-intercalated graphite as an efficient heterogeneous catalyst for ammonia synthesis. Nat Catal 2022;5:222–30. https://doi.org/10.1038/s41929-022-00754-x.
[111] Era K, Sato K, Miyahara S, Naito T, De Silva K, Akrami S, et al. Catalytic behavior of k-doped Fe/MgO catalysts for ammonia synthesis under mild reaction conditions. ChemSusChem 2023;16. https://doi.org/10.1002/cssc.202300942.
[112] Jiang Y, Miyazaki M, Miyashita K, Sasase M, Kishida K, Hosono H, et al. CN $_2^{2-}$ vacancies enhance ammonia synthesis over air-durable alkaline Earth metal cyanamide-supported cobalt catalysts. ACS Catal 2024;14:6349–57. https://doi.org/10.1021/acscatal.4c00830.
[113] Mitchell S, Michels NL, Pérez-Ramírez J. From powder to technical body: the undervalued science of catalyst scale up. Chem Soc Rev 2013;42:6094–112. https://doi.org/10.1039/c3cs60076a.
[114] Matsuishi S, Toda Y, Miyakawa M, Hayashi K, Kamiya T, Hirano M, et al. High-Density Electron Anions in a Nanoporous Single Crystal: [ca $_{24}$ Al $_{28}$ O $_{64}$] $^{4+}$ (4 e^-). Science 1979;301:626–9. https://doi.org/10.1126/science.1083842. 2003.
[115] Gong Y, Li H, Wu J, Song X, Yang X, Bao X, et al. Unique catalytic mechanism for Ru-Loaded ternary intermetallic electrides for ammonia synthesis. J Am Chem Soc 2022;144:8683–92. https://doi.org/10.1021/jacs.2c01899.
[116] Addou A, Sfeir A, Marinova M, Vezin H, Dacquin J, Royer S, et al. Simplified Preparation of BaAl $_2$ O $_{4-y}$ e $^-$ $_y$/C Oxy-Electrides Using Pechini Approach for Ammonia Synthesis. ChemSusChem 2025. https://doi.org/10.1002/cssc.202500682.
[117] Gong Y, Li H, Li C, Yang X, Wang J, Hosono H. LaRuSi electride disrupts the scaling relations for ammonia synthesis. Chem Mater 2022;34:1677–85. https://doi.org/10.1021/acs.chemmater.1c03821.
[118] Zhou Y, Peng X, Zhang T, Cai H, Lin B, Zheng L, et al. Essential role of Ru–Anion interaction in Ru-Based ammonia synthesis catalysts. ACS Catal 2022;12:7633–42. https://doi.org/10.1021/acscatal.2c01486.
[119] Bai Y, Zhang Y, Hu J, Li J, Wan S, Lin J, et al. Hydrogen-assisted dissociation of N $_2$: prevalence and consequences for ammonia synthesis on supported Ru catalysts. ACS Catal 2025;15:1455–66. https://doi.org/10.1021/acscatal.4c06966.
[120] Zhang T, Yue K, Mo J, Zhang M, Zhu J, Lin R, et al. Enhanced ammonia synthesis performance over Ru-Based catalysts via the addition of Ce promoter. Ind Eng Chem Res 2025;64:9070–7. https://doi.org/10.1021/acs.iecr.4c04868.
[121] Peng X, Luo Y, Zhang Y, Zhang S, Zhang M, Mao R, et al. Dissecting the essential role of a molecular promoter C $_{60}$ on a Ru catalyst for ammonia synthesis. ACS Catal 2025;15:2827–38. https://doi.org/10.1021/acscatal.4c06941.
[122] Zhou Y, Xu C-Q, Tan Z, Cai H, Wang X, Li J, et al. Integrating dissociative and associative routes for efficient ammonia synthesis over a TiCN-Promoted Ru-Based catalyst. ACS Catal 2022;12:2651–60. https://doi.org/10.1021/acscatal.1c05613.
[123] Fang B, Zhang C, Yang M, Li J, Li C, Ni J, et al. Introducing trace Co to molybdenum carbide catalyst for efficient ammonia synthesis. AIChE J 2023;69. https://doi.org/10.1002/aic.18163.
[124] Miyazaki M, Ikejima K, Ogasawara K, Kitano M, Hosono H. Ammonia synthesis over fe-supported catalysts mediated by face-sharing nitrogen sites in BaTiO $_{3-x}$ N $_y$ oxynitride. ChemSusChem 2023;16. https://doi.org/10.1002/cssc.202300551.
[125] Woo R, Lee K, An B-S, Kim SH, Ju H, Kim JH, et al. BaCeO3 perovskite-incorporated Co catalyst for efficient NH3 synthesis under mild conditions. Chem Eng J 2023;475:146354. https://doi.org/10.1016/j.cej.2023.146354.
[126] Wang Q, Wen H, Guan Y, Zhang S, Gao W, Guo J, et al. Ruthenium complex hydride catalyst as a platform for ammonia synthesis: the effect of alkali or alkaline Earth elements. ACS Catal 2023;13:9882–90. https://doi.org/10.1021/acscatal.3c02068.
[127] Zhou J, Xia F, Zhang C, Ni J, Lin J, Lin B, et al. Oxygen-induced activation of a ceria-supported Ru catalyst for enhancing ammonia synthesis activity. Ind Eng Chem Res 2023. https://doi.org/10.1021/acs.iecr.3c00392.
[128] Jiang Y, Takashima R, Nakao T, Miyazaki M, Lu Y, Sasase M, et al. Boosted activity of cobalt catalysts for ammonia synthesis with BaAl $_2$ O $_{4-x}$ H $_y$ electrides. J Am Chem Soc 2023;145:10669–80. https://doi.org/10.1021/jacs.3c01074.
[129] Li Z, Lu Y, Li J, Xu M, Qi Y, Park S-W, et al. Multiple reaction pathway on alkaline Earth imide supported catalysts for efficient ammonia synthesis. Nat Commun 2023;14:6373. https://doi.org/10.1038/s41467-023-42050-7.
[130] Vieri HM, Badakhsh A, Choi SH. Comparative study of Ba, Cs, K, and Li as promoters for Ru/La2Ce2O7-Based catalyst for ammonia synthesis. Int J Energy Res 2023;2023:1–11. https://doi.org/10.1155/2023/2072245.
[131] Croisé C, Alabd K, Villesuzanne A, Can F, Courtois X, Gaudin E, et al. Role of hydride ion within Ru/LaScSi and Ru/CeTiGe catalysts for NH3 synthesis: a combination of DFT and experimental nitrogen isotopic exchange studies. Catal Commun 2023;179:106689. https://doi.org/10.1016/j.catcom.2023.106689.
[132] Su K, Huang D, Fang H, Zhou Y, Qi H, Ni J, et al. Boosting N $_2$ conversion into NH $_3$ over Ru catalysts via modulating the Ru-Promoter interface. ACS Appl Mater Interfaces 2023. https://doi.org/10.1021/acsami.3c12531.
[133] Anello G, De Luna G, De Felice G, Saker A, Di Felice L, Gallucci F. Development of ruthenium-based catalysts for ammonia synthesis via polyol reduction method. Int J Hydrogen Energy 2024;86:922–30. https://doi.org/10.1016/j.ijhydene.2024.08.408.
[134] Yamazaki K, Goto Y, Kikugawa M, Sato A, Manaka Y, Nanba T, et al. Effect of support morphology on the ammonia synthesis activity of Ru/CeO2-based catalysts. Int J Hydrogen Energy 2024;94:406–19. https://doi.org/10.1016/j.ijhydene.2024.11.053.
[135] Patkowski W, Zybert M, Ronduda H, Albrecht A, Moszyński D, Fidler A, et al. Toward green ammonia synthesis – exploring the influence of lanthanide oxides as supports on the cobalt catalysts properties. J CO2 Util 2024;80:102699. https://doi.org/10.1016/j.jcou.2024.102699.
[136] Chen Z, Ye Y, Pan X, Bao X. Potassium promoted ferrocene/graphene for ammonia synthesis. Chem Res Chin Univ 2024;40:1004–10. https://doi.org/10.1007/s40242-024-4019-3.
[137] Lee K, Woo R, Woo HC, Ko G, Cho K, Park Y, et al. Unraveling the role of MgO in the Ru-Ba/MgO catalyst for boosting ammonia synthesis: comparative study of MgO and MgAlO supports. J Catal 2024;434:115530. https://doi.org/10.1016/j.jcat.2024.115530.
[138] Zhong G, Liu Y, Yu S, Zhang C, Ni J, Lin J, et al. Strengthening hydrogen spillover in ceria-supported Co–Fe bimetallic catalysts for boosting ammonia synthesis. Ind Eng Chem Res 2024;63:5089–96. https://doi.org/10.1021/acs.iecr.3c04299.
[139] Zhang T, Hu H, Li J, Gao Y, Li L, Zhang M, et al. Tuning clusters-metal oxide promoters electronic interaction of Ru-based catalyst for ammonia synthesis under mild conditions. Chin J Catal 2024;60:209–18. https://doi.org/10.1016/S1872-2067(23)64644-3.
[140] Li R, Liu L, Ju X, Feng J, Wang J, Guo J, et al. Interaction between Ru nanoparticles and Pr6O11 triggers catalytic ammonia synthesis. Catal Lett 2024;154:4814–22. https://doi.org/10.1007/s10562-024-04629-7.
[141] Peng X, Luo Y, Zhang T, Deng J, Zhou Y, Li J, et al. Potassium promoter regulates electronic structure and hydrogen spillover of ultrasmall Ru nanoclusters catalyst for ammonia synthesis. Chem Eng Sci 2024;292:120021. https://doi.org/10.1016/j.ces.2024.120021.
[142] Era K, Sato K, Miyahara S, Naito T, De Silva K, Akrami S, et al. Barium-doped iron nanoparticles supported on MgO as an efficient catalyst for ammonia synthesis under mild reaction conditions. Sustain Energy Fuels 2024;8:2593–600. https://doi.org/10.1039/D4SE00411F.
[143] Jiang Y, Chen Z, Peng T, Jiao L, Pan X, Jiang H, et al. Single-atom Fe catalysts with improved metal loading for efficient ammonia synthesis under mild

conditions. Angew Chem Int Ed 2025;64. https://doi.org/10.1002/anie.202501190.
[144] Kamiguchi S, Asakura K, Shibayama T, Yokaichiya T, Ikeda T, Nakayama A, et al. Catalytic ammonia synthesis on HY-zeolite-supported angstrom-size molybdenum cluster. Chem Sci 2024;15:2914–22. https://doi.org/10.1039/D3SC05447K.
[145] Tian F, Li J, Kong F, Zhang C, Han J, Tang Y, et al. Promoting effect of bulk Cs^{+} over $Cs_{0.68}Ti_{1.83}O_4$ for ammonia synthesis. J Phys Chem C 2024;128:10007–16. https://doi.org/10.1021/acs.jpcc.4c02655.
[146] Croisé C, Alabd K, Tencé S, Gaudin E, Villesuzanne A, Courtois X, et al. Ru/Ce *TX* (*T* =Ti, Sc; *X* =Ge, si) intermetallic catalysts for NH_3 synthesis at low temperature (300 °C): insight into composition and related mechanisms. ChemCatChem 2024. https://doi.org/10.1002/cctc.202400403.
[147] Zhang Z, Miyashita K, Wu T, Kujirai J, Ogasawara K, Li J, et al. Anion vacancies activate N2 to ammonia on Ba–Si orthosilicate oxynitride-hydride. Nat Chem 2025;17:679–87. https://doi.org/10.1038/s41557-025-01737-8.
[148] Mehta P, Barboun P, Herrera FA, Kim J, Rumbach P, Go DB, et al. Overcoming ammonia synthesis scaling relations with plasma-enabled catalysis. Nat Catal 2018;1:269–75. https://doi.org/10.1038/s41929-018-0045-1.
[149] Skubic L, Gyergyek S, Huš M, Likozar B. A review of multiscale modelling approaches for understanding catalytic ammonia synthesis and decomposition. J Catal 2024;429. https://doi.org/10.1016/j.jcat.2023.115217.
[150] Ye TN, Park SW, Lu Y, Li J, Sasase M, Kitano M, et al. Contribution of nitrogen vacancies to ammonia synthesis over metal nitride catalysts. J Am Chem Soc 2020;142:14374–83. https://doi.org/10.1021/jacs.0c06624.
[151] Inoue Y, Kitano M, Kishida K, Abe H, Niwa Y, Sasase M, et al. Efficient and stable ammonia synthesis by self-organized flat Ru nanoparticles on calcium amide. ACS Catal 2016;6:7577–84. https://doi.org/10.1021/acscatal.6b01940.
[152] Hellman A, Honkala K, Remediakis IN, Logadóttir Á, Carlsson A, Dahl S, et al. Insights into ammonia synthesis from first-principles. Surf Sci 2006;600:4264–8. https://doi.org/10.1016/j.susc.2005.11.070.
[153] Kepp KP. Accuracy of theoretical catalysis from a model of iron-catalyzed ammonia synthesis. Commun Chem 2018;1. https://doi.org/10.1038/s42004-018-0063-6.
[154] Cholach AR, Bryliakova AA. Re-Co alloys and single-atom Re catalysts in ammonia synthesis: a DFT study. Mol Catal 2021;513:111801. https://doi.org/10.1016/j.mcat.2021.111801.
[155] Ertl G, Lee SB, Weiss M. Adsorption of nitrogen on potassium promoted Fe(111) and (100) surfaces. Surf Sci 1982;114:527–45. https://doi.org/10.1016/0039-6028(82)90703-8.
[156] Pineda M, Stamatakis M. Kinetic monte carlo simulations for heterogeneous catalysis: fundamentals, current status, and challenges. J Chem Phys 2022;156. https://doi.org/10.1063/5.0083251.
[157] Schaefer D, Stephan S, Langenbach K, Horsch MT, Hasse H. Mass transfer through vapor-liquid interfaces studied by non-stationary molecular dynamics simulations. J Phys Chem B 2023;127:2521–33. https://doi.org/10.1021/acs.jpcb.2c08752.
[158] Mohamed AMO, Bicer Y. Computational exploration of adsorption enhanced haber-bosch using MOFs and ionic Liquid/MOFs. Computer Aided Chem Eng 2021;50:373–9. https://doi.org/10.1016/B978-0-323-88506-5.50059-0.
[159] Albertí M, Amat A, Farrera L, Pirani F. From the (NH3)2–5 clusters to liquid ammonia: molecular dynamics simulations using the NVE and NpT ensembles. J Mol Liq 2015;212:307–15. https://doi.org/10.1016/J.MOLLIQ.2015.09.016.
[160] Patel R, Castro J, Tsapatsis M, Siepmann JI. Molecular simulations probing the adsorption and diffusion of ammonia, nitrogen, hydrogen, and their mixtures in bulk MFI zeolite and MFI nanosheets at high temperature and pressure. J Chem Eng Data 2022;67:1779–91. https://doi.org/10.1021/acs.jced.2c00086.
[161] Lee HW, Jeong GU, Kim MC, Kim D, Kim S, Han SS. Atomistic origin of mechanochemical NH3 synthesis on Fe catalysts. Int J Hydrogen Energy 2023;48:3931–41. https://doi.org/10.1016/J.IJHYDENE.2022.10.193.
[162] Nattino F, Costanzo F, Kroes GJ. N2 dissociation on W(110): an ab initio molecular dynamics study on the effect of phonons. J Chem Phys 2015;142. https://doi.org/10.1063/1.4913979.
[163] Kim SY, Lee HW, Pai SJ, Han SS. Activity, selectivity, and durability of ruthenium nanoparticle catalysts for ammonia synthesis by reactive molecular dynamics simulation: the size effect. ACS Appl Mater Interfaces 2018;10:26188–94. https://doi.org/10.1021/acsami.8b05070.
[164] Rahimi N, McFarland EW, Metiu H, Kristoffersen HH. Properties of negatively charged ruthenium clusters in molten sodium chloride. J Phys Chem C 2019;123:16179–85. https://doi.org/10.1021/acs.jpcc.9b02616.
[165] Fan QY, Liu JL, Gong FQ, Wang Y, Cheng J. Structural dynamics of Ru clusters during nitrogen dissociation in ammonia synthesis. Phys Chem Chem Phys 2022. https://doi.org/10.1039/d2cp00678b.
[166] Lv X, Liu J, Kou L, Ng KW, Wang S, Frauenheim T, et al. Three-dimensional dual-site catalysts for industrial ammonia synthesis at dramatically decreased temperatures and pressures. ACS Catal 2023;13:13561–8. https://doi.org/10.1021/acscatal.3c03160.
[167] Schlögl R. Heterogeneous catalysis. Angew Chem Int Ed 2015;54:3465–520. https://doi.org/10.1002/anie.201410738.
[168] Bonati LI, Polino D, Pizzolitto C, Biasi P, Eckert R, Reitmeier S, et al. The role of dynamics in heterogeneous catalysis: surface diffusivity and N 2 decomposition on Fe, vol 111; 2023. https://doi.org/10.1073/pnas.
[169] Tripathi S, Bonati L, Perego S, Parrinello M. How poisoning is avoided in a step of relevance to the haber-bosch catalysis. ACS Catal 2024;14:4944–50. https://doi.org/10.1021/acscatal.3c06201.
[170] Nakao T, Tada T, Hosono H. First-principles and microkinetic study on the mechanism for ammonia synthesis using Ru-Loaded hydride catalyst. J Phys Chem C 2020;124:2070–8. https://doi.org/10.1021/acs.jpcc.9b10850.
[171] Chiao L, Rinker RG. A kinetic study of ammonia synthesis: modeling high-pressure steady-state and forced-cycling behavior. Chem Eng Sci 1989;44:9–19. https://doi.org/10.1016/0009-2509(89)85227-3.
[172] Green RE, Cornell SJ, Scharlemann JPW, Balmford A. Farming and the fate of wild nature. Science 1979;307:550–5. https://doi.org/10.1126/science.1106049. 2005.
[173] Lang ND, Holloway S, Nørskov JK. Electrostatic adsorbate-adsorbate interactions: the poisoning and promotion of the molecular adsorption reaction. Surf Sci 1985;150:24–38. https://doi.org/10.1016/0039-6028(85)90208-0.
[174] Nørskov JK. Theory nof chemisorption and heterogeneous catalysis. Physica B+C 1984;127:193–202. https://doi.org/10.1016/S0378-4363(84)80030-3.
[175] Dumesic JA, Trevino AA. Kinetic simulation of ammonia synthesis catalysis. J Catal 1989;116:119–29. https://doi.org/10.1016/0021-9517(89)90080-8.
[176] Ertl G, Lee SB, Weiss M. Kinetics of nitrogen adsorption on Fe(111). Surf Sci 1982;114:515–26. https://doi.org/10.1016/0039-6028(82)90702-6.
[177] Aparicio LM, Dumesic JA. Ammonia synthesis kinetics: surface chemistry, rate expressions, and kinetic analysis. Top Catal 1994;1:233–52. https://doi.org/10.1007/BF01492278.
[178] Nørskov JK. Electronic factors in catalysis. Prog Surf Sci 1991;38:103–44. https://doi.org/10.1016/0079-6816(91)90007-Q.
[179] Hinrichsen O. Kinetic simulation of ammonia synthesis catalyzed by ruthenium. Catal Today 1999;53:177–88. https://doi.org/10.1016/S0920-5861(99)00115-7.
[180] Zeinalipour-Yazdi CD, Hargreaves JSJ, Catlow CRA. Low-T mechanisms of ammonia synthesis on Co3Mo3N. J Phys Chem C 2018;122:6078–82. https://doi.org/10.1021/acs.jpcc.7b12364.
[181] Asscher M, Carrazza J, Khan MM, Lewis KB, Somorjai GA. The ammonia synthesis over rhenium single-crystal catalysts: kinetics, structure sensitivity, and effect of potassium and oxygen. J Catal 1986;98:277–87. https://doi.org/10.1016/0021-9517(86)90316-7.
[182] Wittreich GR, Liu S, Dauenhauer PJ, Vlachos DG. Catalytic resonance of ammonia synthesis by simulated dynamic ruthenium crystal strain. Sci Adv 2022;8. https://doi.org/10.1126/sciadv.abl6576.
[183] Fernández C, Bion N, Gaigneaux EM, Duprez D, Ruiz P. Kinetics of hydrogen adsorption and mobility on Ru nanoparticles supported on alumina: effects on the catalytic mechanism of ammonia synthesis. J Catal 2016;344:16–28. https://doi.org/10.1016/J.JCAT.2016.09.013.
[184] Fuller J, Fortunelli A, Goddard WA, An Q. Reaction mechanism and kinetics for ammonia synthesis on the Fe(211) reconstructed surface. Phys Chem Chem Phys 2019;21:11444–54. https://doi.org/10.1039/c9cp01611b.
[185] Fuller J, An Q, Fortunelli A, Goddard WA. Reaction mechanisms, kinetics, and improved catalysts for ammonia synthesis from hierarchical high throughput catalyst design. Acc Chem Res 2022;55:1124–34. https://doi.org/10.1021/acs.accounts.1c00789.
[186] An Q, McDonald M, Fortunelli A, Goddard WA. Si-Doped Fe catalyst for ammonia synthesis at dramatically decreased pressures and temperatures. J Am Chem Soc 2020;142:8223–32. https://doi.org/10.1021/jacs.9b13996.
[187] McDonald M, Fuller J, Fortunelli A, Goddard WA, An Q. Highly efficient Ni-Doped iron catalyst for ammonia synthesis from quantum-mechanics-based hierarchical high-throughput catalyst screening. J Phys Chem C 2019;123:17375–83. https://doi.org/10.1021/acs.jpcc.9b04386.
[188] Qian J, Fortunelli A, Goddard WA. Effect of Co doping on mechanism and kinetics of ammonia synthesis on Fe(1 1 1) surface. J Catal 2019;370:364–71. https://doi.org/10.1016/J.JCAT.2019.01.001.
[189] An Q, Shen Y, Fortunelli A, Goddard WA. QM-Mechanism-Based hierarchical high-throughput in silico screening catalyst design for ammonia synthesis. J Am Chem Soc 2018;140:17702–10. https://doi.org/10.1021/jacs.8b10499.
[190] An Q, McDonald M, Fortunelli A, Goddard WA. Controlling the shapes of nanoparticles by dopant-induced enhancement of chemisorption and catalytic activity: application to Fe-Based ammonia synthesis. ACS Nano 2021;15:1675–84. https://doi.org/10.1021/acsnano.0c09346.
[191] Hellman A, Baerends EJ, Biczysko M, Bligaard T, Christensen CH, Clary DC, et al. Predicting catalysis: understanding ammonia synthesis from first-principles calculations. J Phys Chem B 2006;110:17719–35. https://doi.org/10.1021/jp056982h.
[192] Saidi WA, Shadid W, Veser G. Optimization of high-entropy alloy catalyst for ammonia decomposition and ammonia synthesis. J Phys Chem Lett 2021;12:5185–92. https://doi.org/10.1021/acs.jpclett.1c01242.
[193] Wan M, Yue H, Notarangelo J, Liu H, Che F. Deep learning-assisted investigation of electric field-dipole effects on catalytic ammonia synthesis. JACS Au 2022;2:1338–49. https://doi.org/10.1021/jacsau.2c00003.
[194] Lan T, An Q. Discovering catalytic reaction networks using deep reinforcement learning from first-principles. J Am Chem Soc 2021;143:16804–12. https://doi.org/10.1021/jacs.1c08794.
[195] Jayarathna R, Onsree T, Drummond S, Naglic J, Lauterbach J. Experimental discovery of novel ammonia synthesis catalysts via active learning. J Mater Chem A Mater 2024;12:3046–60. https://doi.org/10.1039/d3ta05939a.
[196] Karakaya C, Huang J, Cadigan C, Welch A, Kintner J, Beach J, et al. Development, characterization, and modeling of a high-performance Ru/B2CA catalyst for ammonia synthesis. Chem Eng Sci 2022;247:116902. https://doi.org/10.1016/J.CES.2021.116902.
[197] Williams T, McCullough K, Lauterbach JA. Enabling catalyst discovery through machine learning and high-throughput experimentation. Chem Mater 2020;32:157–65. https://doi.org/10.1021/acs.chemmater.9b03043.

[198] Deng Z, Zhang L, Miao B, Liu Q, Pan Z, Zhang W, et al. A novel combination of machine learning and intelligent optimization algorithm for modeling and optimization of green ammonia synthesis. Energy Convers Manag 2024;311:118429. https://doi.org/10.1016/J.ENCONMAN.2024.118429.
[199] El-Maghraby RM, Mohamed AY, Hassanean MHM. Improving energy efficiency in ammonia production plants using machine learning. Fuel 2024;363:130910. https://doi.org/10.1016/J.FUEL.2024.130910.
[200] Oliveira Cabral T, Bagheri A, Pourkargar DB. Learning-based model reduction and predictive control of an ammonia synthesis process. Ind Eng Chem Res 2024;63:10325–42. https://doi.org/10.1021/acs.iecr.4c00340.
[201] Wang X, Du X, Chen K, Zheng Z, Liu Y, Shen X, et al. Predicting the ammonia synthesis performance of plasma catalysis using an artificial neural network model. ACS Sustainable Chem Eng 2023;11:4543–54. https://doi.org/10.1021/acssuschemeng.2c04715.
[202] Jiang L, Roskilly AP. Thermal conductivity, permeability and reaction characteristic enhancement of ammonia solid sorbents: a review. Int J Heat Mass Tran 2019;130:1206–25. https://doi.org/10.1016/j.ijheatmasstransfer.2018.11.029.
[203] Kuznika F, Johannesa K. A review on chemisorption heat storage in low-energy buildings. In: Energy procedia, vol. 57. Elsevier Ltd; 2014. p. 2333–41. https://doi.org/10.1016/j.egypro.2014.10.241.
[204] An GL, Wang LW, Gao J, Wang RZ. A review on the solid sorption mechanism and kinetic models of metal halide-ammonia working pairs. Renew Sustain Energy Rev 2018;91:783–92. https://doi.org/10.1016/j.rser.2018.04.032.
[205] Han B, Butterly C, Zhang W, He J, Chen D. Adsorbent materials for ammonium and ammonia removal: a review. J Clean Prod 2021;283. https://doi.org/10.1016/j.jclepro.2020.124611.
[206] Ren Z, Jia B, Zhang G, Fu X, Wang Z, Wang P, et al. Study on adsorption of ammonia nitrogen by iron-loaded activated carbon from low temperature wastewater. Chemosphere 2021;262:127895. https://doi.org/10.1016/j.chemosphere.2020.127895.
[207] Gonçalves M, Sánchez-García L, Oliveira Jardim E De, Silvestre-Albero J, Rodríguez-Reinoso F. Ammonia removal using activated carbons: effect of the surface chemistry in dry and moist conditions. Environ Sci Technol 2011;45:10605–10. https://doi.org/10.1021/es203093v.
[208] Huang CC, Li HS, Chen CH. Effect of surface acidic oxides of activated carbon on adsorption of ammonia. J Hazard Mater 2008;159:523–7. https://doi.org/10.1016/J.JHAZMAT.2008.02.051.
[209] Zheng W, Hu J, Rappeport S, Zheng Z, Wang Z, Han Z, et al. Activated carbon fiber composites for gas phase ammonia adsorption. Microporous Mesoporous Mater 2016;234:146–54. https://doi.org/10.1016/j.micromeso.2016.07.011.
[210] Zhang Y, Xiao J, Zhang TC, Ouyang L, Yuan S. Synthesis of CuSiO3-loaded P-doped porous biochar derived from phytic acid-activated lemon peel for enhanced adsorption of NH3. Sep Purif Technol 2022;283. https://doi.org/10.1016/j.seppur.2021.120179.
[211] Qajar A, Peer M, Andalibi MR, Rajagopalan R, Foley HC. Enhanced ammonia adsorption on functionalized nanoporous carbons. Microporous Mesoporous Mater 2015;218:15–23. https://doi.org/10.1016/j.micromeso.2015.06.030.
[212] Bae C, Gu M, Jeon Y, Kim D, Kim J. Metal–organic frameworks for NH3 adsorption by different NH3 operating pressures. Bull Kor Chem Soc 2023;44:112–24. https://doi.org/10.1002/bkcs.12640.
[213] Vikrant K, Kumar V, Kim KH, Kukkar D. Metal-organic frameworks (MOFs): potential and challenges for capture and abatement of ammonia. J Mater Chem A Mater 2017;5:22877–96. https://doi.org/10.1039/c7ta07847a.
[214] Jasuja H, Peterson GW, Decoste JB, Browe MA, Walton KS. Evaluation of MOFs for air purification and air quality control applications: ammonia removal from air. Chem Eng Sci 2015;124:118–24. https://doi.org/10.1016/J.CES.2014.08.050.
[215] Rieth AJ, Tulchinsky Y, Dincă M. High and reversible ammonia uptake in mesoporous azolate metal-organic frameworks with open Mn, Co, and Ni sites. J Am Chem Soc 2016;138:9401–4. https://doi.org/10.1021/jacs.6b05723.
[216] Chen Y, Shan B, Yang C, Yang J, Li J, Mu B. Environmentally friendly synthesis of flexible MOFs M(NA)2 (M = Zn, Co, Cu, Cd) with large and regenerable ammonia capacity. J Mater Chem A Mater 2018;6:9922–9. https://doi.org/10.1039/c8ta02845a.
[217] Lu W, De Alwis Jayasinghe D, Schröder M, Yang S. Ammonia storage in metal–organic framework materials: recent developments in design and characterization. Acc Mater Res 2024;5:1279–90. https://doi.org/10.1021/accountsmr.4c00183.
[218] Rieth AJ, Wright AM, Dincă M. Kinetic stability of metal–organic frameworks for corrosive and coordinating gas capture. Nat Rev Mater 2019;4:708–25. https://doi.org/10.1038/s41578-019-0140-1.
[219] Van Humbeck JF, McDonald TM, Jing X, Wiers BM, Zhu G, Long JR. Ammonia capture in porous organic polymers densely functionalized with brønsted acid groups. J Am Chem Soc 2014;136:2432–40. https://doi.org/10.1021/ja4105478.
[220] Luo L, Liu Y, Wu Z, Liu J, Cao X, Lin J, et al. Macromolecular-metal complexes induced by Co(II) with polymer and flexible ligands for ammonia uptake compared with MOFs. Chem Eng J 2022;448:137626. https://doi.org/10.1016/J.CEJ.2022.137626.
[221] Li Y, Li L, Yu J. Applications of zeolites in sustainable chemistry. Chem 2017;3:928–49. https://doi.org/10.1016/j.chempr.2017.10.009.
[222] Lucero JM, Crawford JM, Wolden CA, Carreon MA. Tunability of ammonia adsorption over NaP zeolite. Microporous Mesoporous Mater 2021;324. https://doi.org/10.1016/j.micromeso.2021.111288.
[223] Helminen J, Helenius J, Paatero E, Turunen I. Comparison of sorbents and isotherm models for NH 3 -gas separation by adsorption. AIChE J 2000;46:1541–55. https://doi.org/10.1002/aic.690460807.
[224] Cheng H, Zhu Q, Xing Z. Adsorption of ammonia nitrogen in low temperature domestic wastewater by modification bentonite. J Clean Prod 2019;233:720–30. https://doi.org/10.1016/j.jclepro.2019.06.079.
[225] Wang H, Song T, Li Z, Qiu J, Zhao Y, Zhang H, et al. Exceptional high and reversible ammonia uptake by two dimension few-layer BiI3Nanosheets. ACS Appl Mater Interfaces 2021;13:25918–25. https://doi.org/10.1021/acsami.1c03261.
[226] Liu CY, Aika KI. Ammonia absorption on alkaline Earth halides as ammonia separation and storage procedure. Bull Chem Soc Jpn 2004;77:123–31. https://doi.org/10.1246/bcsj.77.123.
[227] Aoki T, Miyaoka H, Inokawa H, Ichikawa T, Kojima Y. Activation on ammonia absorbing reaction for magnesium chloride. J Phys Chem C 2015;119:26296–302. https://doi.org/10.1021/acs.jpcc.5b07965.
[228] Sørensen R Z, Hummelshøj J S, Klerke A, Birke Reves J, Vegge T, Nørskov J K, et al. Indirect, reversible high-density hydrogen storage in compact metal ammine salts. J Am Chem Soc 2008;130:8660–8. https://doi.org/10.1021/ja076762c.
[229] Zamljen A, Likozar B. Catalytic reactor-utilized ammonia adsorption, absorption, and storage materials: mechanism, nanostructure, and *Ab Initio* design. ACS Sustainable Chem Eng 2024. https://doi.org/10.1021/acssuschemeng.4c06100.
[230] Aoki T, Ichikawa T, Miyaoka H, Kojima Y. Thermodynamics on ammonia absorption of metal halides and borohydrides. J Phys Chem C 2014;118:18412–6. https://doi.org/10.1021/jp5049474.
[231] Grinderslev JB, Amdisen MB, Skov LN, Møller KT, Kristensen LG, Polanski M, et al. New perspectives of functional metal borohydrides. J Alloys Compd 2022;896. https://doi.org/10.1016/j.jallcom.2021.163014.
[232] Jepsen LH, Ley MB, Filinchuk Y, Besenbacher F, Jensen TR. Tailoring the properties of ammine metal borohydrides for solid-state hydrogen storage. ChemSusChem 2015;8:1452–63. https://doi.org/10.1002/cssc.201500029.
[233] He T, Cao H, Chen P. Complex hydrides for energy storage, conversion, and utilization. Adv Mater 2019;31. https://doi.org/10.1002/adma.201902757.
[234] Yamamoto H, Miyaoka H, Hino S, Nakanishi H, Ichikawa T, Kojima Y. Recyclable hydrogen storage system composed of ammonia and alkali metal hydride. Int J Hydrogen Energy 2009;34:9760–4. https://doi.org/10.1016/j.ijhydene.2009.10.034.
[235] Yuan Y, Zhang H, Yang F, Zhang N, Cao X. Inorganic composite sorbents for water vapor sorption: a research progress. Renew Sustain Energy Rev 2016;54:761–76. https://doi.org/10.1016/J.RSER.2015.10.069.
[236] Yan T, Li TX, Li H, Wang RZ. Experimental study of the ammonia adsorption characteristics on the composite sorbent of CaCl2 and multi-walled carbon nanotubes. Int J Refrig 2014;46:165–72. https://doi.org/10.1016/j.ijrefrig.2014.02.014.
[237] Wang ZX, Wang LW, Gao P, Yu Y, Wang RZ. Analysis of composite sorbents for ammonia storage to eliminate NOx emission at low temperatures. Appl Therm Eng 2018;128:1382–90. https://doi.org/10.1016/j.applthermaleng.2017.09.084.
[238] Phillip WA, Martono E, Chen L, Hillmyer MA, Cussler EL. Seeking an ammonia selective membrane based on nanostructured sulfonated block copolymers. J Membr Sci 2009;337:39–46. https://doi.org/10.1016/j.memsci.2009.03.013.
[239] Richard S, Verde V, Kezibri N, Makhloufi C, Saker A, Garguilo I, et al. Power-to-ammonia synthesis process with membrane reactors: techno- economic study. Int J Hydrogen Energy 2024;73:462–74. https://doi.org/10.1016/J.IJHYDENE.2024.06.041.
[240] Wei Q, Lucero JM, Crawford JM, Way JD, Wolden CA, Carreon MA. Ammonia separation from N2 and H2 over LTA zeolitic imidazolate framework membranes. J Membr Sci 2021;623. https://doi.org/10.1016/j.memsci.2021.119078.
[241] Duan X, Kim D, Narasimharao K, Al-Thabaiti S, Tsapatsis M. High-performance ammonia-selective MFI nanosheet membranes. Chem Commun 2021;57:580–2. https://doi.org/10.1039/d0cc07217f.
[242] Yang B, Bai L, Zeng S, Luo S, Liu L, Han J, et al. NH3 separation membranes with self-assembled gas highways induced by protic ionic liquids. Chem Eng J 2021;421:127876. https://doi.org/10.1016/J.CEJ.2020.127876.
[243] Laciak DV, Pez GP, Burban PM. Molten salt facilitated transport membranes. Part 2. Separation of ammonia from nitrogen and hydrogen at high temperatures. J Membr Sci 1992;65:31–8. https://doi.org/10.1016/0376-7388(92)87049-4.
[244] Padinjarekutt S, Sengupta B, Li H, Friedman K, Behera D, Lecaros R, et al. Synthesis of Na+-gated nanochannel membranes for the ammonia (NH3) separation. J Membr Sci 2023;674:121512. https://doi.org/10.1016/J.MEMSCI.2023.121512.
[245] Himstedt HH, Huberty MS, Mccormick AV, Schmidt LD, Cussler EL. Ammonia synthesis enhanced by magnesium chloride absorption. AIChE J 2015;61:1364–71. https://doi.org/10.1002/aic.14733.
[246] David WIF, Agnew GD, Bañares-Alcántara R, Barth J, Bøgild Hansen J, Bréquigny P, et al. 2023 roadmap on ammonia as a carbon-free fuel. JPhys Energy 2024;6. https://doi.org/10.1088/2515-7655/ad0a3a.
[247] Smith C, Torrente-Murciano L. Guidance for targeted development of ammonia synthesis catalysts from a holistic process approach. Chem Catal 2021;1:1163–72. https://doi.org/10.1016/j.checat.2021.09.015.
[248] Malmali M, Wei Y, McCormick A, Cussler EL. Ammonia synthesis at reduced pressure via reactive separation. Ind Eng Chem Res 2016;55:8922–32. https://doi.org/10.1021/acs.iecr.6b01880.
[249] Palys MJ, McCormick A, Cussler EL, Daoutidis P. Modeling and optimal design of absorbent enhanced ammonia synthesis. Processes 2018;6. https://doi.org/10.3390/PR6070091.

[250] Smith C, McCormick AV, Cussler EL. Optimizing the conditions for ammonia production using absorption. ACS Sustainable Chem Eng 2019;7:4019–29. https://doi.org/10.1021/acssuschemeng.8b05395.
[251] Smith C, Torrente-Murciano L. Low temperature and pressure single-vessel integrated ammonia synthesis and separation using commercial KATALCO catalysts: green ammonia synthesis using renewable energy. Johnson Matthey Technol Rev 2022;66:435–42. https://doi.org/10.1595/205651322X16577001040526.
[252] Kunz T, Cholewa T, Güttel R. Potential of sorption-enhanced ammonia synthesis—an equilibrium and reactor modeling study. ACS Eng Au 2025;5:140–53. https://doi.org/10.1021/acsengineeringau.4c00056.
[253] Onuoha CE, Kale MJ, Malmali M, Dauenhauer PJ, McCormick AV. Improving absorbent-enhanced ammonia separation for efficient small-scale ammonia synthesis. Ind Eng Chem Res 2024;63:5608–17. https://doi.org/10.1021/acs.iecr.3c04351.
[254] Zhang Z, Way JD, Wolden CA. Design and operational considerations of catalytic membrane reactors for ammonia synthesis. AIChE J 2021;67. https://doi.org/10.1002/aic.17259.
[255] Kucuk E, Hasan Koybasi H, Avci AK. Beyond equilibrium ammonia synthesis in a membrane and heat exchange integrated microreactor: a modeling study. Fuel 2024;357:129858. https://doi.org/10.1016/J.FUEL.2023.129858.
[256] Wakimoto K, Yan WW, Hattori M, Hara M, Moriyama N, Nagasawa H, et al. Green ammonia production via recycle membrane reactor: experiment and process simulation. Chem Eng J 2024;496. https://doi.org/10.1016/j.cej.2024.153754.
[257] Tm I. Kinetics of ammonia synthesis on promoted iron catalysts. Acta Physiochim URSS 1940;12:327–56.
[258] Chimique G, Annarle D. CHEMICAL ENGINEERING SCIENCE application of the temkin kinetic equation to ammonia synthesis in large-scale reactors. 1952.
[259] Nielsen A, Kjaer J, Hansen B. Rate equation and mechanism of ammonia synthesis at industrial conditions. J Catal 1964;3:68–79. https://doi.org/10.1016/0021-9517(64)90094-6.
[260] Sehested J, Jacobsen CJH, Törnqvist E, Rokni S, Stoltze P. Ammonia synthesis over a multipromoted iron catalyst: extended set of activity measurements, microkinetic model, and hydrogen inhibition. J Catal 1999;188:83–9. https://doi.org/10.1006/jcat.1999.2628.
[261] Dyson DC, Simon JM. A kinetic expression with diffusion correction for ammonia synthesis on industrial catalyst. Ind Eng Chem Fund 1968;7:605–10. https://doi.org/10.1021/i160028a013.
[262] Rossetti I, Pernicone N, Ferrero F, Forni L. Kinetic study of ammonia synthesis on a promoted Ru/C catalyst. Ind Eng Chem Res 2006;45:4150–5. https://doi.org/10.1021/ie051398g.
[263] Tripodi A, Compagnoni M, Bahadori E, Rossetti I. Process simulation of ammonia synthesis over optimized Ru/C catalyst and multibed Fe + Ru configurations. J Ind Eng Chem 2018;66:176–86. https://doi.org/10.1016/j.jiec.2018.05.027.
[264] Nikačević N, Jovanović M, Petkovska M. Enhanced ammonia synthesis in multifunctional reactor with in situ adsorption. Chem Eng Res Des 2011;89:398–404. https://doi.org/10.1016/j.cherd.2010.08.011.
[265] Nikzad A, Iranshahi D, Ranjbaran M, Bagherpour-Ardakani E. Conceptual comparison of three novel configurations in the spherical radial flow reactor for ammonia production. Fuel 2022;321. https://doi.org/10.1016/j.fuel.2022.123945.
[266] Nikzad A, Iranshahi D, Ranjbaran M. Comparative evaluation of spherical radial flow reactor, spherical axial flow reactor, and tubular reactor in ammonia production by using CFD simulation. Fuel 2023;350. https://doi.org/10.1016/j.fuel.2023.128772.
[267] Tyrański M, Bujalski JM, Orciuch W, Makowski Ł. Computational fluid dynamics of ammonia synthesis in axial-radial bed reactor. Energies 2023;16:6680. https://doi.org/10.3390/en16186680.
[268] Gu T, Araya SS, Yin C, Liso V. Exploring decentralized ammonia synthesis for hydrogen storage and transport: a comprehensive CFD investigation with experimental validation and parametric study. Energy Convers Manag 2023;295. https://doi.org/10.1016/j.enconman.2023.117604.
[269] Zhang X, Li G, Zhou Z, Nie L, Dai Y, Ji X, et al. How to achieve flexible green ammonia production: insights via three-dimensional computational fluid dynamics simulation. Ind Eng Chem Res 2024;63:12547–60. https://doi.org/10.1021/acs.iecr.4c01118.
[270] Zhang S, Zhao X, Bayyuk S. Generalized formulations for the rhie-chow interpolation. J Comput Phys 2014;258:880–914. https://doi.org/10.1016/j.jcp.2013.11.006.
[271] Guo J, Chen P, Catalyst. NH3 as an energy carrier. Chem 2017;3:709–12. https://doi.org/10.1016/j.chempr.2017.10.004.
[272] Khan MA, Young C, Mackinnon CB, Layzell DB. The techno-economics of hydrogen compression. Transition Accelerator Tech Briefs 2021;1:1–36.
[273] Ishaq H, Dincer I. Dynamic modelling of a solar hydrogen system for power and ammonia production. Int J Hydrogen Energy 2021;46:13985–4004. https://doi.org/10.1016/j.ijhydene.2021.01.201.
[274] Bahnamiri FK, Khalili M, Pakzad P, Mehrpooya M. Techno-economic assessment of a novel power-to-liquid system for synthesis of formic acid and ammonia, based on CO2 electroreduction and alkaline water electrolysis cells. Renew Energy 2022;187:1224–40. https://doi.org/10.1016/J.RENENE.2022.01.085.
[275] Cesaro Z, Ives M, Nayak-Luke R, Mason M, Bañares-Alcántara R. Ammonia to power: forecasting the levelized cost of electricity from green ammonia in large-scale power plants. Appl Energy 2021;282:116009. https://doi.org/10.1016/j.apenergy.2020.116009.
[276] Liu H, Yu M, Tong X, Wang Q, Chen M. High temperature solid oxide electrolysis for green hydrogen production. Chem Rev 2024. https://doi.org/10.1021/acs.chemrev.3c00795.
[277] Cameli F, Kourou A, Rosa V, Delikonstantis E, Galvita V, Van Geem KM, et al. Conceptual process design and technoeconomic analysis of an e-ammonia plant: Green H2 and cryogenic air separation coupled with haber-bosch process. Int J Hydrogen Energy 2024;49:1416–25. https://doi.org/10.1016/J.IJHYDENE.2023.10.020.
[278] Zhang H, Wang L, Van herle J, Maréchal F, Desideri U. Techno-economic comparison of green ammonia production processes. Appl Energy 2020;259:114135. https://doi.org/10.1016/J.APENERGY.2019.114135.
[279] Zhou H, Chen Z, Meng W, Yang S. Design, global energy integration, and sustainability analyses of a process coupling renewable energy water electrolysis for hydrogen production with ammonia synthesis. J Environ Chem Eng 2024;12:112892. https://doi.org/10.1016/J.JECE.2024.112892.
[280] Asgharian H, Pignataro V, Iov F, Pagh Nielsen M, Liso V. Exceeding equilibrium limitations: enhanced temperature control for sustainable decentralized green ammonia production – a techno-economic analysis. Energy Convers Manag 2024;315:118764. https://doi.org/10.1016/J.ENCONMAN.2024.118764.
[281] Waugh KC, Butler D, Hayden BE. The mechanism of the poisoning of ammonia synthesis catalysts by oxygenates O2, CO and H2O: an in situ method for active surface determination. Catal Lett 1994;24:197–210. https://doi.org/10.1007/BF00807390.
[282] Morgan ER, Manwell JF, McGowan JG. Sustainable ammonia production from U. S. offshore wind farms: a techno-economic review. ACS Sustainable Chem Eng 2017;5:9554–67. https://doi.org/10.1021/acssuschemeng.7b02070.
[283] Haug P, Koj M, Turek T. Influence of process conditions on gas purity in alkaline water electrolysis. Int J Hydrogen Energy 2017;42:9406–18. https://doi.org/10.1016/j.ijhydene.2016.12.111.
[284] Bacquart T, Arrhenius K, Persijn S, Rojo A, Auprêtre F, Gozlan B, et al. Hydrogen fuel quality from two main production processes: steam methane reforming and proton exchange membrane water electrolysis. J Power Sources 2019;444. https://doi.org/10.1016/j.jpowsour.2019.227170.
[285] Moghaddam AA, Krewer U. Poisoning of ammonia synthesis catalyst considering off-design feed compositions. Catalysts 2020;10:1–16. https://doi.org/10.3390/catal10111225.
[286] Kopp M, Coleman D, Stiller C, Scheffer K, Aichinger J, Scheppat B. Energiepark mainz: technical and economic analysis of the worldwide largest power-to-gas plant with PEM electrolysis. Int J Hydrogen Energy 2017;42:13311–20. https://doi.org/10.1016/J.IJHYDENE.2016.12.145.
[287] Weiß A, Siebel A, Bernt M, Shen T-H, Tileli V, Gasteiger HA. Impact of intermittent operation on lifetime and performance of a PEM water electrolyzer. J Electrochem Soc 2019;166:F487–97. https://doi.org/10.1149/2.0421908jes.
[288] Palys MJ, Daoutidis P. Power-to-X: a review and perspective. Comput Chem Eng 2022;165:107948. https://doi.org/10.1016/J.COMPCHEMENG.2022.107948.
[289] Ruuskanen V, Koponen J, Kosonen A, Hehemann M, Keller R, Niemelä M, et al. Power quality estimation of water electrolyzers based on current and voltage measurements. J Power Sources 2020;450:227603. https://doi.org/10.1016/J.JPOWSOUR.2019.227603.
[290] Armijo J, Philibert C. Flexible production of green hydrogen and ammonia from variable solar and wind energy: case study of Chile and Argentina. Int J Hydrogen Energy 2020;45:1541–58. https://doi.org/10.1016/J.IJHYDENE.2019.11.028.
[291] Qi M, Vo DN, Yu H, Shu CM, Cui C, Liu Y, et al. Strategies for flexible operation of power-to-X processes coupled with renewables. Renew Sustain Energy Rev 2023;179. https://doi.org/10.1016/j.rser.2023.113282.
[292] Bouaboula H, Ouikhalfan M, Saadoune I, Chaouki J, Zaabout A, Belmabkhout Y. Addressing sustainable energy intermittence for green ammonia production. Energy Rep 2023;9:4507–17. https://doi.org/10.1016/j.egyr.2023.03.093.
[293] Nayak-Luke R, Bañares-Alcántara R, Wilkinson I. "green" ammonia: impact of renewable energy intermittency on plant sizing and levelized cost of ammonia. Ind Eng Chem Res 2018;57:14607–16. https://doi.org/10.1021/acs.iecr.8b02447.
[294] Smith C, Torrente-Murciano L. The importance of dynamic operation and renewable energy source on the economic feasibility of green ammonia. Joule 2024;8:157–74. https://doi.org/10.1016/j.joule.2023.12.002.
[295] Campion N, Nami H, Swisher PR, Vang Hendriksen P, Münster M. Techno-economic assessment of green ammonia production with different wind and solar potentials. Renew Sustain Energy Rev 2023;173:113057. https://doi.org/10.1016/J.RSER.2022.113057.
[296] Nami H, Rizvandi OB, Chatzichristodoulou C, Hendriksen PV, Frandsen HL. Techno-economic analysis of current and emerging electrolysis technologies for green hydrogen production. Energy Convers Manag 2022;269:116162. https://doi.org/10.1016/J.ENCONMAN.2022.116162.
[297] Fúnez Guerra C, Reyes-Bozo L, Vyhmeister E, Jaén Caparrós M, Salazar JL, Clemente-Jul C. Technical-economic analysis for a green ammonia production plant in Chile and its subsequent transport to Japan. Renew Energy 2020;157:404–14. https://doi.org/10.1016/j.renene.2020.05.041.
[298] Ong CW, Chang N, Tsai ML, Chen CL. Decarbonizing the energy supply chain: ammonia as an energy carrier for renewable power systems. Fuel 2024;360. https://doi.org/10.1016/j.fuel.2023.130627.
[299] Wang C, Walsh SDC, Longden T, Palmer G, Lutalo I, Dargaville R. Optimising renewable generation configurations of off-grid green ammonia production systems considering haber-bosch flexibility. Energy Convers Manag 2023;280. https://doi.org/10.1016/j.enconman.2023.116790.
[300] Cesaro Z, Ives M, Nayak-Luke R, Mason M, Bañares-Alcántara R. Ammonia to power: forecasting the levelized cost of electricity from green ammonia in large-

scale power plants. Appl Energy 2021;282:116009. https://doi.org/10.1016/J.APENERGY.2020.116009.
[301] Osman O, Sgouridis S, Sleptchenko A. Scaling the production of renewable ammonia: a techno-economic optimization applied in regions with high insolation. J Clean Prod 2020;271. https://doi.org/10.1016/j.jclepro.2020.121627.
[302] Mohamed AMO, Economou IG, Bicer Y. Navigating ammonia production routes: life cycle assessment insights for a sustainable future. Curr Opin Green Sustainable Chem 2024;49:100947. https://doi.org/10.1016/J.COGSC.2024.100947.
[303] Bicer Y, Dincer I, Zamfirescu C, Vezina G, Raso F. Comparative life cycle assessment of various ammonia production methods. J Clean Prod 2016;135:1379–95. https://doi.org/10.1016/J.JCLEPRO.2016.07.023.
[304] Bicer Y, Dincer I, Vezina G, Raso F. Impact assessment and environmental evaluation of various ammonia production processes. Environ Manage 2017;59:842–55. https://doi.org/10.1007/s00267-017-0831-6.
[305] Lee B, Winter LR, Lee H, Lim D, Lim H, Elimelech M. Pathways to a green ammonia future. ACS Energy Lett 2022;7:3032–8. https://doi.org/10.1021/acsenergylett.2c01615.
[306] Chisalita DA, Petrescu L, Cormos CC. Environmental evaluation of european ammonia production considering various hydrogen supply chains. Renew Sustain Energy Rev 2020;130:109964. https://doi.org/10.1016/J.RSER.2020.109964.
[307] Liu X, Elgowainy A, Wang M. Life cycle energy use and greenhouse gas emissions of ammonia production from renewable resources and industrial by-products. Green Chem 2020;22:5751–61. https://doi.org/10.1039/d0gc02301a.
[308] Lee K, Liu X, Vyawahare P, Sun P, Elgowainy A, Wang M. Techno-economic performances and life cycle greenhouse gas emissions of various ammonia production pathways including conventional, carbon-capturing, nuclear-powered, and renewable production. Green Chem 2022;24:4830–44. https://doi.org/10.1039/d2gc00843b.
[309] Wen D, Kuo PC, Saeidi S, Özdemir F, Maréchal F. Renewable synthesis fuels for a circular economy: a life cycle assessment. Resour Conserv Recycl 2024;211:107851. https://doi.org/10.1016/J.RESCONREC.2024.107851.
[310] Unigel to retrofit plant in camaçari. https://ammoniaenergy.org/articles/brazils-first-electrolysis-based-ammonia-plant-takes-shape/; 2022 (accessed November 5, 2024).
[311] World's first of its kind green ammonia plant inaugurated by skovgaard energy, vestas, and topsoe. https://www.topsoe.com/press-releases/worlds-first-of-its-kind-green-ammonia-plant-inaugurated-by-skovgaard-energy-vestas-and-topsoe; 2024 (accessed November 5, 2024).
[312] China: scaling-up "flexible" ammonia production powered by renewable energy. https://ammoniaenergy.org/articles/china-scaling-up-flexible-ammonia-production-powered-by-renewable-energy/; 2023 (accessed November 5, 2024).
[313] HØST PtX esbjerg. https://hoestptxesbjerg.dk/. [Accessed 5 November 2024].
[314] Oman project. https://www.acme-ghc.in/oman-project. [Accessed 5 November 2024].
[315] World's largest green ammonia plant for nelson mandela Bay, South Africa. https://www.hiveenergy.co.uk/2021/12/15/worlds-largest-green-ammonia-plant-for-nelson-mandela-bay-south-africa/; 2021 (accessed November 5, 2024).
[316] Topsoe signs agreement on first commercial size dynamic green ammonia plant in China 2023. https://www.topsoe.com/press-releases/topsoe-signs-agreement (accessed November 5, 2024).
[317] Ohmium announces collaboration with SwitcH2 BV and BW offshore for floating green ammonia plant. https://www.ohmium.com/news/ohmium-announces-collaboration-with-switch2-bv-and-bw-offshore-for-floating-green-ammonia-plant; 2024 (accessed November 5, 2024).
[318] ACWA power to develop Uzbekistan's first green hydrogen and green ammonia projects. https://www.acwapower.com/news/acwa-power-to-develop-uzbekistans-first-green-hydrogen-and-green-ammonia-projects/; 2023 (accessed November 5, 2024).
[319] Sungrow hydrogen won the bidding for the world's largest green hydrogen, ammonia and methanol integrated project 2024. https://www.prnewswire.com/apac/news-releases/sungrow-hydrogen-won-the-bidding-for-the-worlds-largest-green-hydrogen-ammonia-and-methanol-integrated-project-302184486.html (accessed November 5, 2024).
[320] Project nujio'qonik. chrome-extension://efaidnbmnnnibpcajpcglclefindmkaj/https://ammoniaenergy.org/wp-content/uploads/2024/06/Project-Features-speaker-slides-June-2024.pdf, ; 2024 (accessed November 5, 2024).
[321] The generalitat valenciana and IGNIS sign an MOU to promote the Castellón green ammonia and hydrogen project. https://ignis.es/en/the-generalitat-valenciana-and-ignis-sign-an-mou-to-promote-the-castellon-green-ammonia-and-hydrogen-project/. [Accessed 5 November 2024].
[322] Using surplus hydroelectricity for ammonia production in Paraguay 2023. chrome-extension://efaidnbmnnnibpcajpcglclefindmkaj/https://ammoniaenergy.org/wp-content/uploads/2023/04/Project-Features-speakers-slides-April-2023.pdf (accessed November 5, 2024).
[323] Topsoe is selected technology provider by Indian frontrunner in green ammonia, hygenco 2024. https://www.topsoe.com/press-releases/topsoe-is-selected-technology-provider-by-indian-frontrunner-in-green-ammonia-hygenco (accessed December 4, 2024).
[324] Energy China: 200,000 tons of renewable ammonia capacity online this September. https://AmmoniaenergyOrg/Articles/Energy-China-Engineering-Corporation-200000-Tons-of-Renewable-Ammonia-Capacity-Online-This-September/ [n.d.].
[325] Yu S, Xiang T, Alharbi NS, Al-aidaroos BA, Chen C. Recent development of catalytic strategies for sustainable ammonia production. Chin J Chem Eng 2023;62:65–113. https://doi.org/10.1016/j.cjche.2023.03.028.
[326] Odenweller A, Ueckerdt F. The green hydrogen ambition and implementation gap. Nat Energy 2025;10:110–23. https://doi.org/10.1038/s41560-024-01684-7.